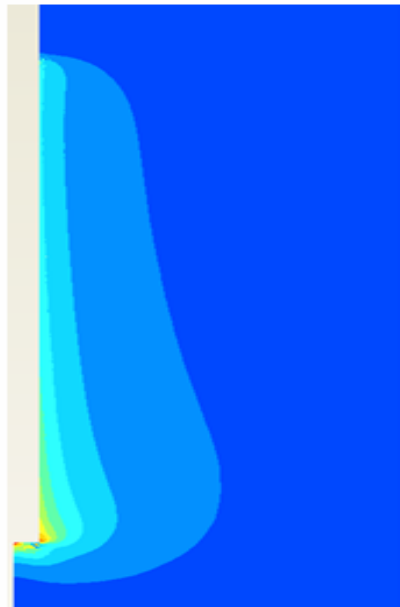


Modelling of Installation Effect of Driven Piles by Hypoplasticity

Delft, December 2009



MSc Thesis

Pham Huy Dung

Modelling of Installation Effect of Driven Piles by Hypoplasticity

MASTER OF SCIENCE THESIS

Graduation committee:

Chairman:
Prof.Ir. A.F. Van Tol

Supervisor:
Dr.Ir. R.B.J. Brinkgreve

Ir. J.G. De Gijt

Dr.Ir. J. Dijkstra

Daily assistance:
Ir. A. Rohe
H.K. Engin, MSc

Coordinator:
Ir. J.P. Oostveen

Student: Pham Huy Dung

Section of Geotechnical Engineering
Water Resources University - Vietnam

Section of Geotechnical Engineering
Faculty of Civil Engineering & Geosciences
Delft University of Technology – The Netherlands

Table of contents

Acknowledgements	6
Abstract	7
1 Introduction	8
1.1 Motivation	8
1.2 Objectives of study	9
1.3 Structure of report	9
2 Background Knowledge	11
2.1 Introduction	11
2.2 Literature study on driven piles	11
2.2.1 Analytical methods	11
2.2.2 Experimental methods	12
2.2.3 Numerical methods	13
2.3 Soil models	16
2.3.1 Mohr-Coulomb model (MC)	16
2.3.2 Hardening Soil model (HS)	17
2.3.3 Hypoplastic model (HP)	18
2.4 Numerical framework	19
2.5 Interface elements	19
2.6 Conclusion	20
3 Hypoplasticity	21
3.1 Introduction	21
3.2 Constitutive equation	22
3.3 Parameter determination	23
3.3.1 Critical state parameter φ_c	24
3.3.2 Stiffness parameter h_s and n	25
3.3.3 Minimum void ratio at zero pressure e_{d0}	26
3.3.4 Maximum void ratio at zero pressure e_{i0}	27
3.3.5 Critical void ratio e_{c0} at zero pressure	27
3.3.6 Exponent α	28
3.3.7 Exponent β	28
3.4 Intergranular strain (IGS)	29
3.5 Conclusion	31
4 Parametric Sensitivity Analysis	33
4.1 Introduction	33
4.2 Verification and validation of the HP model	33

4.2.1	Comparison with Baskarp sand	33
4.2.2	Comparison with Karlsruhe sand	35
4.3	Sensitivity of the hypoplastic parameters.....	36
4.3.1	Parameter variation.....	36
4.3.2	Influence of parametric variation on drained triaxial tests	37
4.3.3	Influence of parametric variation on oedometer tests	41
4.4	Effects of intergranular strain.....	43
4.4.1	Intergranular strain parameters for Karlsruhe sand	43
4.4.2	Simulation of oedometer test.....	43
4.4.3	Simulation of triaxial test	45
4.4.4	Sensitivity of IGS parameters.....	46
4.5	Conclusion.....	48
5	Numerical Modelling of Pile Jacking	50
5.1	Introduction	50
5.2	Centrifuge pile test	51
5.2.1	Test set-up.....	51
5.2.2	Test results	52
5.3	Numerical modeling of pile jacking.....	54
5.3.1	Mesh and boundary conditions.....	54
5.3.2	Simulation of installation effect	56
5.3.3	Constitutive model and parameters	57
5.3.4	Calculation procedures	58
5.3.4.1	Initial stresses.....	58
5.3.4.2	Calculation phases	59
5.3.5	Numerical results.....	60
5.3.5.1	Change of void ratio	61
5.3.5.2	Stress distributions.....	63
5.3.5.3	Void ratio evolution	65
5.3.6	Influence of prescribed displacements	66
5.3.7	Modelling of shearing effect.....	68
5.4	Conclusion.....	71
6	Numerical Modelling of Cyclic Loading on Pile Shaft	74
6.1	Introduction	74
6.2	Mesh and boundary conditions	75
6.3	Simulation of installation effect	76
6.4	Constitutive model and parameters	77
6.5	Calculation procedures.....	78
6.5.1	Initial stresses	78
6.5.2	Calculation phases.....	78

6.6	Result and discussions.....	79
6.6.1	Dense case.....	79
6.6.1.1	After jacking process.....	79
6.6.1.2	After cyclic loading process.....	82
6.6.2	Loose case.....	88
6.6.2.1	After jacking process.....	88
6.6.2.2	After cyclic loading process.....	90
6.6.3	Modelling of shearing effect.....	93
6.7	Conclusion.....	94
7	Conclusions and Recommendations	96
7.1	General.....	96
7.2	Conclusions.....	96
7.2.1	Hypoplasticity.....	96
7.2.2	Modelling of pile jacking.....	97
7.2.3	Modelling of cyclic loading.....	99
7.3	Recommendations.....	100
	Appendix A	101
	Estimation of intergranular strain parameters for Baskarp sand.....	101
	Appendix B	104
	Estimation of Hardening soil parameters for Baskarp sand.....	104
	References.....	107

Acknowledgements

Doing the final thesis has been the most challenged work in my study. This report would not have been finished without the help from my supervisors.

Firstly, I would like to express my thankfulness to Professor van Tol for accepting me as his MSc student and his guidance and encouragement. I also deeply acknowledge Dr. R.B.J. Brinkgreve as my main supervisor with the continuous guidance and advice for my thesis.

Secondly, I am grateful to Ir. A. Rohe and Ir. H.K. Engin for their daily assistance and suggestions as well as for correcting my report.

I also would like to thank Dr. J. Dijkstra and Ir. J.G. De Gijt for their comments and suggestions during the meetings.

I want to thank CICAT organisation for the support relating to the fund and all procedures during my studying, also the help from Plaxis staffs and valuable guidance from my coordinator Ir. J.P. Oostveen.

I also specially thank all of my colleagues at Geotechnical Engineering Section of Water Resources University, Vietnamese friends in Delft and international students for the help in studying as well as in the daily life.

Finally, I am grateful to my family, my parents; greatly indebted to my wife N.T.N. Thanh and my little child P.T. Minh for their continuous encouragement and belief. They are always in my inspiration and motivation.

Delft, December 2009

Pham Huy Dung

Abstract

Driven piles have been selected as a powerful technique to deal with the construction on soft soil. Many case studies have been carried out to capture the soil behaviour during the pile installation, both numerical and experimental methods. In terms of the numerical method, it is proved to be difficult due to the large displacement in the installation process, leading to a significant change of stress and void ratio. Therefore, it is required to have some special techniques such as Arbitrary Lagrangian Eulerian or Particle methods, and also a proper constitutive model to describe the continuous changing of stress and void ratio during the installation.

On the other hand, the installation effect of driven piles is proved to be modelled by using a conventional small strain analysis in Plaxis 2D finite element code, whereas the installation effect is taken into account by increasing the volume of the pile cluster, e.g. using the prescribed displacements at the pile-soil boundary or volumetric expansion. Moreover, the hypoplastic model with intergranular strain concept is a powerful constitutive law to describe the soil behaviour for granular soil. It uses a unique equation; the stress rate is a function of the stress tensor, the current void ratio and the strain rate as $\dot{\mathbf{T}} = \mathbf{F}(\mathbf{T}, e, \mathbf{D})$. The dependency of stress and density are also accounted in this model, whilst the excessive accumulation of deformations in the region of small stress cycles is overcome by the introduction of intergranular strain.

This study proposes a procedure to simulate the pile jacking method in Plaxis 2D finite element code with the improvements based on the suggestions as showed by previous authors [6, 33], where the installation effect is taken into account by applying the prescribed displacements at the pile-soil boundary. A centrifuge pile test [10] is chosen in order to validate the numerical simulations. In the analyses, the hypoplastic model formulated by Von Wolfferdorff with intergranular strain is used. The hypoplastic parameters are derived from laboratory tests as shown in [13], while the intergranular strain parameters are derived from the numerical simulations. The results show a good agreement with the experimental and other numerical results. Besides, a simplified procedure is also used in order to investigate the cyclic loading effect in the vicinity of the pile shaft. Promisingly, the numerical results fit quite well with the soil response found in reality and other numerical results. It shows that a compaction results from the continuous cyclic loading, leading to a reduction of stresses around the pile.

Chapter 1

Introduction

1.1 Motivation

Driven piles have been commonly used as a technical solution for deep foundations. Consequently, many case studies have been executed to establish a reliable approach for determining the bearing capacity of a single pile. Most of the methods use soil parameters such as friction angle, cohesion, cone resistance, etc., which are collected from standard site investigations carried out before pile installation (e.g. CPT, SPT). However, during the pile installation process the surrounding soil is displaced and compacted, leading to large stress increases around the pile and an associated increase in strength and stiffness of the soil [6]. Definitely, the soil properties will change, influencing in the correctness of above-mentioned parameters.

Thanks to the modern development of the finite element method (FEM) and the increase of computational power, many complex geotechnical problems can be solved in the numerical frameworks. However, when the modelling of pile foundations is attempted in the finite element code, the installation phase is often not taken into account, partly due to the inability to cope with large strains and mainly due to the limited knowledge of the material behaviour around driven piles [11]. Hence, it is very important to have an appropriate model that can simulate the real soil behaviour and soil-pile interaction caused by the pile installation process.

A huge number of studies in modelling of driven piles using soil models like Mohr-Coulomb, Drucker-Prager or Hardening Soil, have been published, but its results are still not completely according to experimental ones [9, 11, 13]. The main reason is the inability of those models to capture the soil behaviour, taking into account the continuously changing soil properties during the pile installation process. Promisingly, the hypoplastic model which is developed by Kolymbas [22] is proved to be a good model for granular soil. For this model, the soil behaviour is defined by stress state and the current void ratio so that the continuous changing of stresses and void ratio during the installation phase could be taken into account. However, the shortcoming of this model is the over-accumulation of deformation for small stress cycles. For this reason, the concept of intergranular strain is introduced by Niemunis & Herle [28] to take this behaviour into consideration. As a result, the hypoplastic model with the intergranular strain is chosen as the main model to simulate the installation effect of driven piles.

1.2 Objectives of study

The objective of this study is the investigation of the installation effect of driven piles in sand using the finite element method while the change of stresses and void ratio is looked into more detail. Therefore, this study mainly focuses:

- ✓ To evaluate the possibilities and limitations of the Hardening soil and the Hypoplastic models in describing the installation effect.
- ✓ To describe a procedure using the FEM (Plaxis 2D) for analysing the installation effect of driven piles in sand.
- ✓ To visualise the installation effect of driven piles in terms of stresses and void ratio.
- ✓ To evaluate the bearing capacity of driven piles in terms of the shaft friction.

1.3 Structure of report

This is the report of the study on the investigation of the installation effect of driven piles using the FEM. The report begins with Chapter 1 in which some information of the study is introduced and analysed roughly in order to choose the research methodology. Then, Chapter 2 illustrates literature review in which previous studies on driven piles and soil models are described. Next, the hypoplastic model with the intergranular strain concept are described in more detail in Chapter 3, including

parameter determinations. Chapter 4 verifies the validity of the hypoplastic model and investigates the influences of various hypoplastic parameters on the soil behaviour. In Chapter 5, the installation effect of the pile jacking method is analysed using the commercial available Plaxis 2D package. Here, the installation effect is taken into account by applying the volumetric expansion or prescribed displacements at the pile shaft and pile tip. Then, the impact of cyclic loading is examined in Chapter 6 whilst the possibilities and limitations of the hardening soil and the hypolastic models are evaluated. At the end, Chapter 7 gives the conclusions and recommendations obtained from this study.

Chapter 2

Background Knowledge

2.1 Introduction

In this chapter, a series of researches on driven piles are reviewed in order to get a general idea on the developments of this field. Then several soil models which are already applied in numerical methods on driven piles are expressed. Finally, the hypoplastic model, Plaxis 2D finite element code and the interface element are described briefly, too.

2.2 Literature study on driven piles

2.2.1 Analytical methods

Gorbunov & Posadov [15] analysed the displacement and compaction of soil by a driven pile. They assumed that during the pile driving, the soil being displaced is moved only horizontally, whereas in reality the pile displaces the soil also vertically. The state of stresses in the soil established in this study will correspond to the original state after driving. The results from their study suggested that the points immediately adjacent to the central pile axis should be displaced to the edge of the pile. However, the radius of the displaced zone decreases with a reduction of penetration depth (z) of the pile (Fig. 2.1).

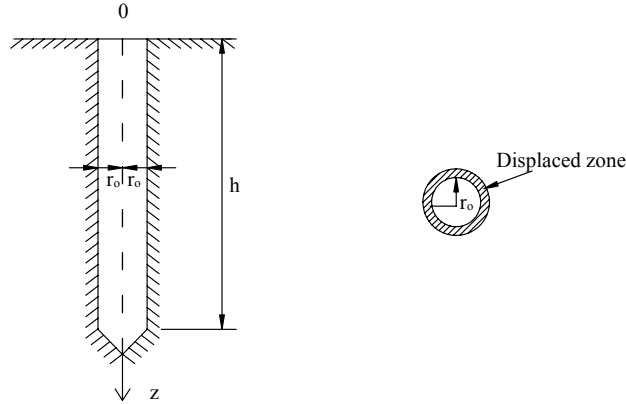


Fig. 2.1: Longitude (left) and cross section (right) of the pile [15]

If $z = h$ (h being the length of the pile) then the radius of the gap reaches $1.15r_0$ (r_0 being the radius of the pile) this value reduces to $1.03r_0$ when $0.4 < z/h < 0.6$ and remains $0.5r_0$ with smaller penetration depth. Please note that, above results are found from the case of $h/r_0 = 10$.

2.2.2 Experimental methods

A series of model pile tests are carried out in the centrifuge in sand by Klotz & Coop [20]. Some remarkable conclusions can be found from their results. Firstly, the base resistance and the average shaft friction at a certain depth of the penetration increase with an increase of the acceleration levels. However, no clear trend of the average radial stress can be found relating to the acceleration level except the fact that this value increases along the penetration depth. Moreover, the mobilised friction angle of the interface between the pile and soil had a very low value compared to the internal friction angle of the soil. Surprisingly, after increasing along to the depth of penetration, the radial stress shows a decrease towards the pile tip.

On the other hand, drum centrifuge tests have been conducted by White & Lehane [37] to examine the development of the horizontal stress acting on the pile shaft during the installation with respect to different methods. The horizontal stress distribution is relatively similar to the findings by Klotz & Coop [20], but no reduction of this stress towards the pile tip could be found. The results show an independence of the ratio between the horizontal stress and the cone resistance corresponding to an independence of the friction ratio. However, the horizontal stress degrades significantly during both cyclic installation and cyclic load test, this phenomenon leads to a considerable reduction of the shaft friction. This effect can be seen in the Fig. 2.2.

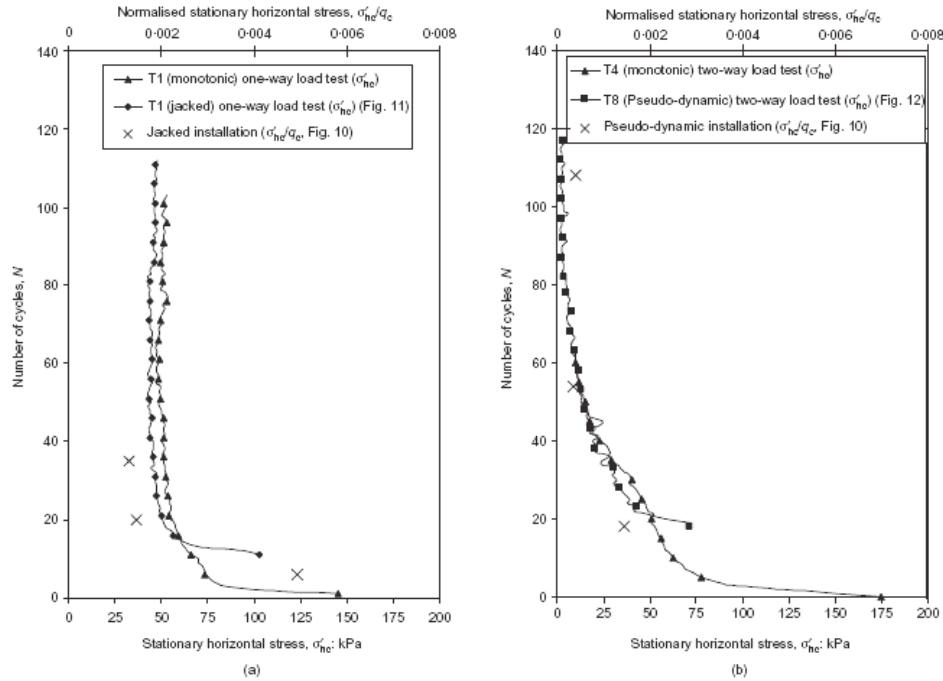


Fig. 2.2: Degradation of stationary horizontal stress with cycling during load tests
 (a) one-way compression load test, (b) two-way compression load test [37]

Furthermore, Bement and Selby [4] also conducted several tests to quantify a potential compaction settlements of granular soil due to vibration, typical of these experiments when piles are installed by vibrodriver. The tests are carried out in a Rowe cell (70 mm x 150 mm diameter) in which samples is kept at a constant vertical stress (10, 20, 50 or 100 kPa). After this process, the entire cell is shaken vertically at an increments of acceleration (typically of 0.1 g, 0.2 g, 0.3 g, 0.4 g, 0.5 g, 0.6 g, 0.8 g, 1.0 g and 2.0 g, and in some tests up to 6.0 g), while the vertical effective stress is maintained. The trend of results show that: increased surcharge pressure reduced the subsequent vibratory compaction; well-graded soil showed greater compaction than more uniform sands; compaction raised markedly when acceleration exceeded 1g; saturated soil demonstrated lager compaction than dry and unsaturated soil and compaction is influenced little by frequency within the range from 25 Hz to 120 Hz although rate of compaction reduced with frequency increase.

2.2.3 Numerical methods

Dijkstra et al. [12] used the FEM for the modelling of stress and strain development in the soil due to the installation effect of a displacement pile. The first analysis used small strain finite element method in PLAXIS package with the Mohr-Coulomb and the Hardening models, whilst the second one used Arbitrary Lagrangian Eularian (ALE)

numerical scheme with the Drucker-Prager model. Then, the results of both methods are compared with experimental outcomes of a jacked pile in sand. For the first method, they used interfaces element along the pile in analysis, it is shown that the results fit best the experimental test when it is applied a prescribed horizontal displacement equal to 7.5% of the pile radius at the pile shaft and a prescribed vertical displacement equal to 7.5 times of the pile radius at the pile tip (Fig. 2.3). On the other hand, in the ALE environment it is difficult to get results using advanced soil models or even the Mohr-Coulomb model so it is only applicable for determining the stress change due to the pile installation.

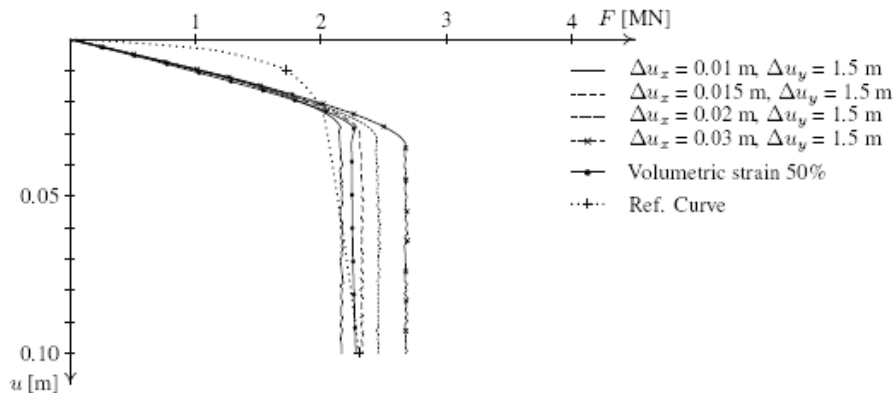


Fig. 2.3: Load-displacement curves for fine meshes with interfaces ($R = 0.75$) along the pile, for HS model with $\psi = 0$ [12]

The same principle is used to model the bearing capacity of displacement piles in sand in which the prescribed displacements are applied at pile-soil boundary to simulate the installation effect. Broere & Van Tol [6] found that the results are strongly influenced by the horizontal displacement rather than the vertical displacement. However, even with advanced model-Hardening soil, the horizontal stress along the pile are differ from findings by White and Lehane [37], resulting in a difference in terms of the shaft friction after the pile installation process and at failure in comparison with Lehane et al. [25]. They concluded that the Hardening model does not capture all installation effects so that another model would be developed in order to deal with the large strain happening during the pile installation.

Henke & Grabe [17] published a paper investigating the influence of the installation method (jacking, impact driving and vibratory driving) on the soil-plug behaviour inside open-ended piles using numerical simulation. Here, an open-ended pile with a diameter of 61 cm is penetrated into medium dense Karlsruhe sand. The commercial code ABAQUS with the hypoplastic model and the intergranular strain is used to simulate the pile penetration process in all analyses. The results showed that the jacked pile exhibited high horizontal stress inside the pile than impact driving or

vibro-driving methods. In contrast, vibro-driven piles showed a high compaction inside the pile down to the minimum void ratio caused by the continuous cyclic shearing.

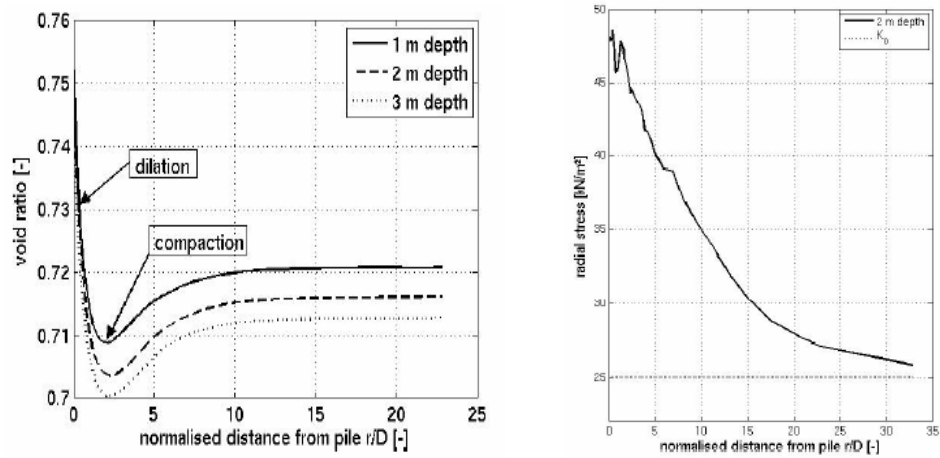


Fig. 2.4: Void ratio around the jacked pile (left) and radial stress distribution (right) at certain depth after 4 m of pile jacking [18]

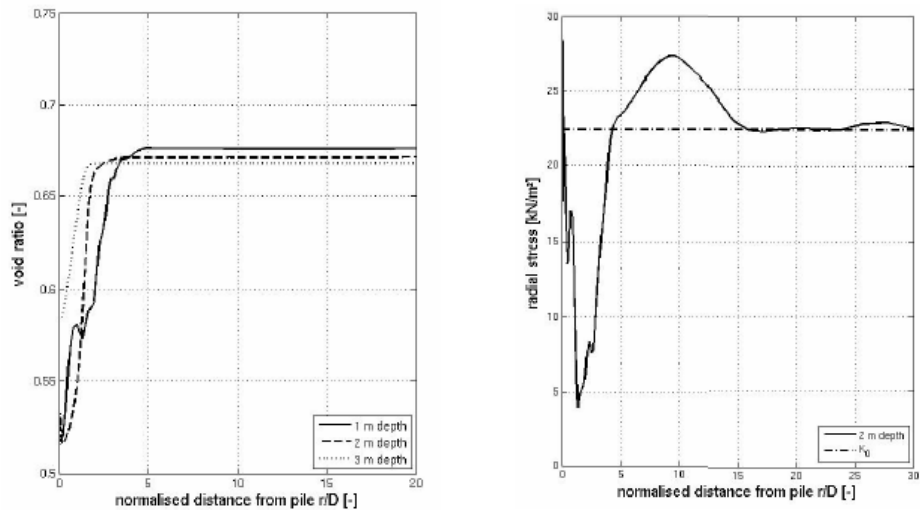


Fig. 2.5: Void ratio around the jacked pile (left) and radial stress distribution (right) at certain depth after 4 m of vibratory pile driving [18]

Finally, a special technique is introduced by Henke & Grabe [18] in a three-dimensional finite element model to simulate the pile installation effect. A tube of 1 mm radius is modelled at the axis of penetration. The contact between the tube and the surrounding soil is only activated during the pile penetration in which the pile slides over the tube and the soil separates from the tube. The hypoplastic model with intergranular strain is used in the commercial code ABAQUS. The results from jacking method show that a dilatant zone appears close to the pile shaft while the soil is

compacted at a distance from the pile. Moreover, the radial stress increases around the pile during the pile penetration. On the other hand, the results from vibrating method display difference behaviour from the jacking method. Around the vibrating pile, the soil is compacted leading to a decrease of void ratio and radial stress. Furthermore, the influenced area is much wider for pile jacking than vibratory pile driving and the radial stress for jacked pile is also higher than for vibrating pile (Fig. 2.4 and Fig. 2.5).

2.3 Soil models

2.3.1 Mohr-Coulomb model (MC)

The Mohr-Coulomb (MC) model is an elastic- perfectly plastic model; it is very simple to approximate the soil behaviour in the first approach. The basic principle of this model includes an elastic part with the reversible strain and a plastic part with the irreversible strain [5]. In the elastic part, the stress-strain relation follows Hooke's law while the MC failure criterion is used in the plastic part. A yield function (f) is introduced in order to evaluate the appearance of the plasticity. The plasticity occurs when $f = 0$. The full MC model yield condition includes six yield functions:

$$f_{1a} = \frac{1}{2}(\sigma'_{xx} - \sigma'_{zz}) + \frac{1}{2}(\sigma'_{xx} + \sigma'_{zz}) \sin \varphi - C \cos \varphi \leq 0 \quad (2.1)$$

$$f_{1b} = \frac{1}{2}(\sigma'_{zz} - \sigma'_{xx}) + \frac{1}{2}(\sigma'_{xx} + \sigma'_{zz}) \sin \varphi - C \cos \varphi \leq 0 \quad (2.2)$$

$$f_{2a} = \frac{1}{2}(\sigma'_{yy} - \sigma'_{xx}) + \frac{1}{2}(\sigma'_{yy} + \sigma'_{xx}) \sin \varphi - C \cos \varphi \leq 0 \quad (2.3)$$

$$f_{2b} = \frac{1}{2}(\sigma'_{xx} - \sigma'_{yy}) + \frac{1}{2}(\sigma'_{yy} + \sigma'_{xx}) \sin \varphi - C \cos \varphi \leq 0 \quad (2.4)$$

$$f_{3a} = \frac{1}{2}(\sigma'_{zz} - \sigma'_{yy}) + \frac{1}{2}(\sigma'_{zz} + \sigma'_{yy}) \sin \varphi - C \cos \varphi \leq 0 \quad (2.5)$$

$$f_{3b} = \frac{1}{2}(\sigma'_{yy} - \sigma'_{zz}) + \frac{1}{2}(\sigma'_{yy} + \sigma'_{zz}) \sin \varphi - C \cos \varphi \leq 0 \quad (2.6)$$

Although this model describes quite well the failure behaviour of the soil, it involves many limitations for the real soil behaviour. First, the linear elasticity occurs until failure so it includes neither stress-dependency nor stress-path dependency of stiffness. Furthermore, care must be taken in undrained condition due to unrealistic stress path [5]. Lastly, this model also does not include either hardening or softening rules.

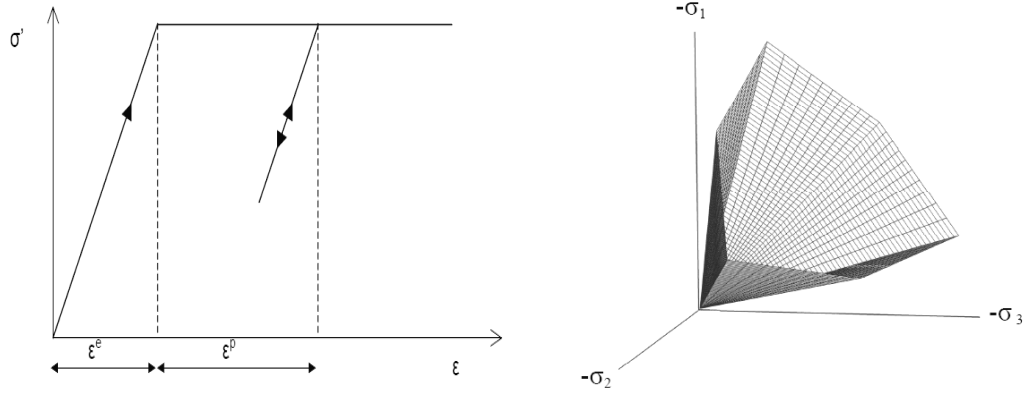


Fig. 2.6: Basic principle of MC model (left) and MC yield surface in principal stress space with $c=0$ (right) [5]

2.3.2 Hardening Soil model (HS)

The Hardening Soil model (HS) can be considered as an advanced model for the soil behaviour. The main difference with the MC model is the taking into account the stress-dependent and stress-path dependent stiffness. The basic idea for the formulation of the HS model is the hyperbolic relationship between the vertical strain ϵ_1 and the deviatoric stress q in primary triaxial loading [34]. This relation is as the following:

$$\epsilon_1 = \frac{q_a}{2E_{50}} \frac{q}{q_a - q} \quad \text{for } q < q_f \quad (2.7)$$

$$q_f = \frac{6 \sin \phi}{3 - \sin \phi} (p + c \cdot \cot \phi) \quad \text{with } q_a = \frac{q_f}{R_f} \quad (2.8)$$

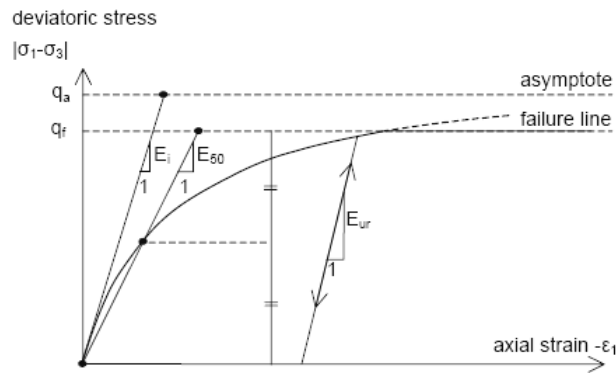


Fig. 2.7: Hyperbolic stress-strain relation in HS model [5]

Moreover, the soil behaviour is described much more accurately by using three different stiffnesses: triaxial loading stiffness E_{50} , triaxial unloading stiffness E_{ur} and the oedometer loading stiffness E_{cod} . The dependence of soil stiffness is accounted for as the

following:

$$E_{\text{oed}} = E_{\text{oed}}^{\text{ref}} \left(\frac{\sigma}{p^{\text{ref}}} \right)^m \quad (2.9)$$

$$E_{50} = E_{50}^{\text{ref}} \left(\frac{c \cdot \cos \varphi + \sigma_3 \cdot \sin \varphi}{c \cdot \cos \varphi + p^{\text{ref}} \cdot \sin \varphi} \right)^m \quad (2.10)$$

$$E_{\text{ur}} = E_{\text{ur}}^{\text{ref}} \left(\frac{c \cdot \cos \varphi + c \cdot \cot \varphi}{\sigma^{\text{ref}} + c \cdot \cot \varphi} \right)^m \quad (2.11)$$

Here, $E_{\text{oed}}^{\text{ref}}$, E_{50}^{ref} , $E_{\text{ur}}^{\text{ref}}$ are the corresponding modules at reference pressure $p^{\text{ref}} = 100$ kPa and m is the power to account for stress-level dependency of stiffness. The MC criterion at failure behaviour is also utilized for the HS model.

Besides the advantages of stress-dependency and memory of pre-consolidation stress, the HS model still has a number of limitations. Firstly, this model does not capture the softening behaviour caused by dilatancy and de-bonding effects [5]. In the HS model, the dilatancy continues to infinity, unless the dilatancy cut-off option is used. Moreover, the HS model does not take into account the increase of stiffness at small strain in comparison with reduced stiffness at large strain level. Lastly, this model also has a shortcoming in the region of small stress cycles due to an excessive accumulation of deformations in cyclic loading.

2.3.3 Hypoplastic model (HP)

The hypoplastic model (HP) has been developed since 1985 by Kolymbas [22] and is considered as a good model for granular materials. First, the hypoplastic constitutive law describes the stress rate ($\dot{\sigma}$) as a function of the strain rate ($\dot{\epsilon}$) and the stress tensor (σ). Then, it was improved by many following authors like Bauer, Herle, Gudehus, Von Wolfferdorff, etc., and Kolymbas himself. The outstanding of this model is the introduction of void ratio (e) as a state variable. The HP model recognizes anelastic deformation without using any additional notions such as yield surface or plastic potential [21]. However, this model has a shortcoming in the region of small stress cycles as an excessive accumulation of deformation occurs and therefore the displacements are overpredicted. Thereafter, the concept of intergranular strain is introduced by Niemunis & Herle [28] allows to account for this behaviour. In short, the HP model includes eight parameters describing the soil behaviour at different states and five parameters representing the intergranular strain. The HP model will be explained in more detail in Chapter 3.

2.4 Numerical framework

Plaxis is a two-dimensional FE program to model geotechnical problems in which a real situation may be modelled by a plane strain or axisymmetric analysis. One of the special features of this software is the use of a simple graphical input procedure in order to provide detailed computational results [5]. Herein, specific elements will be used to model a structure (e.g. plates, anchors, geogrids). A series of soil models can be utilized to simulate the soil behaviour while interface elements are used to model soil-structure interaction. Soil layers and other volume cluster can be modelled by 6-node or 15-node triangular elements. In the numerical scheme, stresses and strains at Gauss points are interpolated and calculated from displacements at nodes. Moreover, several analyses may be applied to perform deformation and stability analyses such as staged construction, consolidation or safety analysis. Lastly, in case of a conventional small strain analysis may lead to a significant change of geometry, updated Lagrangian analysis could be used to take into account the continuous changing of the FE mesh.

2.5 Interface elements

One notable feature of Plaxis finite element code is the possibility to use interface elements. A typical application of interfaces would be to model the interaction between a structure and the soil, which is intermediate between smooth and fully rough [5]. So this element could be used in the modelling of the pile installation process as suggestions by many authors [6, 33]. Interface elements are defined by a pair of nodes (Fig. 2.8). In this figure, the interface element can be seen to have certain thickness but in the calculation the coordinates of each node pair are identical, so the element has zero thickness.

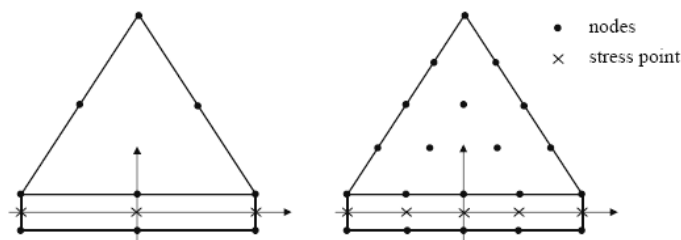


Fig. 2.8: Illustration of interface elements

The MC model is used to describe the behaviour of interfaces for the modelling of soil-structure interaction. The main interface parameter is the strength reduction factor R_{inter} which is taken into account the strength decrease of interface element in the corresponding soil layer.

2.6 Conclusion

As can be seen so far, there are a lot of studies on driven piles using not only experiments but also analytical or numerical methods. However, the results of numerical methods can not completely reproduce the experimental results. Moreover, the experimental results are even not completely in accordance with each other [20, 25, 37]. The measurements only focus on the soil behaviour nearby the pile, but not inspecting the soil behaviour at a distance from the pile. In the FEM, the fundamental problem is the use of such models could describe the soil behaviour which changes continuously during the pile installation. Obviously, the MC model has many limitations for the real soil behaviour and it seems not to be used in this case. This model only includes an elastic part with the reversible strain and a plastic part with the irreversible strain [5]. The HS model can be considered as an advanced model to simulate the soil behaviour. However, some important features are still not involved in the HS model. For example, this model does not capture the softening behaviour caused by dilatancy and de-bonding effects [5], also including a shortcoming in the region of small stress cycles as an excessive accumulation of deformations in cyclic loading. Indeed, the HP model seems to be the currently most suitable model for driven piles because of the introduction of the void ratio as a state variable and the intergranular strain concept. As a result, this study aims to investigate the soil behaviour under the installation effect of driven piles by using a conventional small strain analysis with the application of an advanced soil model-HP model in Plaxis 2D finite element code.

Chapter 3

Hypoplasticity

3.1 Introduction

As referred in Chapter 2, the hypoplastic model is selected for modelling of the soil behaviour of driven piles. This model is considerably introduced by Kolymbas [22], which describes the stress-strain behaviour of granular materials in a rate form. It is developed from the stress rate, written as a function of the stress tensor and the strain rate. Later on, the void ratio is added as an additional state variable by following authors (e.g. Gudehus [16], Bauer [3]). The outstanding of this model is its simplicity, this model recognizes anelastic deformation without using any additional notions such as yield surface or plastic potential [21]. However, small deformation due to cyclic loading and creep are not included, leading to an excessive accumulation of deformations under stress cycles. Then the concept of intergranular strain is introduced by Niemunis and Herle [28] allows to account for this behaviour. Currently, the hypoplastic model could be able to use for not only cohesiveless materials but also clays and organics. Nevertheless, the purpose of this study only limits for sand, the constitutive law given by Von Wolffersdorff [36] with the improvement of intergranular strain would be sufficient.

3.2 Constitutive equation

The hypoplastic model by Von Wolffersdorff [36] is selected since this version has advantages compared to previous hypoplastic formulations. For example, more realistic friction angles are obtained for deviatoric loadings other than conventional triaxial tests. Also, the upper limit is defined by comparing different proportional compression curves [36]. Moreover, this model could be used with and without intergranular strain.

The general form of the hypoplastic model is:

$$\dot{\mathbf{T}} = \mathbf{F}(\mathbf{T}, e, \mathbf{D}) \quad (3.1)$$

Where: $\dot{\mathbf{T}}$ being the stress rate

\mathbf{T} being the current Cauchy stress

e being the void ratio

\mathbf{D} being the stretching tensor

The modified constitutive equation given by Von Wolffersdorff is as follows:

$$\dot{\mathbf{T}} = f_b f_e \frac{1}{tr(\hat{\mathbf{T}}^2)} \left\{ F^2 \mathbf{D} + a^2 tr(\hat{\mathbf{T}} \mathbf{D}) \hat{\mathbf{T}} + f_d a F (\hat{\mathbf{T}} + \hat{\mathbf{T}}^*) \|\mathbf{D}\| \right\} \quad (3.2)$$

In which:
$$a = \frac{\sqrt{3}(3 - \sin \varphi_c)}{2\sqrt{2} \sin \varphi_c} \quad (3.3)$$

The factor F is a function of $\hat{\mathbf{T}}^*$

$$F = \sqrt{\frac{1}{8} \tan^2 \psi + \frac{2 - \tan^2 \psi}{2 + 2 \tan \psi \cos 3\theta}} - \frac{1}{2\sqrt{2} \tan \psi} \quad (3.4)$$

$$\tan \psi = \sqrt{3} \|\hat{\mathbf{T}}^*\|; \quad \cos 3\theta = -\sqrt{6} \frac{tr(\hat{\mathbf{T}}^{*3})}{[tr(\hat{\mathbf{T}}^{*2})]^{\frac{3}{2}}} \quad (3.5)$$

Herein, $\hat{\mathbf{T}}^* = \hat{\mathbf{T}} - \frac{1}{3} \mathbf{I}$ is the deviatoric part of the stress ratio tensor $\hat{\mathbf{T}}$. \mathbf{I} is the unit tensor and $\hat{\mathbf{T}} = \mathbf{T} / tr \mathbf{T}$, $p_s = -tr \mathbf{T} / 3$.

The hypoplastic model includes three characteristic functions of limiting void ratios as a function of mean skeleton pressure p_s , e_i describes the loosest possible state, e_c corresponds to the critical state and e_d denotes the maximum densification. According to Bauer [3] these limiting void ratios decrease with increasing p_s . They reach the limit values e_{d0} , e_{i0} , e_{c0} at vanishing mean skeleton pressure and approach zero for very high p_s , following the equation:

$$\frac{e_i}{e_{i0}} = \frac{e_c}{e_{c0}} = \frac{e_d}{e_{d0}} = \exp \left[- \left(\frac{3p_s}{h_s} \right)^n \right] \quad (3.6)$$

Typically, the influence of stress level on soil properties (an increase of stress level leads to a decrease of the dilatant angle but an increase of the stiffness) in the hypoplastic model is taken into account by introducing barotropy factor f_b . f_b is directly determined from the consistency requirement that the simulation of a perfect isotropic compression must provide the same exponential relationship between the current void ratio and the mean pressure as assumed in the Equation 3.6:

$$f_b = \left(\frac{e_i}{e_c} \right)^\beta \frac{h_s}{n} \frac{1+e_i}{e_i} \left(\frac{-tr\mathbf{T}}{h_s} \right)^{1-n} \left[3 + a^2 - a\sqrt{3} \left(\frac{e_{i0} - e_{d0}}{e_{c0} - e_{d0}} \right)^\alpha \right]^{-1} \quad (3.7)$$

Moreover, the influence of density is denoted by pycnotropy factor and f_d and f_e . For $e_c > e > e_d$ the factor f_d controls the maximum stress ratio $\hat{\mathbf{T}}$ at peak as well as the dilatancy connected with this ratio. The pycnotropy factor f_e controls the influence of the void ratio e on the incremental stiffness.

$$f_d = \left(\frac{e - e_d}{e_c - e_d} \right)^\alpha \quad (3.8)$$

$$f_e = \left(\frac{e_c}{e} \right)^\beta \quad (3.9)$$

3.3 Parameter determination

Parameter determination is the central key of the model. It is discussed in several publications (e.g. Gudehus [16], Bauer [3], Von Wolffersdorff [36]). Here, the methods of determination are taken from Herle & Gudehus [19]. For the case of an axially symmetric compression ($|T_1| > |T_2| = |T_3|$), the tensorial Equation 3.1 then reduces as follows:

$$\dot{T}_1 = f_s \frac{(T_1 + 2T_2)^2}{T_1^2 + 2T_2^2} \left[D_1 + a^2 \frac{T_1 D_1 + 2T_2 D_2}{(T_1 + 2T_2)^2} T_1 + f_d \frac{a}{3} \frac{5T_1 - 2T_2}{T_1 + 2T_2} \sqrt{D_1^2 + 2D_2^2} \right] \quad (3.10)$$

$$\dot{T}_2 = f_s \frac{(T_1 + 2T_2)^2}{T_1^2 + 2T_2^2} \left[D_2 + a^2 \frac{T_1 D_1 + 2T_2 D_2}{(T_1 + 2T_2)^2} T_2 + f_d \frac{a}{3} \frac{4T_2 - T_1}{T_1 + 2T_2} \sqrt{D_1^2 + 2D_2^2} \right] \quad (3.11)$$

The subscript 1 denotes the axial direction and 2 the radial one. Other factors are already mentioned above. The factor f_s is defined as the product of the pycnotropy factor f_e and the barotropy factor f_b , written as:

$$f_s = \left(\frac{e_i}{e} \right)^\beta \frac{h_s}{n} \frac{1+e_i}{e_i} \left(\frac{-tr\mathbf{T}}{h_s} \right)^{1-n} \left[3 + a^2 - a\sqrt{3} \left(\frac{e_{i0} - e_{d0}}{e_{c0} - e_{d0}} \right)^\alpha \right]^{-1} \quad (3.12)$$

In short, the hypoplastic model given by Von Wolffersdorff includes eight parameters that allow for a realistic description of granular material behavior over a wide range of stresses and densities. The proposed methods of determination are given in the Table 3. 1:

Table 3. 1: Parameter determinations in the HP model

Parameter	Physical meaning	Method of definition
φ_c	Critical friction angle	Angle of repose
$e_{d0}; e_{i0}, e_{c0}$	Minimum, maximum and critical void ratio at zero pressure	Index tests
h_s	Granular hardness	Oedometer compression test
n	Exponent relates to sensitivity of granular skeleton to changes of pressure	Oedometer compression test
α	Exponent describes the transition between peak and critical stress	Monotonic triaxial test
β	Exponent represents the change of stiffness at current density	Oedometer compression test

3.3.1 Critical state parameter φ_c

The critical state is reached during large monotonic shearing if both the tress rate and the volumetric deformation rate vanish [35]. It means:

$$\dot{T}_1 = \dot{T}_2 = D_1 + 2D_2 = 0 \quad (D_1 \neq 0) \quad (3.13)$$

Substituting into Equations 3.10 and 3.11, we have:

$$\sin \varphi = \max \left(\frac{T_1 - T_2}{T_1 + T_2} \right) \quad (3.14)$$

Then the relation between the parameter a and φ_c in the critical state:

$$a = \frac{\sqrt{3}(3 - \sin \varphi_c)}{2\sqrt{2} \sin \varphi_c} \quad (3.15)$$

A simple estimation of φ_c can be obtained from the angle of repose of a dry granular material. This simple method almost gives the same result with shear test or triaxial test methods. Herle and Gudehus [19] suggested to use a small excavation at the toe of the slope in order to reduce the influence of the heap preparation.

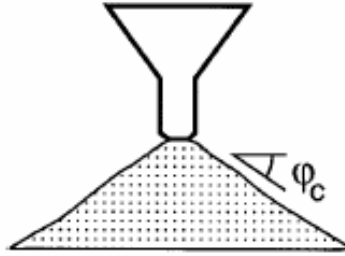


Fig. 3.1: Determination of φ_c from the angle of repose [19]

3.3.2 Stiffness parameter h_s and n

h_s represents the *granulate hardness* of material and is used as a reference pressure. The exponent n takes into account the pressure-sensitivity of a grain skeleton here, is the non-proportional increase of the incremental stiffness with increasing mean granulate pressure p_s ($p_s = -tr\mathbf{T}/3$). The relation between void ratios and p_s is described by the equation:

$$e_p = e_{p0} \exp \left[- \left(\frac{3p_s}{h_s} \right)^n \right] \quad (3.16)$$

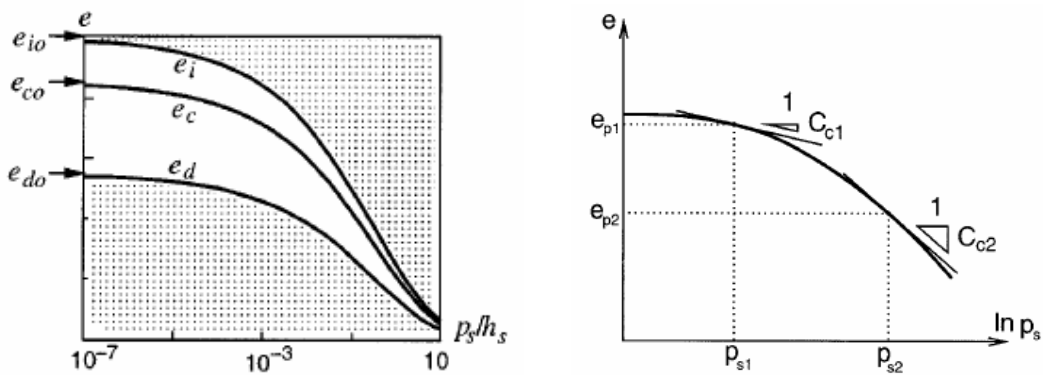


Fig. 3.2: Relation between e_i , e_c , e_d and p_s (left) and determination of n (right) [19]

For the determination of h_s and n , a compression test with an initially very loose specimen must be carried out. In practice, an eodometer test is chosen since it is simpler than isotropic compression test. Formulations for determining h_s and n are given below:

$$n = \frac{\ln(e_{p1}C_{c2} / e_{p2}C_{c1})}{\ln(p_{s2} / p_{s1})} \quad (3.17)$$

$$h_s = 3p_s \left(\frac{ne_p}{C_c} \right)^{1/n} \quad (3.18)$$

Where: e_p being the void ratio during a proportional compression
 e_{p0} being the void ratio at zero pressure
 C_c being the compression index
 n being the constant value in a specific range of stress

Obviously, the determinations of h_s and n are valid in a certain stress range. Parameter n reflects the curvature of a compression curve, and h_s the its slope. If grain crushing takes place, values of h_s and n will change with changes of granulometric properties.

3.3.3 Minimum void ratio at zero pressure e_{d0}

The best densification of granular material can be generally reached by mean of cyclic shearing with small amplitude under constant pressure. The relation between the minimum void ratio at zero pressure e_{d0} and minimum void ratio e_d as followed:

$$e_{d0} = e_d \left[\left(\frac{3p_s}{h_s} \right)^n \right] \quad (3.19)$$

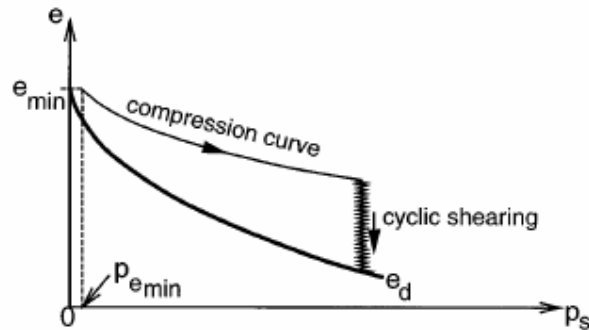


Fig. 3.3: Pressure dependent minimum void ratio e_d [19]

In practice, a minimum void ratio e_{min} is determined from index tests described

in various standards is chosen. These densification tests are performed at certain pressure ($p_s = p_{emin}$) and they are not effective as cyclic shearing, so the value of e_{min} lies above the one of e_d in Fig. 3.3. The value of e_d depends mainly on non-uniformity and grain shape. e_d decreases with the increase of the coefficient of uniformity C_u due to filling the voids between big grains by smaller ones. Moreover, the decrease of e_d also results from diminishing angularity of grains.

In comparison, e_{d0} and e_{min} are proved close each other, so in reality the minimum void ratio at zero pressure is taken from index test, $e_{d0} \approx e_{min}$.

3.3.4 Maximum void ratio at zero pressure e_{i0}

The parameter e_{i0} can be explained as the maximum void ratio of a simple grain skeleton. In theory, this situation is reached during an isotropic consolidation of grain suspension in a gravity-free space. It is considered as a percolation threshold related with the birth of a grain skeleton (Fig. 3.4). However, it is proved that impossible to determine experimentally but we can be approximated by relation with maximum void ratio e_{max} , taken from index test. Normally, the relation $\frac{e_{i0}}{e_{max}} \approx 1.15$ to 1.2 can be assumed.

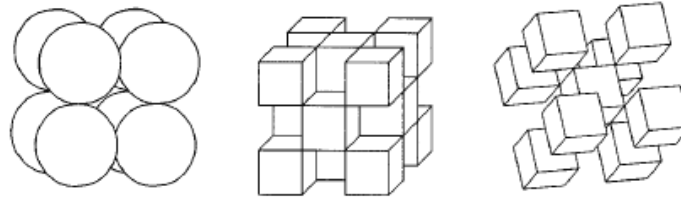


Fig. 3.4: Idealized packings of spheres and cubes at minimum density ([19])

3.3.5 Critical void ratio e_{c0} at zero pressure

The decrease of the critical void ratio e_c with the mean pressure is described by next equation:

$$e_{c0} = e_c \exp \left[\left(\frac{3p_s}{h_s} \right)^n \right] \quad (3.20)$$

e_c can be obtained together with φ_c from a shear test on a soil sample. But it is difficult to keep a homogeneous deformation up to the critical state. In practice, e_{c0} can be assumed to be equal to e_{max} .

3.3.6 Exponent α

Exponent α describes the transition between the peak and critical state. This is determined by using a triaxial compression test. At the peak state, the axial stress rate vanishes ($\dot{T}_1 = 0$). Then substituting into Equation 3.10, we obtain:

$$\alpha = \frac{\ln \left[6 \frac{(2 + K_p)^2 + a^2 K_p (K_p - 1 - \tan \nu_p)}{a(2 + K_p)(5K_p - 2)\sqrt{4 + 2(1 + \tan \nu_p)^2}} \right]}{\ln \left(\frac{e - e_d}{e_c - e_d} \right)} \quad (3.21)$$

with the peak ratio:
$$K_p = \frac{T_1}{T_2} = \frac{1 + \sin \varphi_p}{1 - \sin \varphi_p} \quad (3.22)$$

$$\tan \nu_p = -\frac{D_1 + 2D_2}{D_1} \quad (3.23)$$

$$\sin \varphi_p = \left(\frac{T_1 - T_2}{T_1 + T_2} \right)_p \quad (3.24)$$

in which ν is the dilatancy angle.

φ_p is the friction angle at peak

3.3.7 Exponent β

Exponent β represents the change of stiffness at current density. β plays an important role if e substantially lower than e_i , i.e. for a dense soil. According to Equation 3.12, the incremental stiffness $E = \dot{T}_1 / D_1$ increases with increasing density and pressure. For the case of an isotropic compression, the stress rate is given by:

$$\dot{T}_1 = f_s(3 + a^2 - f_a a \sqrt{3})D_1 \quad (3.25)$$

Substituting into Equation 3.10, we have:

$$\beta = \frac{\ln \left[E \frac{3+a^2 - f_{d0} a \sqrt{3}}{3+a^2 - f_d a \sqrt{3}} \frac{e_i}{1+e_i} \frac{n}{h_s} \left(\frac{3p_s}{h_s} \right)^{n-1} \right]}{\ln(e_i / e)} \quad (3.26)$$

in which
$$f_{d0} = \frac{e_{i0} - e_{d0}}{e_{c0} - e_{d0}} \quad (3.27)$$

For simplification, β can be determined by considering the ratio of the stiffness modulus at two different void ratios e_1 and e_2 , but the same pressure, in order to eliminate the influence of p_s :

$$\beta = \frac{\ln(\beta_o E_2 / E_1)}{\ln(e_1 / e_2)} \quad (3.28)$$

with
$$\beta_o = \frac{3+a^2 - a\sqrt{3}f_{d1}}{3+a^2 - a\sqrt{3}f_{d2}} \quad (3.29)$$

3.4 Intergranular strain (IGS)

The original hypoplastic model (e.g. Gudehus [16], Bauer [3], von Wolffersdorff [36]) has a shortcoming in the region of small stress cycles as an excessive accumulation of deformation occurs and therefore the displacements are overpredicted. This model predicts saw-tooth-like diagram instead of loops, such phenomenon is called ratcheting [28]. According to measurements [2, 30], the soil stiffness at a given state defined by stress and void ratio depends strongly on the deformation history and the direction of strain rate. The maximum value of stiffness is reached when the direction of strain path is reversed.

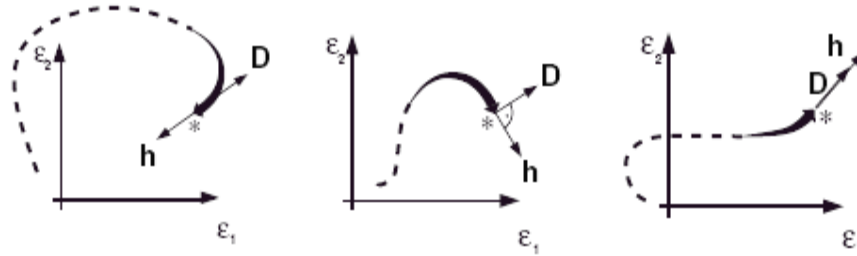


Fig. 3.5: Different intergranular strains \mathbf{h} related with different deformation histories [28]

However, if the strain is continued in a fixed direction, the stiffness decreases gradually, and get almost the same stiffness at a certain strain path $\epsilon = \epsilon_{SOM}$. Subsequently, in order to improve the performance of the hypoplastic model in the

range of small load cycles, Niemunis and Herle [28] have introduced a new state variable called *intergranular strain*, \mathbf{h} . This tensorial state variable is supposed to take into account the deformation of intergranular interface layer and rearrangement of the particles during application of small strains.

When the intergranular strain is included in the hypoplastic model, the current stiffness is controlled by the difference in the direction of the actual strain rate and the intergranular strain rate as well as the magnitude of the intergranular strain rate. The magnitude of the intergranular strain rate, $\rho = \|\mathbf{h}\|/R$, can not become larger than the intergranular strain radius, R , a material parameter which varies between 10^{-7} for very large grains and 10^{-3} for very small grains [24]. The evolution of stiffness degradations are described by Niemunis [27] in Fig. 3.6.

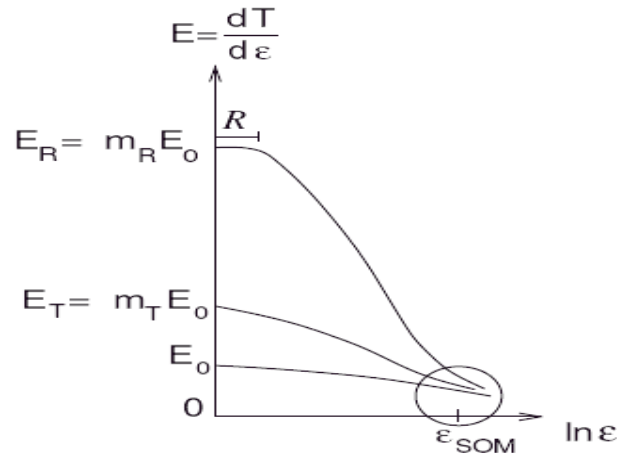


Fig. 3.6: Characteristic stiffness values for the hypoplastic model [27]

As can be seen, the 180° reversal strain path direction leads to an elastic behaviour with an increased granular stiffness by a factor m_R ($m_R = E_R/E_0$). The 90° change of strain path direction also leads to an increased granular stiffness by a factor m_T ($m_T = E_T/E_0$). For other changes of the strain path direction, a steady interpolation is carried out.

The parameter β_R influences the evolution of intergranular strain and can be correlated with ε_{SOM} . This value is defined as the length of a strain path, need for the additional stiffness to decline in 90% (Fig. 3.6). Then the stiffness evolution is followed:

$$\begin{aligned}
 E &= m_R \cdot E_0 & \text{for } \varepsilon < R & & (3.30) \\
 E &= E_0 + E_0(m_R - 1)(1 - \rho^\beta) & \text{for } \varepsilon > R & &
 \end{aligned}$$

The parameter χ ($\chi > 1$) describes the degradation of the stiffness from E_R to E_0 during the monotonic deformation. Fig. 3.7 depicts the correlation of β_R and the strain for different value of χ .

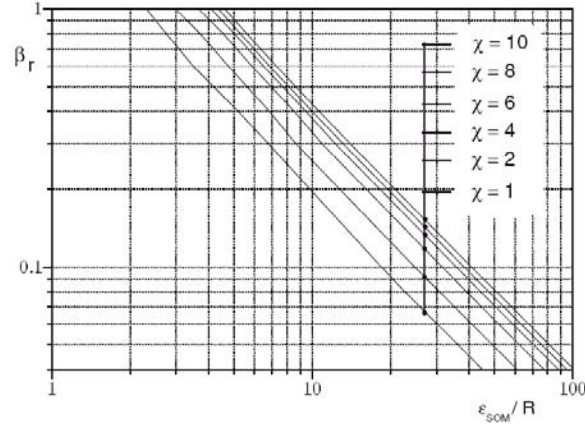


Fig. 3.7: Correlation of β_R vs ϵ_{SOM}/R for different value of χ [27]

For the determinations of the intergranular strain parameters, the methods given in the Table 3.2 could be used. In fact, the factor m_T and m_R are usually taken the value of 2.0 and 5.0 respectively, as the “rule of thumb”. The radius of elastic range R varies between 10^{-7} and 10^{-3} , normally is taken as 10^{-4} . The remaining parameters need to be defined by the cyclic tests at small strain.

Table 3.2: Parameter determinations of intergranular strain [31]

Parameter	Physical meaning	Method of definition
m_T	Stiffness increase for a 90° change of strain path direction	Cyclic shear test
m_R	Stiffness increase for a 180° reversal	Biaxial test
R	Radius of elastic range	Cyclic triaxial test
β_R	Material constant controls the rate $\dot{\mathbf{h}}$	Cyclic triaxial test
χ	Material constant represents stiffness degradation	Cyclic triaxial test

3.5 Conclusion

This chapter describes the hypoplastic model given by von Wolffersdorff [36] in more detail. The constitutive law is given in the rate form, the stress rate is a function of the stress tensor, the current void ratio and the strain rate as $\dot{\mathbf{T}} = \mathbf{F}(\mathbf{T}, e, \mathbf{D})$. The outstanding

of this model is using an unique equation, this model recognizes anelastic deformation without using any additional notions such as yield surface or plastic potential [21]. Typically, the influence of the stress level on soil properties (an increase of the stress level leads to a decrease of the dilatant angle but an increase of the stiffness) in the hypoplastic model is taken into account by introducing barotropy factor f_b . Moreover, the influence of density is also denoted by pycnotropy factors and f_d and f_e .

This model requires eight parameters. The critical angle φ_c is defined in the case of both the stress rate and the volumetric deformation rate vanish. For simplification, φ_c can be taken from the angle of repose of a dry granular material.

The granular hardness h_s and the exponent n are determined from the oedometer test and valid in a certain stress range. Parameter n reflects the curvature of a compression curve, and h_s the its slope.

Three characteristic void ratios, e_d , e_c , and e_i denote the maximum densification, the critical state and the loosest state, respectively. These limiting void ratios decrease with increasing p_s , according to Bauer's formulas [3]. They reach the limit values e_{d0} , e_{c0} , e_{i0} at vanishing mean skeleton pressure and approach zero for very high p_s . Due to the difficulties in testing, these limit void ratios are assumed to be e_{min} , e_{max} and approximately $1.2e_{max}$.

Exponent α describes the transition between the peak and critical state. This is determined by using a triaxial compression test at the peak state ($\dot{T}_1 = 0$). On the other hand, exponent β represents the change of stiffness at current density. It is defined by comparing the ratio of the stiffness modulus at two different void ratios, but the same pressure in an oedometer test.

A shortcoming of this model is an excessive accumulation of deformations in the region of small stress cycles is overcome by the introduction of intergranular strain \mathbf{h} . The intergranular remembers the deformation history and the current stiffness is controlled by the direction of strain rates.

The intergranular strain includes five parameters. The factor m_R and m_T take into account the increase of the stiffness for the 180° and 90° change of strain path direction. The radius of elastic range R varies between 10^{-7} and 10^{-3} , normally is taken as 10^{-4} . The parameter β_R influences the evolution of intergranular strain and the parameter χ describes the degradation of the stiffness. They are determined by using a cyclic triaxial test.

Chapter 4

Parametric Sensitivity Analysis

4.1 Introduction

In this chapter, the influences of various hypoplastic parameters on the model behaviour are investigated. First, a series of drained triaxial tests using the hypoplastic parameters are simulated, its results are then compared to measured results, in order to check the reliability of the hypoplastic model. Next, the influences of individual parameter are evaluated by varying this parameter and keeping the others constant. The effects of intergranular strain on the soil behaviour under cyclic loading are also examined.

4.2 Verification and validation of the HP model

In order to check the reliability of the HP model, the drained triaxial tests are simulated by using the *Soil test* facility in Plaxis 2D, the results are then compared with those which are measured and simulated on Baskarp and Karlsruhe sand.

4.2.1 Comparison with Baskarp sand

A series of drained triaxial tests on Baskarp sand are performed in [13]. After completion of isotropic consolidation, the void ratios are measured. For initially dense samples, Baskarp sand shows the high dilatancy behaviour. The results of drained triaxial tests with different cell pressures are plotted in Fig. 4.1. On the other hand, the numerical simulations of drained triaxial using element tests in the FEAT program with model parameters in Table 4.2 are also plotted in Fig. 4.2 (see Elmi Anaraki [13] for more detail).

Similarly, drained triaxial tests are also simulated in Plaxis 2D using the *Soil test* facility. One thing need to be remembered is that the state variable (e_0) of the HP model in Plaxis 2D is the void ratio at zero pressure. Using Bauer's formula as referred in Chapter 3, the initial void ratios (e_0) are 0.598, 0.611 and 0.615 respectively in order to get comparable soil states at cell pressure as performed in [13].

As can be seen, both softwares, the FEAT and Plaxis 2D give completely similar soil responses in drained triaxial tests. Moreover, the peak and residual shear strengths from both simulated tests are in accordance with laboratory experiments. Also the initial simulated stiffness is as expected, except for the confining pressure of 50 kPa. This is explained by logging error in the measurement as mentioned by Elmi Anaraki [13]. For the volumetric strain and dilatancy angle, the simulated results are qualitatively in accordance with experimental results. Both numerical results show a smaller dilatancy angle compared with measured results (see Fig. 4.1 to Fig. 4.3).

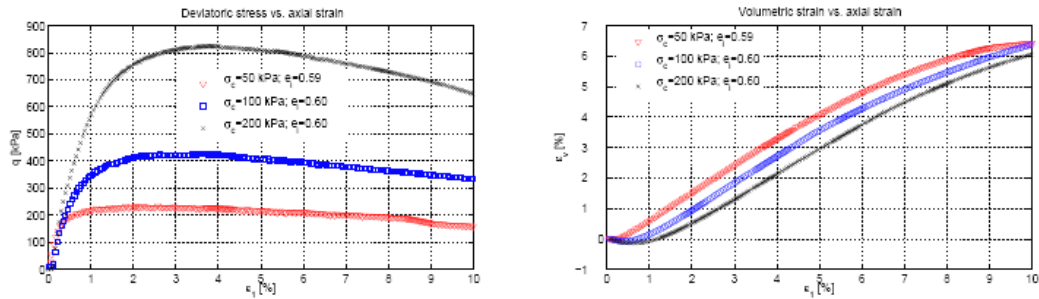


Fig. 4.1: Measured results of triaxial compression tests with Baskarp sand [13], the initial void ratios are measured at cell pressure

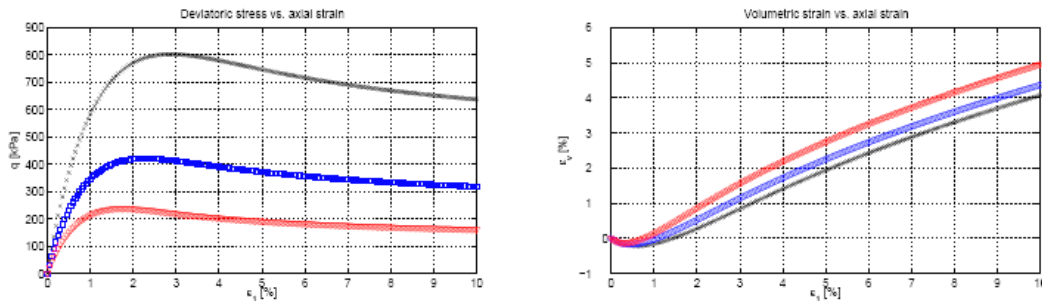


Fig. 4.2: Simulated results of triaxial compression tests with Baskarp sand [13], using FEAT program

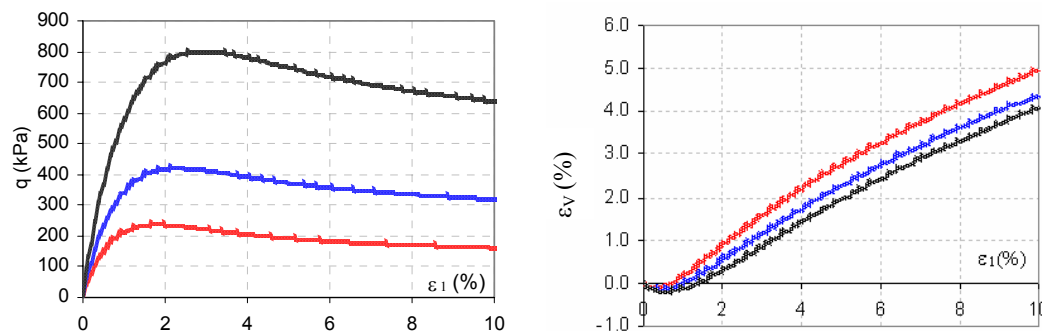


Fig. 4.3: Simulated results of triaxial compression tests with Baskarp sand, using *Soil test* in Plaxis 2D

4.2.2 Comparison with Karlsruhe sand

Likely, a series of drained triaxial tests on Karlsruhe sand are also performed in [23]. All tests have the same initial void ratio (e_0) of 0.53 after isotropic consolidation. Outputs of standard triaxial compression tests [23] with a dense Karlsruhe sand at different cell pressures are plotted in Fig. 4.4. The results show the trend: the stress deviator increases with the cell pressure whereas the dilatancy decreases. The initial stiffness, the secant stiffness and the differences between the peak strength and residual strength also increase with cell pressure. Additionally, the numerical simulations of triaxial tests with hypoplastic model parameters derived by Herle & Gudehus (Table 4.1) are also plotted in Fig. 4.5.

Table 4.1: Hypoplastic parameters for Karlsruhe sand [19]

Parameters	φ_c (°)	h_s (MPa)	n	e_{d0}	e_{c0}	e_{i0}	α	β
Values	30	5800	0.28	0.53	0.84	1.0	0.13	1.0

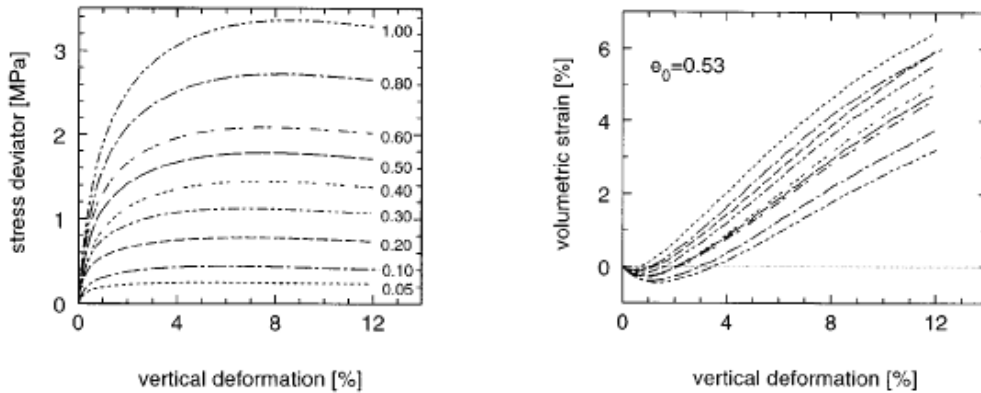


Fig. 4.4: Measured results of triaxial compression tests with Karlsruhe sand [23].

Numbers donate the cell pressure in MPa

Once again, drained triaxial tests are also performed in Plaxis 2D using the *Soil test* facility. The void ratio at zero pressure also calculated using Bauer's formula to make sure that the initial void ratio reaches the value of 0.53 at the cell pressure as in measurements. The results are plotted in Fig. 4.6.

As can be seen that the simulated results from Plaxis 2D are completely the same as the simulated results by Herle & Gudehus [19]. These simulated results fit the measured ones also very well. There is only a small difference results in terms of the peak strength and the residual strength at very high cell pressure.

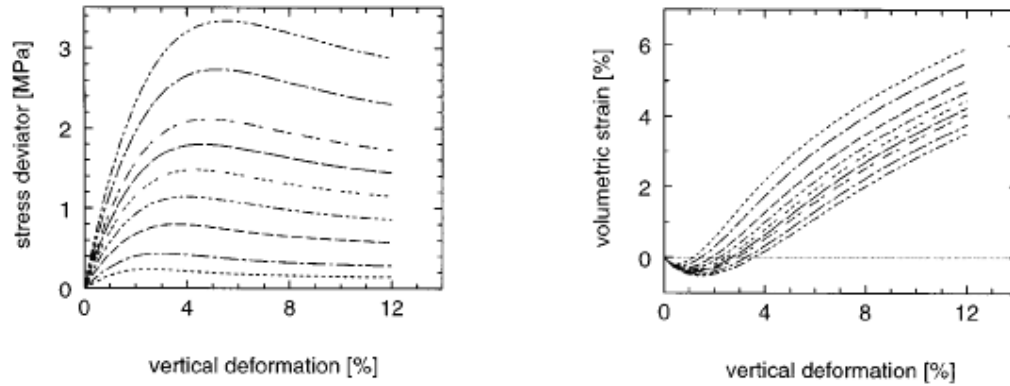


Fig. 4.5: Simulated result of triaxial compression tests with Karlsruhe sand [19] using the HP model

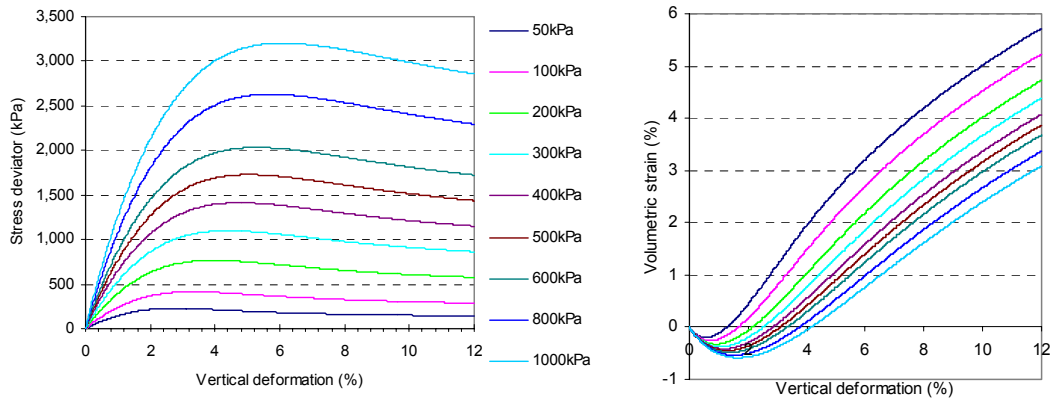


Fig. 4.6: Simulated results of triaxial compression tests from *Soil test* in Plaxis 2D with Karlsruhe sand using the HP model

4.3 Sensitivity of the hypoplastic parameters

4.3.1 Parameter variation

The hypoplastic parameters for Baskarp sand in which they were derived from laboratory tests by Elmi Anaraki [13] are chosen as a reference set (see Table 4.2). Then each parameter is varied by increasing 30% of the reference value while keeping the others constant. Next, a drained triaxial test with different cell pressure and an oedometer test are simulated in Plaxis 2D in order to see the influence of parameter changing.

Table 4.2. Hypoplastic parameters for Baskarp sand [13]

Parameters	φ_c (o)	h_s (MPa)	n	e_{d0}	e_{c0}	e_{i0}	α	β	e_0
Ref	30	4000	0.42	0.548	0.929	1.08	0.12	0.96	0.709
Changes	9	1200	0.126	0.164	0.279	0.324	0.036	0.288	0.213
+30%	39	5200	0.546	0.712	1.208	1.404	0.156	1.248	0.922

4.3.2 Influence of parametric variation on drained triaxial tests

Fig. 4.7 shows the numerically simulated response of drained triaxial tests for varying the initial void ratio. As can be seen, the initial void ratio has a big influence on the soil response. As expected, an increase of the initial void ratio leads to a significant reduction of the strength, stiffness and dilatancy. But, the dependence on cell pressure decreases with the increase of the initial void ratio.

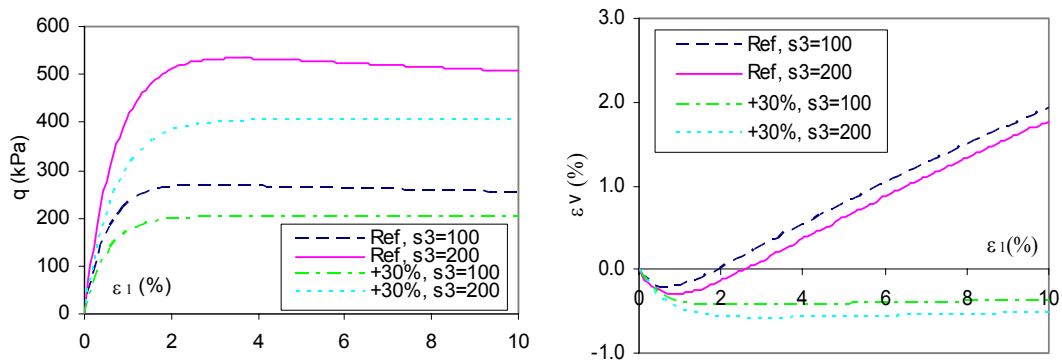


Fig. 4.7: Influence of initial void ratio (e_0) on drained triaxial test

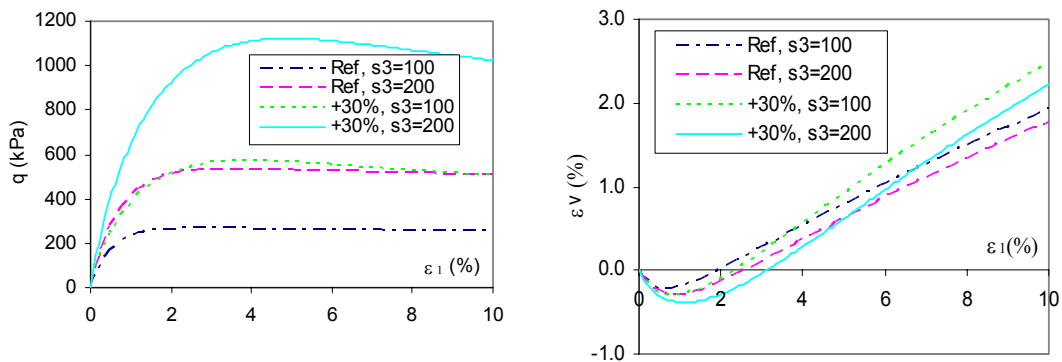


Fig. 4.8: Influence of φ_c on drained triaxial test

On the other hand, the critical friction angle has the positive effect on the peak strength, the residual strength and the initial stiffness. An increase of the critical friction angle results in the rise of those values. The dilatancy angle also enhances with smaller influence however. Different from the initial void ratio, the dependence on cell pressure increases with the increase of the critical friction angle.

The influence of the granulate hardness h_s and exponent n can be seen on the Fig. 4.9 and Fig. 4.10. Both parameters have more or less the same influences on the soil behaviour as they are the stiffness parameters and determined as a pair. Only initial stiffness is slightly increased by rising the granulate hardness, other influences can be negligible. On the other hand, the higher of exponent n causes the noteworthy raise of initial stiffness. A reduction of this exponent delays the happening of dilatant behaviour, but does not influence the dilatancy angle. The peak strength and residual strength mostly are not influenced by both h_s and n parameters.

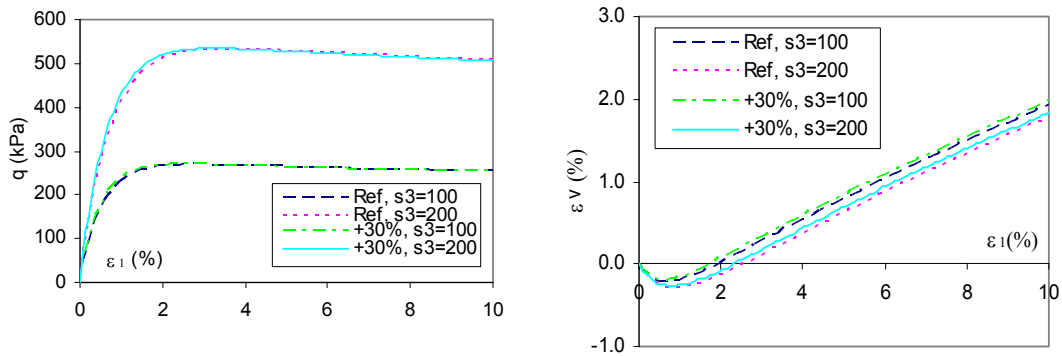


Fig. 4.9: Influence of h_s on drained triaxial test

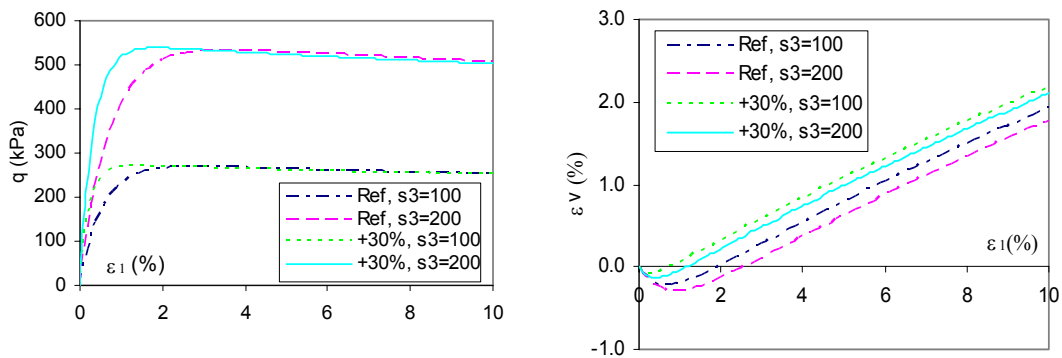


Fig. 4.10: Influence of n on drained triaxial test

As can be seen in Fig. 4.11 and Fig. 4.12, the limit void ratios e_{d0} and e_{c0} have the same influence on the dilatant behaviour. Its higher values lead to the strongly dilatancy behaviour of the soil. However, e_{d0} shows stronger influences on initial stiffness and strength. Especially, the higher value of e_{d0} causes a significant increase of the peak strength and a small increase of the residual strength. The bigger cell pressure also result in the larger differences of the stiffness and strength.

The influence of the limit void ratio e_{i0} and the exponent β can be considered as the same. Only small increment of the initial stiffness can be found when enhancing these parameters. Its effects on the strength and dilatancy behaviour are negligible. Finally, the exponent α has the similar impacts on the soil behaviour as the limit void ratio e_{c0} . Both the strength and the dilatancy angle increase when increasing the exponent α . However, its influence on initial stiffness is little.

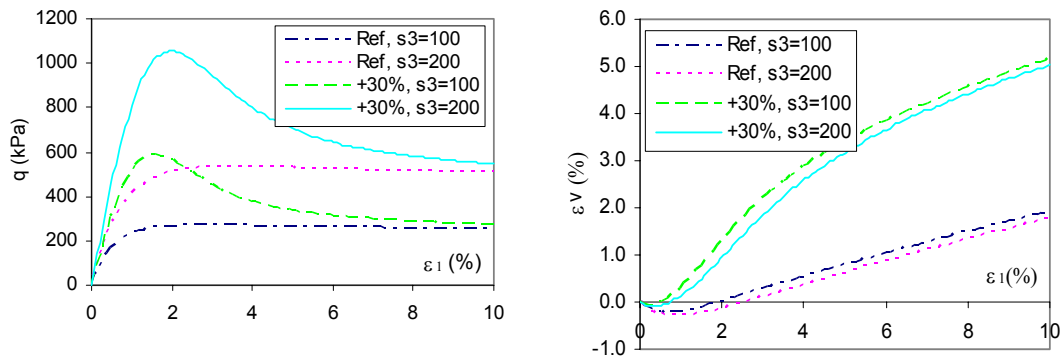


Fig. 4.11: Influence of e_{d0} on drained triaxial test

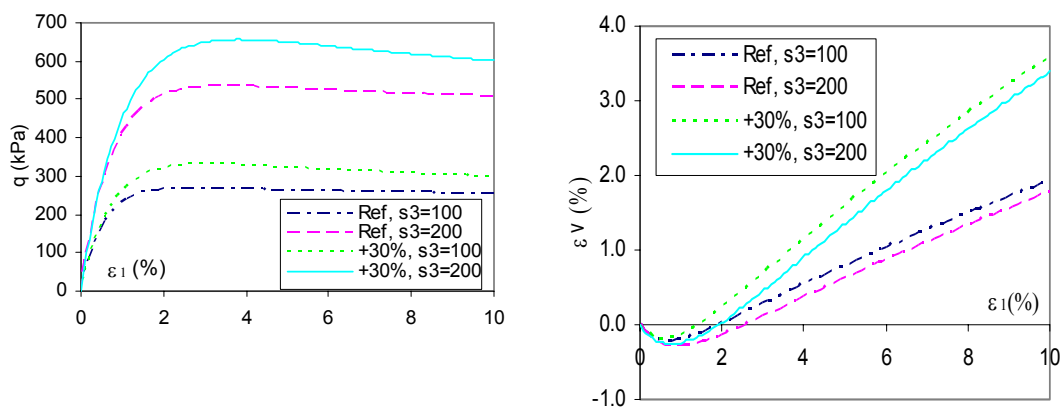


Fig. 4.12: Influence of e_{c0} on drained triaxial test

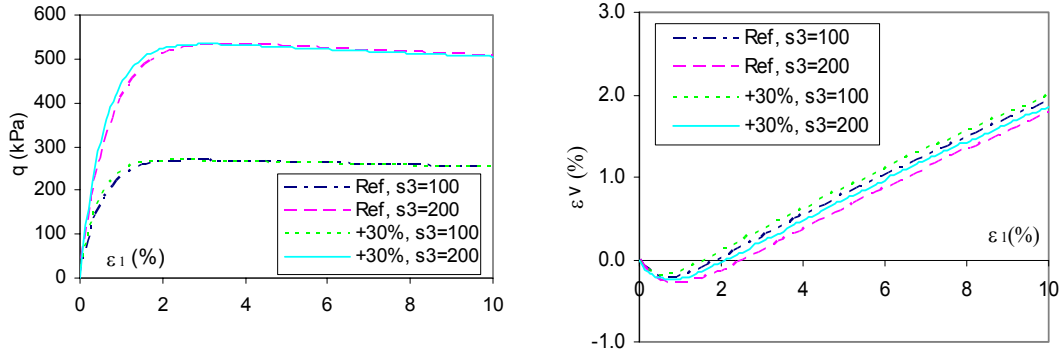


Fig. 4.13: Influence of e_{i0} on drained triaxial test

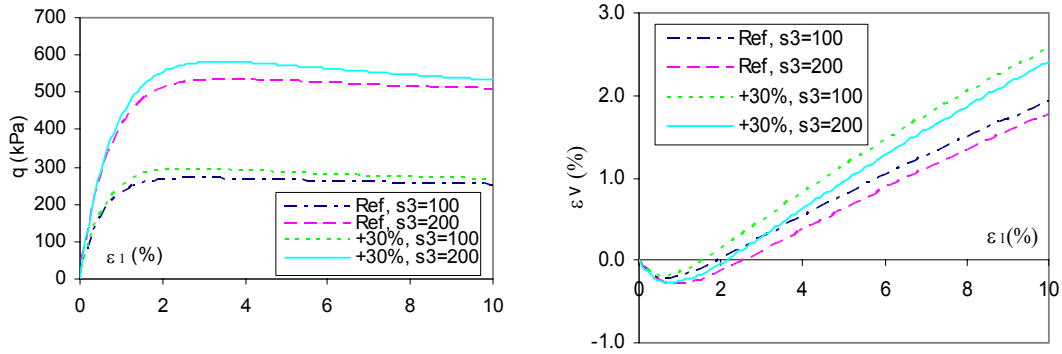


Fig. 4.14: Influence of a on drained triaxial test

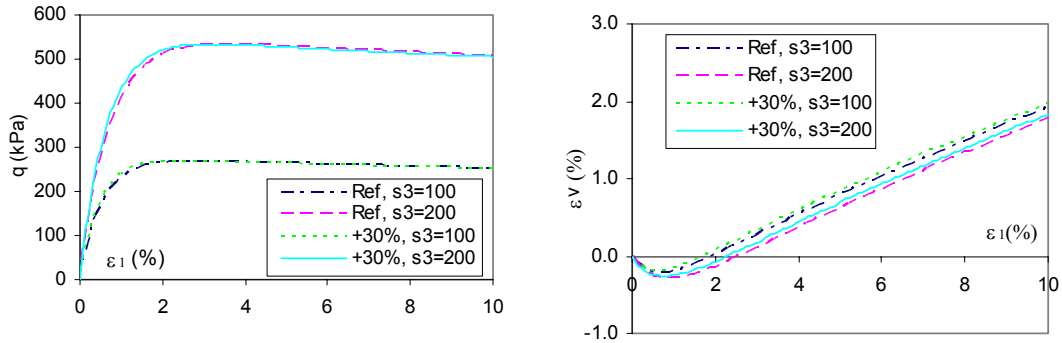


Fig. 4.15: Influence of β on drained triaxial test

To summarise, the initial void ratio controls the soil behaviour as it is a state variable in the hypoplastic model. A reduction of the void ratio leads to a significant increase of the initial stiffness and strength. A stronger dilatancy also occurs with a reduction of the initial void ratio. As can be seen, the dilatancy behaviour strongly

influenced by e_{d0} and e_{c0} , a smaller impact can be found from φ_c and α , while the influence from other parameters can be negligible. This means that the increase of e_{d0} and e_{c0} lead to the significance of the dilatancy angle but smaller increase for φ_c and α . In terms of the strength, the biggest influence is caused by φ_c , followed by e_{d0} , e_{c0} and α . This soil property is not controlled by h_s , n , e_{i0} and β . Finally, the initial stiffness are mainly controlled by φ_c , n , and e_{d0} , other parameters only include little influence on the initial stiffness.

4.3.3 Influence of parametric variation on oedometer tests

Similarly, the influence of individual parameter on an oedometer test is also investigated. The parameter set for Baskarp sand is also given in Table 4.2. In the simulations, the axial stress is increased until 10 MPa to make sure that a large stress range is covered. As can be seen in Fig. 4.16, the initial void ratio has a significant influence on the stiffness. The higher initial void ratio leads to the decrease of the stiffness. This decrease is larger with stress level. The critical friction angle also has a slight influence on the stiffness at high stress level.

On the other hand, the stiffness increases when enhancing other remaining parameters. But their importances are different. The exponent n has a huge influence, followed by e_{d0} , e_{i0} , h_s and β . Finally, the exponent α , e_{c0} and φ_c have only a slight effect on the stiffness at high stress level.

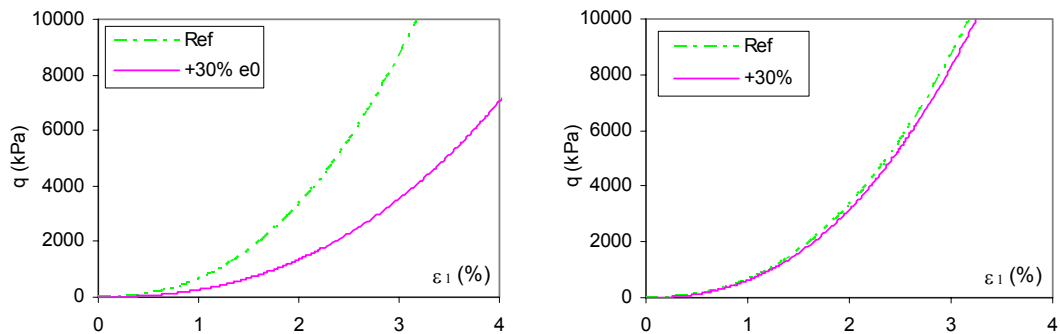


Fig. 4.16: Influence of initial void ratio (left) and φ_c (right) on oedometer test

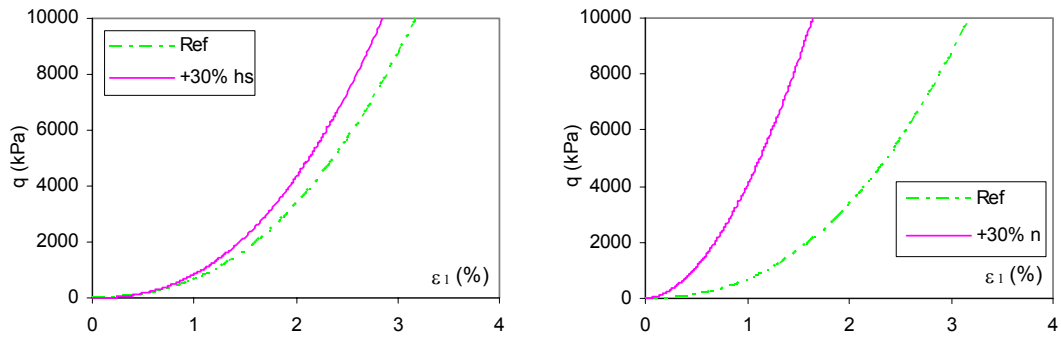


Fig. 4.17: Influence of h_s (left) and n (right) on oedometer test

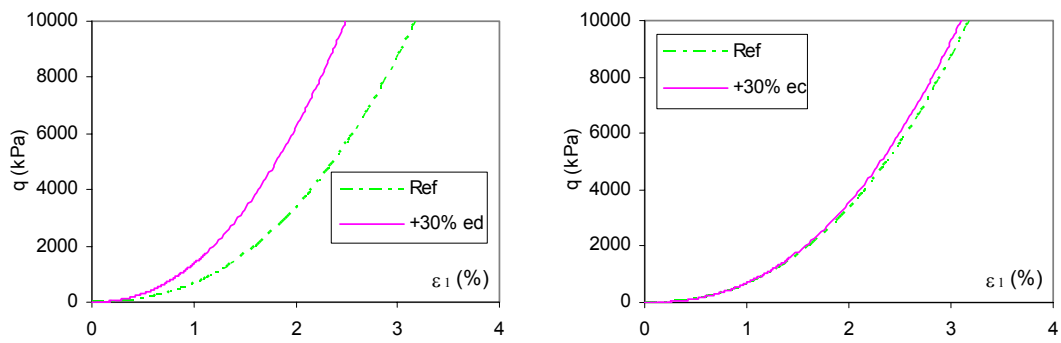


Fig. 4.18: Influence of e_{d0} (left) and e_{c0} (right) on oedometer test

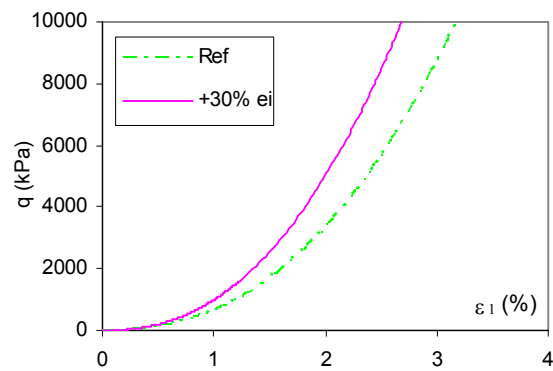


Fig. 4.19: Influence of e_{i0} on oedometer test

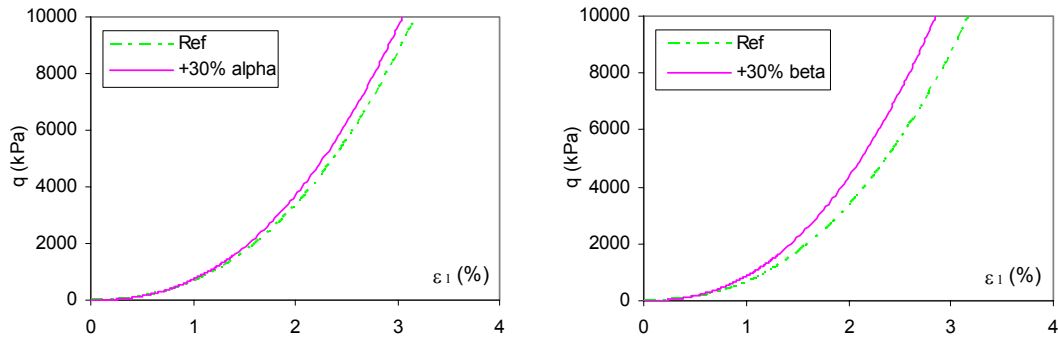


Fig. 4.20: Influence of α (left) and β (right) on oedometer test

4.4 Effects of intergranular strain

4.4.1 Intergranular strain parameters for Karlsruhe sand

As mentioned the hypoplastic model developed by many authors (e.g. Kolymbas [22], Gudehus [16], Bauer [3]) does not account for an excessive accumulation of deformation for small stress cycles. Then the concept of intergranular strain (IGS) is introduced by Niemunis & Herle [28] to take this behaviour into consideration. Here, a stress cycle during an oedometer compression and triaxial tests are simulated using Plaxis 2D in order to verify the effect of intergranular strain. Its results are compared for the case of using the intergranular strain and not used. Karlsruhe sand is selected to examine this behaviour. The intergranular strain parameters of Karlsruhe sand defined by Niemunis & Herle [28] are given in the Table 4.3.

Table 4.3 Parameters for intergranular strain for Karlsruhe sand [28]

Parameters	m_T	m_R	R_{max}	β_r	χ
Values	2	5	0.0001	0.5	6.0

4.4.2 Simulation of oedometer test

An oedometer compression test is simply modelled in Plaxis 2D by mean of an axisymmetric mesh. The dimensions of the model are a square of 1 m. These dimensions does not influence the results, provided that the soil weight is not taken into account [5]. The right and left sides of model are applied horizontal fixities so that similar the real situations in an oedometer test. The bottom is fixed both horizontally

and vertically. Also a distributed load is applied on the top.

In order to simulate a stress cycle during compression test, the distributed load is increased step by step, subsequently it is un-loaded and re-loaded at certain stress range. As a result, in the calculation phases, the distributed load is increased from 0 kPa to 100, 300, 1000 and 2000 kPa respectively. Then, this load is cycled between 1000 kPa and 2000 kPa.

These analyses are carried out on Karlsruhe sand. First, the HP model with parameters defined by Herle and Gudehus [19] given in Table 4.1 is used. This model does not include the intergranular strain. Next, the IGS given in Table 4.3 is involved in the HP model in order to see the effect of the intergranular strain. Both results are plotted in Fig. 4.22. It is evident that the HP model with IGS accumulates much less strain than for the case not using IGS.

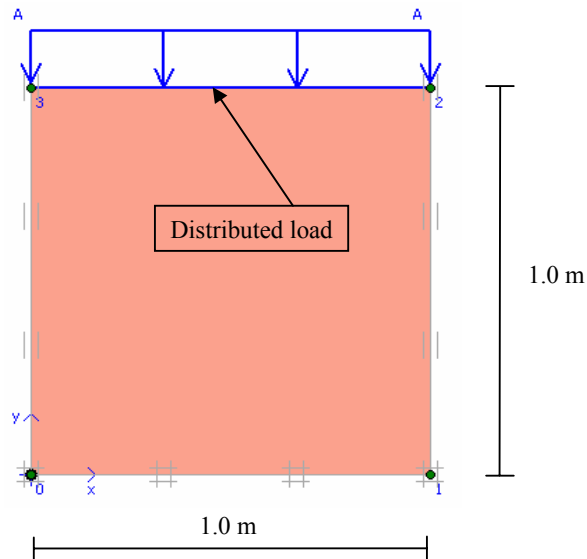


Fig. 4.21: Simplified modelling of an oedometer test

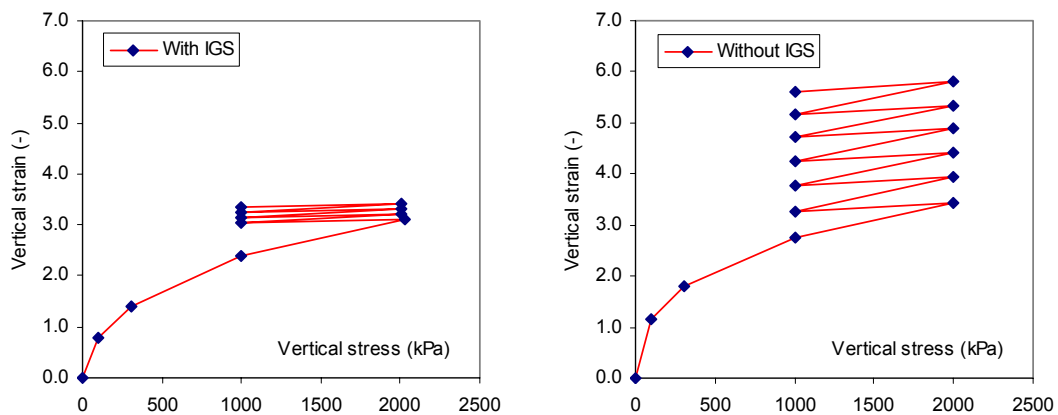


Fig. 4.22: Oedometer compression stress cycles

4.4.3 Simulation of triaxial test

Similarly, a drained triaxial test is also simply modelled in Plaxis 2D by mean of an axisymmetric mesh. The dimensions of the model are also a square of 1 m. Once again, these dimensions does not influence the results, provided that the soil weight is not taken into account [5]. However, only the left side of model are applied horizontal fixities while the bottom is fixed both horizontally and vertically. The distributed load is applied on the top and the right side.

The simulation of the triaxial test under stress cycle is performed as the following. First, the distributed load of 100 kPa is applied on the top and the right side in order to create the confining pressure. Then all displacements from this phase are reset to zero. Subsequently, the vertical load is increased gradually until 200, 300 and 400 kPa respectively, while the horizontal load is kept constant at 100 kPa. After that, the vertical load is cycled between 300 kPa and 400 kPa.

Karlsruhe sand is used in this analysis. As can be seen from Fig. 4.24, the effect of the intergranular strain is evident under stress cycle. The use of IGS also leads to the very small accumulation of strain.

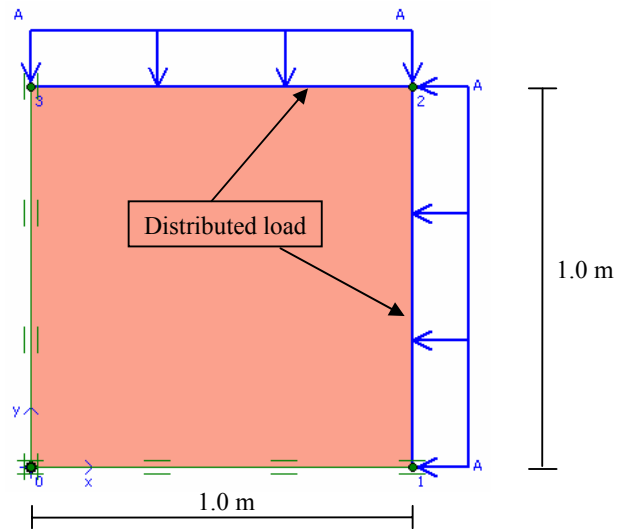


Fig. 4.23: Simplified modelling of a drained triaxial test

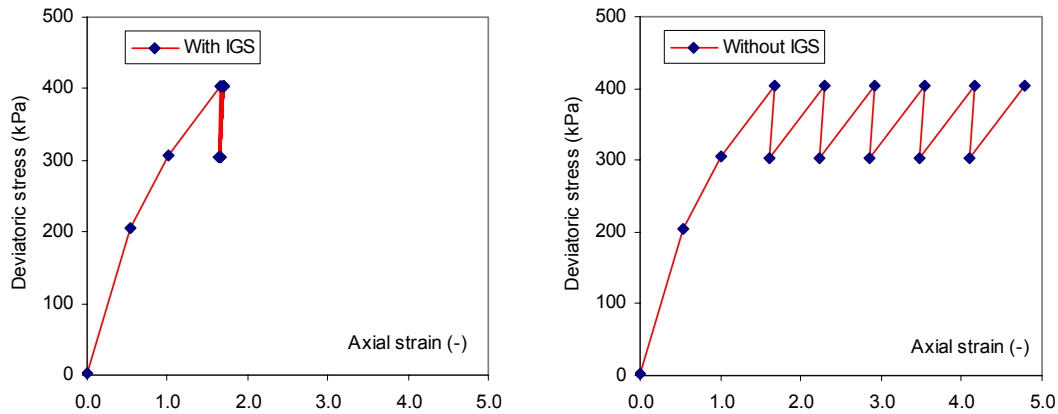


Fig. 4.24: Drained triaxial stress cycles

4.4.4 Sensitivity of IGS parameters

This section evaluates the sensitivity of the simulated response of triaxial and oedometer tests to parametric variation of intergranular strain parameters. As mentioned, the intergranular strain includes 5 parameters. However, the increase of granular stiffness for 90° and 180° change of strain path direction by the factor m_T and m_R are usually taken the value of 2.0 and 5.0 respectively, as the “rule of thumb”. The radius of elastic range R varies between 10^{-7} and 10^{-3} , but normally is taken as 10^{-4} . As a result, this section only considers the variation of parameters β_r and χ .

As can be seen from Fig. 4.25, the change of β_r only influences the initial stiffness on the triaxial test. Obviously, this effect only occurs at very small strain. The increase of β_r leads to the decrease of the initial stiffness and delays the occurrence of the dilatancy behaviour but does not influence on the magnitude of dilatancy angle. In the oedometer test, the increase of β_r also results in the decrease of the modulus at high stress level (Fig. 4.26).

On the other hand, the parameter χ has different effects on the soil response. The increase of this parameter leads to an increase of the initial stiffness, but speeds up the occurrence of dilatancy behaviour. Once again the increase of χ also results in an increase of the modulus at high stress level in the oedometer test.

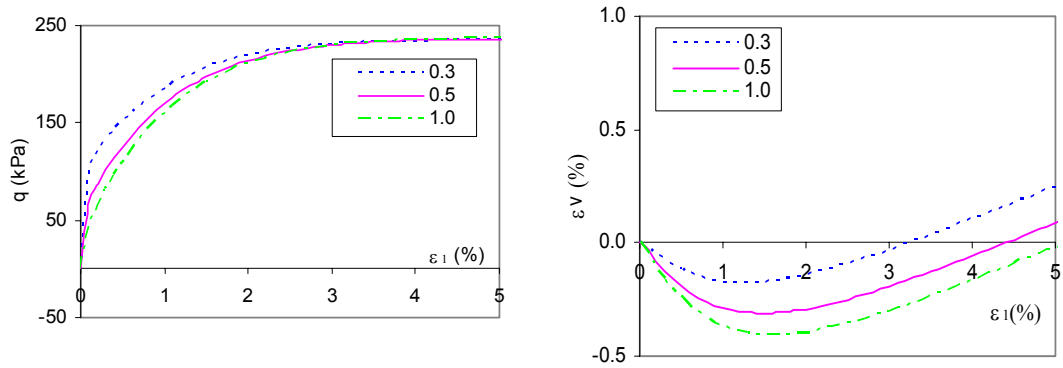


Fig. 4.25: Influence of β_r on drained triaxial test

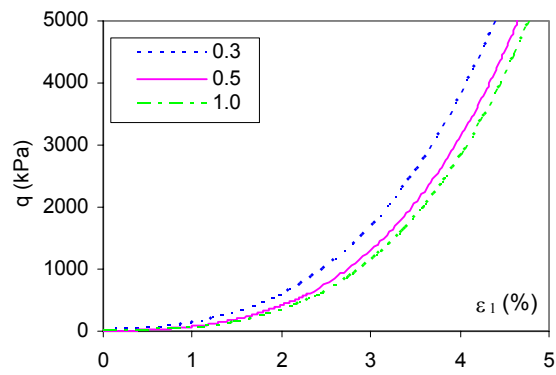


Fig. 4.26: Influence of β_r on oedometer test

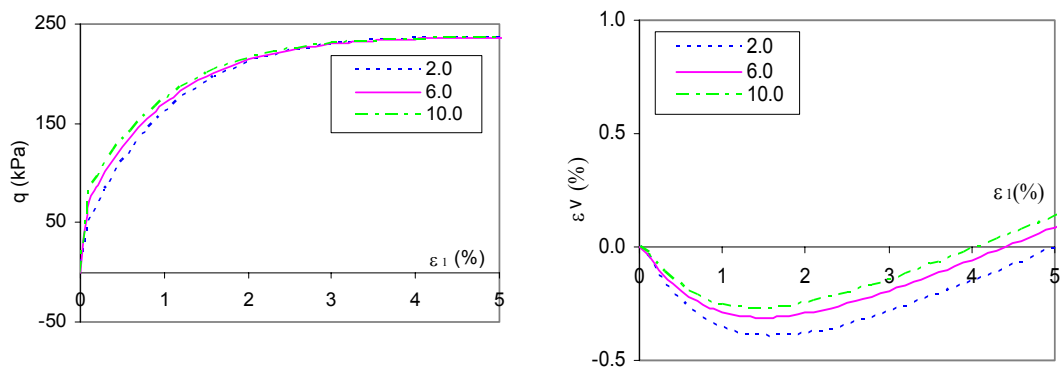


Fig. 4.27: Influence of χ on drained triaxial test

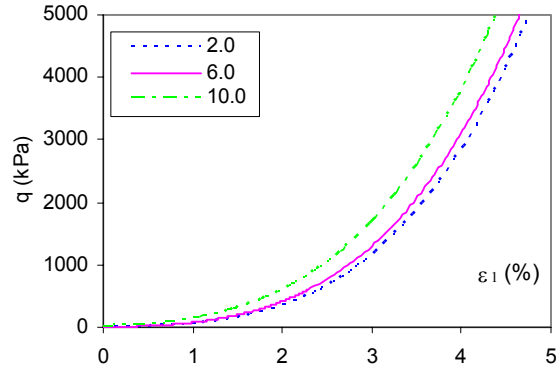


Fig. 4.28: Influence of χ on oedometer test

4.5 Conclusion

A series of drained triaxial tests using the HP model without IGS are simulated by using the *Soil test* facility in Plaxis 2D. These results show good agreements with other numerical and measured results for both Baskarp and Karlsruhe sands. Especially, the simulated results on dense sand show the softening behaviour after the peak strength has been reached that reflecting the real soil behaviour in drained triaxial tests. This phenomenon overcomes the limitations of the HS model. There is only a small difference of the peak strength at very high cell pressure. Moreover, the shortcoming of the HP model as an excessive accumulation of deformation for small stress cycles is improved by the introduction of the intergranular strain, is also examined. The numerical results show that, the accumulation of deformation is much smaller when the intergranular strain is included in the HP model. If combined with the characteristic of the HP model that given in conclusion part of Chapter 3, subsequently, the HP model seems to be a good model to simulate the real soil behaviour which occurs in driven piles.

As can be seen from the simulations, the initial void ratio (e_0) controls the soil behaviour as it is a state variable in the hypoplastic model. A reduction of the void ratio leads to a significant increase of the stiffness and strength of the soil. A stronger dilatancy also occurs with a reduction of the initial void ratio.

From the simulations of drained triaxial and oedometer tests, it is shown that individual parameters have a different influence on the soil response. Among other parameters φ_c , e_{c0} , and e_{d0} have the significant influence on the soil response in triaxial tests. The parameters e_{i0} and β only have a small effect in terms of the initial stiffness. On the other hand, the exponent n has a huge influence on oedometer tests, followed by e_{d0} , e_{i0} , h_s and β . The exponent α and e_{c0} only have slight effects on the stiffness at high stress level.

Finally, the influences of intergranular strain parameters are only found at very small strain and high pressure. An increase of β_r leads to a decrease of the initial stiffness and delays the occurrence of the dilatancy behaviour but does not have an influence on the magnitude of dilatancy angle. In the oedometer test, an increase of β_r also results in a decrease of the modulus at high stress level. On the other hand, the influences of the parameter χ on soil response are reversed in comparison with the parameter β_r .

Chapter 5

Numerical Modelling of Pile Jacking

5.1 Introduction

Driven piles have been commonly used as a technical solution for deep foundations. Consequently, many case studies have been executed to describe the soil behaviour in driven piles, not only experimental but also analytical or numerical methods [1, 10, 15, 33]. However, the soil behaviour around a driven pile is not completely understood. Even that the results from some experiments are not totally in accordant (e.g.[25, 37]). Obviously, in driven piles the surrounding soil is distorted and compacted, leading to the continuous changing of stresses and void ratio. In the FEM, the modeling of the pile installation effect becomes difficult, due to the limited knowledge of the soil behaviour and large displacements during the installation process [11]. A series of studies using the FEM investigate the soil behaviour in driven piles, but the outcomes are still not totally reasonable in comparison with experimental results [6, 12, 13]. Hence, it is very important to have an appropriate model that can simulate the real soil behaviour and soil-pile interaction caused by the pile installation process. As mentioned in Chapter 4, the hypoplastic model is a currently good model to simulate the real soil behaviour which occurs in driven piles. As a result, this chapter will focus on the investigation of the soil behaviour in driven piles with respect to a jacked pile method. A conventional small strain analysis is used in a commercially available FEM package, Plaxis 2D [5]. The hypoplastic model with intergranular strain is chosen for the simulation of the soil behaviour.

However, it is confirmed that it is impossible to model completely the pile installation process, in which the pile is jacked continuously from the surface to its final installation depth in Plaxis 2D finite element code [6]. Therefore, this study aims to find a suitable procedure in order to model properly the installation effect at final depth of the penetration. Then the changes of the soil behaviour will be evaluated in term of stress and void ratio. The basic principle are based on the proposals as showed in [6], [33]. They

suggested that it is possible to model the installation effect by increasing the volume of the pile cluster by volumetric expansion or applying prescribed displacements at the pile-soil boundary. Then the numerical results are validated by means of comparison with centrifuge pile test performed in [10].

5.2 Centrifuge pile test

The centrifuge pile test performed by Dijkstra et al. [10] is chosen to validate the numerical simulation of the installation effect of pile jacking. During the test, the continuous changing of the soil porosity near the pile shaft is evaluated from the change in electric resistance of the saturated soil. Moreover, the load-displacement curves are also produced.

5.2.1 Test set-up

In these tests, a closed-ended model pile with a 405 mm length and 15 mm diameter are used. For a 35g test, this would represent a real pile of approximately 14 m in length and 0.5 m in diameter. The pile already initially embedded by 205 mm into the sand. Then it is hydraulically jacked a further 200 mm into the soil body. Three sensors are attached at certain positions on the pile shaft in order to measure the density changes during the installation process. Moreover, the forces on the pile head and pile base and the displacement of the pile head are also continuously measured. (See Fig. 5.1).

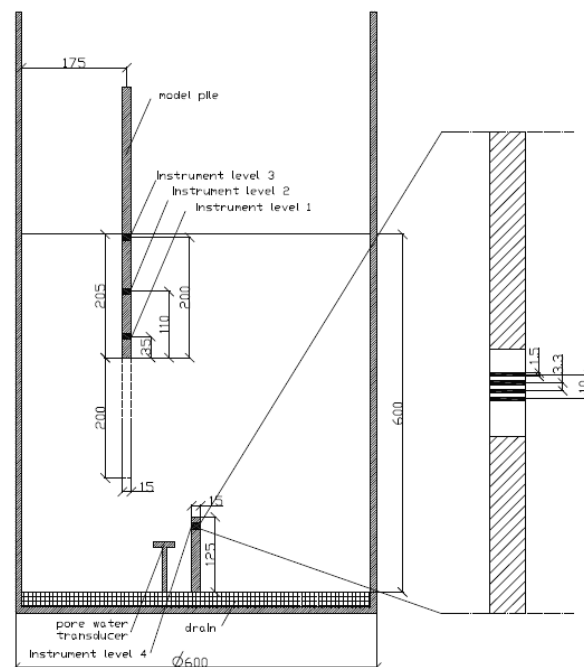


Fig. 5.1: Pile model set-up [10]

Baskarp sand is used as the material for the soil body. First, the pile model is fixed in the model container. Then the sand is pumped in until certain level so that the pile is embedded a length of 205 mm. By this way, the loosest state of the soil body is created with an initial porosity (n) of about 0.455. The denser states are made by using a shock wave, allowing the sand to consolidate.

5.2.2 Test results

Dijkstra J. et al. [10] carried out five tests in which the initial porosity ranges from 0.386 to 0.439. His results showed a significant increase of measured force on the pile head and pile base when the porosity changes from the loose to dense condition. At the installation level of 200 mm, the measured force on the pile head is 85% bigger than those on the pile base with the dense sand while for the medium and loose sand the differences are 55% and 42% respectively. This trend shows the reasonable soil behaviour that the shaft friction for dense case is much higher for either medium or loose case. However, there are big discrepancies of these forces for dense case in comparison with medium and loose cases. The detailed results are shown on the Fig. 5.2.

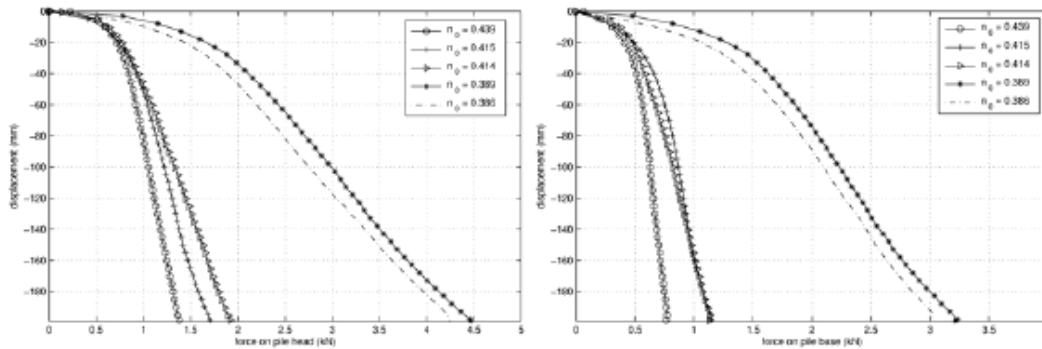


Fig. 5.2: Measured force (kN) on the pile head (left) and pile base (right) during installation [10]

In terms of porosity changes, the results show that there is an increase of the porosity near the pile shaft during the installation process. Generally, the porosity at the instrument level 2 is little higher than either at the instrument level 1 or 3. Besides, the porosity at the instrument level 3 rises gradually over the penetration depth of the pile, while the porosity at the instrument level 1 increased very fast until 40 mm of the penetration depth then stays stable until the end. Unfortunately, no clear relation between the development of the porosity and the penetration depth could be found. Furthermore, the effect of the initial relative density on the change of the porosity is not discovered (see Fig. 5.3)

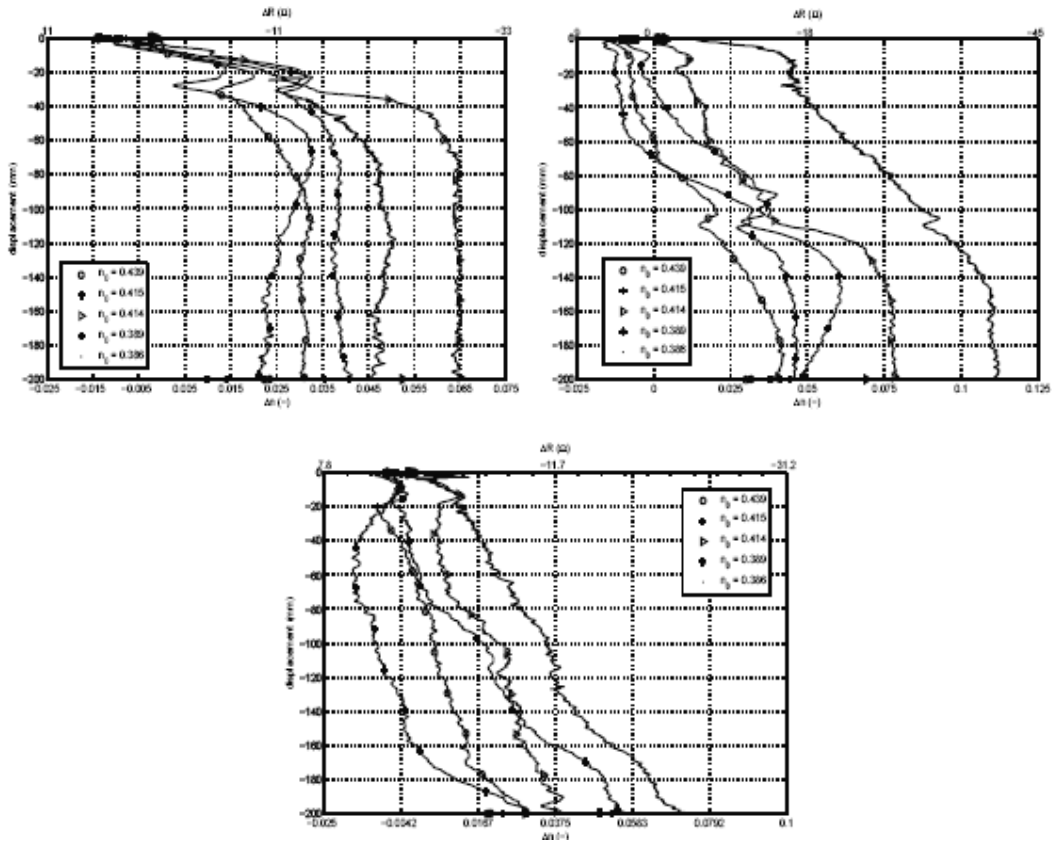


Fig. 5.3: Measured change of porosity during pile installation at instrument level 1 (left), level 2 (right) and level 3 (below) [10]

Three samples are selected from Dijkstra's experiments for comparison with the FE, representing three conditions: dense ($n_o = 0.389$), medium dense ($n_o = 0.415$) and loose ($n_o = 0.439$). The results at 200 mm of installation depth show that the void ratios near by pile shaft increase by in average of 18%, 16% and 14% for dense, medium dense and loose sands respectively. Moreover, there is a significant increment in the vertical stress at the pile tip when the soil condition changes from the loose to dense state. These results will be used to evaluate the numerical simulation (Table 5.1).

Table 5.1: Void ratio and vertical stress at 200 mm of the installation depth

Case	Initial porosity n_o	Initial void ratio, e_o	Void ratio at level 1	Void ratio at level 2	Void ratio at level 3	Average void ratio at pile shaft	Average σ_{yy} (kPa) at pile tip
Dense	0.389	0.637	0.692	0.767	0.802	0.754	18,150
Medium	0.415	0.709	0.835	0.841	0.792	0.823	6,507
Loose	0.439	0.783	0.883	0.919	0.876	0.893	4,244

5.3 Numerical modeling of pile jacking

In this analysis, a procedure is described to simulate the pile installation process in the FEM by a commercially available package, Plaxis 2D. Since it is proved impossible to model the pile installation process, jacking from the surface in Plaxis 2D [6], therefore the pile is modeled at its final depth of the penetration. Then the stresses and void ratio, after the installation process of the numerical simulation, are compared with those obtained from the centrifuge pile test (see Table 5.1).

5.3.1 Mesh and boundary conditions

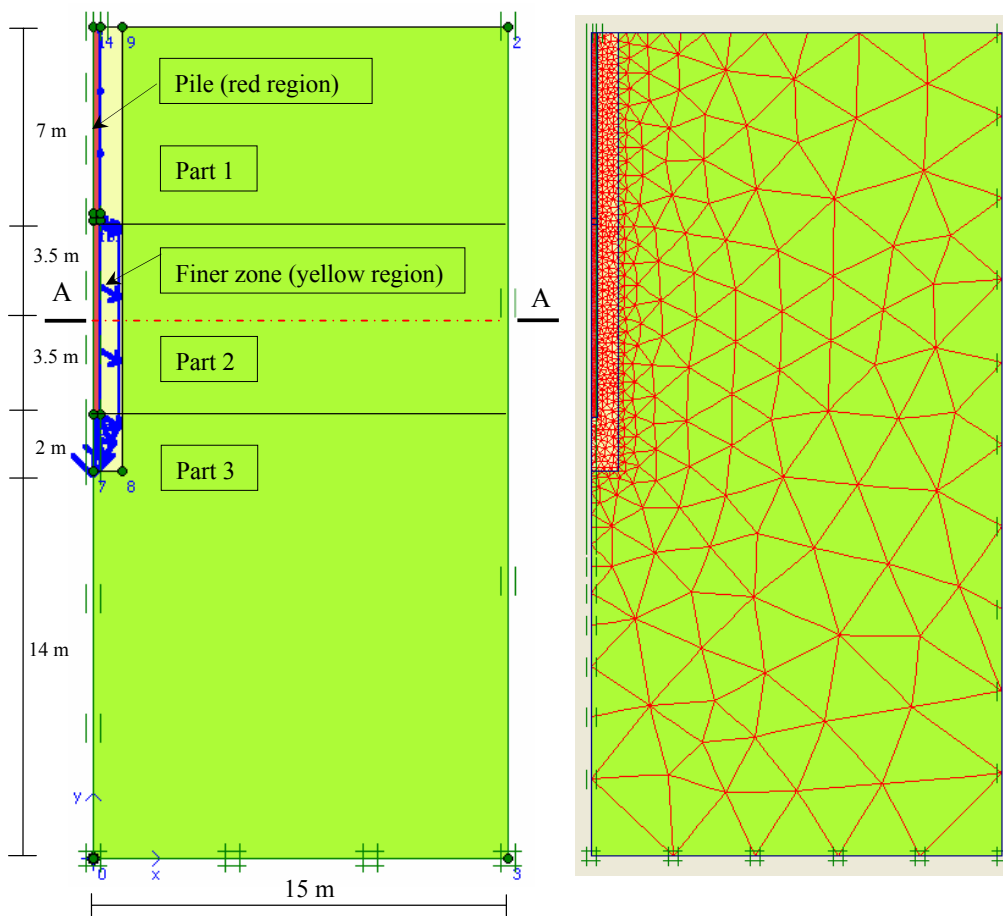


Fig. 5.4: Model geometry (left) and numerical mesh (right)

The numerical simulations are performed using Plaxis 2D [5] in which the geometry is defined in an axisymmetric mesh. In this analysis, the pile dimensions are 14 m length and 0.5 m diameter so that representing the pile model in the centrifuge test [10]. The boundaries are chosen such that their influence is negligible. As the result, the width and the length of the mesh are 15 m and 30 m respectively. The soil cluster is modeled

by 15-noded triangular elements. The left and the right sides of the geometry are applied horizontal fixities whereas the bottom is fixed both horizontally and vertically.

In order to get a better prediction of the soil behavior around the pile, where a big displacement occurs, a zone near the pile is refined (Fig. 5.4). This requirement is realized by choosing a different *Local element size factor* in Plaxis 2D. Firstly, three points (point number 7, 8 and 9 in Fig. 5.5) are added to make a cluster near the pile. Subsequently, the *Local element size factor* at point numbers 0, 2 and 3 (Fig. 5.5) are reset to 2.0 while the remaining points are reset to 0.1. By this way, the mesh is shown in the Fig. 5.4. Since the pile model in the centrifuge test is already embedded 205 mm in the sand body before jacking hydraulically a further 200 mm. Thus, in the numerical model, a transitional zone is created at the middle of the pile cluster (point 11 and 12) to transit from the part 1 (from the surface to the level of 7 m depth) to the part 2 (from the level of 7 m depth to the pile tip), in which they show a different behaviour due to the installation process (see Fig. 5.4 and Fig. 5.5 for more detail).

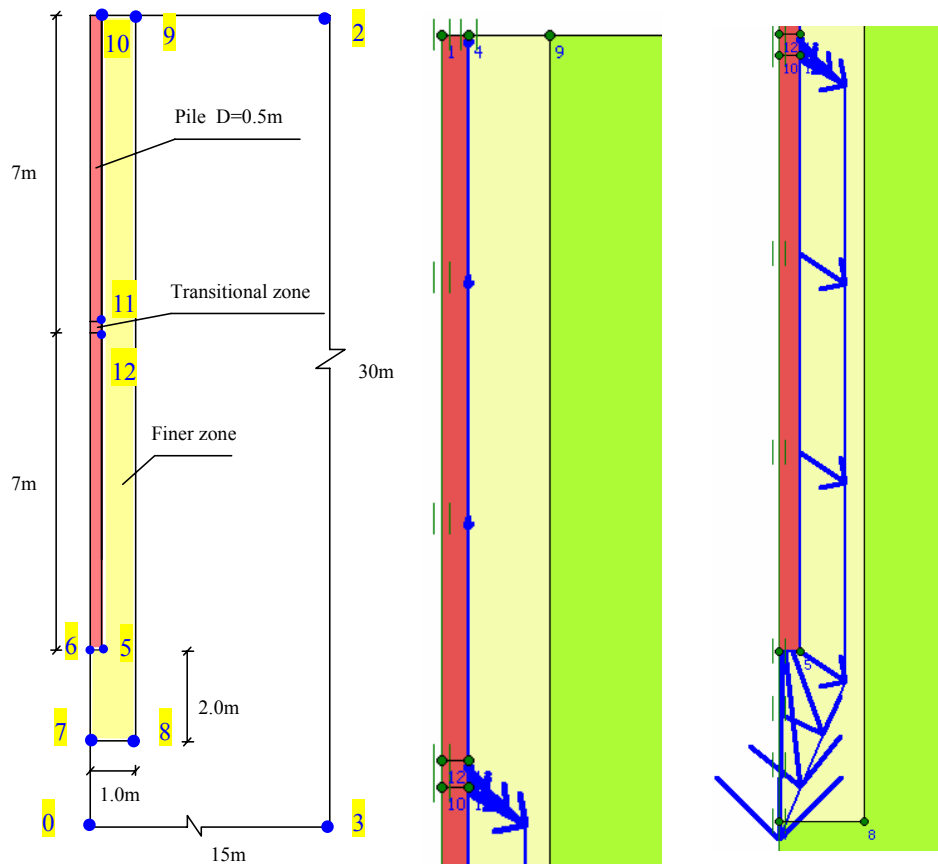
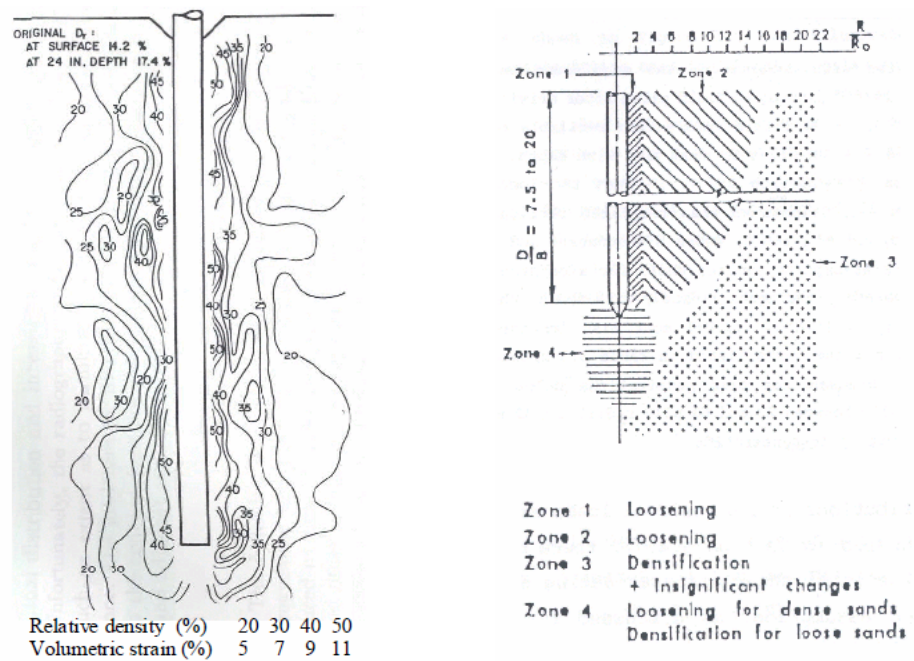


Fig. 5.5: Detailed pile model (left) and prescribed displacements (right)

5.3.2 Simulation of installation effect



Robinsky and Morrison [32]

Chong [8]

Fig. 5.6: Observed changes in density during the installation

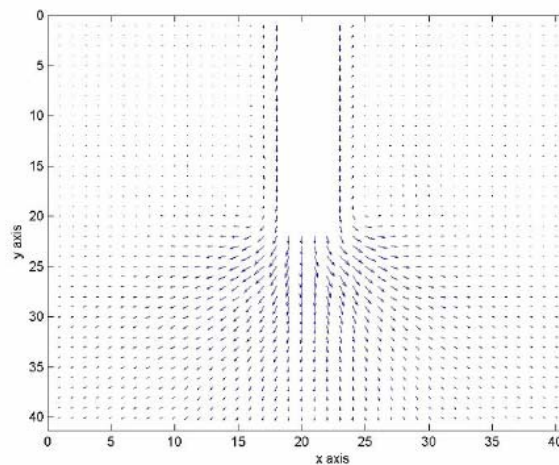


Fig. 5.7: Displacement field during the installation [7]

In the centrifuge test, the pile initially embeds by 205 mm into the sand and is hydraulically jacked a further 200 mm into the soil. Logically, in the part 1 of the numerical model (from the surface to the level of 7 m depth) the pile is moved vertically and continuously leading to the mostly vertical movement of the soil particles close to the pile shaft, when going further from the pile shaft the soil body can be considered stable. However, the soil surrounding the pile in the part 2 (from the level of 7 m depth

to the pile tip) behaves in a different way during the pile installation. Near the pile shaft, the soil particles move both vertically and horizontally, subsequently leading to a dilating zone [8, 15, 32], whilst at a further distance the soil body is densified and compacted [8, 18]. Furthermore, the soil skeletons below the pile tip (part 3) express the outward and downward movement from the axis of the pile [7]. As a result, the models need to consider a different behaviour of the soil body in three parts.

The fundamental principles of modelling the pile installation using regular FEM are based on the proposals as showed by Broere & Van Tol [6] and Said et al. [33], where the installation effect is taken into account by applying prescribed displacements at the pile-soil boundary. In their analyses, the horizontal prescribed displacement is applied at the pile shaft while the vertical prescribed displacement is applied at the pile tip. By this way, the bearing capacity of the pile founded from the FEM fits relatively well to the experimental results [6]. However, these simulations lead to an incompatibility at the corner of the pile in which different directions of the prescribed displacements are applied at the corner point. These problems will be considered in this analysis. In order to model more or less properly the soil behaviour due to installation effect in the jacking pile method as in the centrifuge tests, it is recommended as the following:

- Along the pile shaft (part 1) is only applied the vertical prescribed displacement.
- Along the pile shaft (part 2) and below the pile tip (part 3) is applied both horizontal and vertical prescribed displacements.
- However, care should be taken at the corner point (point 5) and the center point (point 6) of the pile tip. In order to make the compatibility with the pile shaft movement, the magnitude of the horizontal prescribed displacement at the point 5 must be equal to those applied along the pile shaft (part 2). Furthermore, no horizontal displacement is applied at the center point (point 6) of the pile tip due to axisymmetric geometry.
- Additionally, two transitional points are added at the pile-soil boundary (point 11 and 12) in order to transit the differences of the prescribed displacements between part 1 and 2.

5.3.3 Constitutive model and parameters

All analyses are realized on saturated Baskarp sand as performed in the centrifuge tests. Baskarp sand is an uniform sand, the grains are classified as angular to sub-angular with D_{50} of approximately 140 μm [13]. This sand has a total unit weight of 20 kN/m^3 , a friction angle of 37° and a dilatancy angle of 8° [10]. Dijkstra et al. [10] carried out five tests in which the initial porosity ranges from 0.386 to 0.439 (the initial void ratio ranges from 0.629 to 0.783). However, for the validation of the numerical simulation,

first the medium dense sample ($e_o = 0.709$) is selected to define the appropriate prescribed displacements applied at the pile-soil boundary. Then these values are verified again with dense sample ($e_o = 0.637$) and loose sample ($e_o = 0.783$).

In the FEM, the hypoplastic model formulated by Von Wolfferdorff [36] is used for the soil material. All parameters are derived from laboratory tests in [13] given in the Table 5.2. For this model, the soil behaviour is defined by the stress history and the current void ratio. However, the excessive accumulation of strains and stresses due to cyclic loadings is still a drawback of the hypoplastic model [14]. Later, Niemunis and Herle [28] have introduced an intergranular strain tensor as an additional state variable to take this behaviour into account. In these analyses, the parameters for intergranular strain are estimated by using the *Soil tests* facility in Plaxis 2D, in such a way that the soil responses from the HP model without intergranular strain are similar to those obtained from the HP model with intergranular strain (see appendix A for more detail). The intergranular strain parameters are recommended in Table 5.3.

Table 5.2: Hypoplastic parameters for Baskarp sand [13]

Parameters	φ_c (o)	h_s (MPa)	n	e_{d0}	e_{c0}	e_{i0}	α	β
Values	30	4000	0.42	0.548	0.929	1.08	0.12	0.96

Table 5.3: Estimated parameters of the intergranular strain for Baskarp sand

Parameters	m_T	m_R	R_{max}	β_r	χ
Values	2	5	0.0001	1.0	2.0

5.3.4 Calculation procedures

5.3.4.1 Initial stresses

In Plaxis 2D, the initial stresses in the soil body are influenced by the weight of the material [5]. The initial horizontal stress is calculated from the initial vertical stress by using K_o procedure ($K_o = 1 - \sin\phi$). Furthermore, the water level is also selected at the ground surface level to make a fully saturated soil mass.

For the hypoplastic model the void ratio is a state variable which is dependent on the pressure level. Therefore, after the initial stresses are generated, the void ratio in the soil body varies according to Bauer's formula [3]. In the analysis, the stress level at the middle cross-section A-A of the part 2 is chosen to define the initial void ratio (Fig. 5.4). As a result, the initial void ratios at zero pressure using in Plaxis 2D is determined as $e_o = 0.720$ (back-calculating for the mean stress using Bauer's formula) in order to get the similarly initial soil state for medium dense sample obtained from centrifuge test.

5.3.4.2 Calculation phases

This phase is applied directly after the initial phase. All calculation phases are carried out under drained analysis. In order to simulate the installation effect of driven piles in the numerical framework, the prescribed displacements are applied at the pile-soil boundary as mentioned on the section 5.3.2. Care should be taken during this phase is that all displacements from the initial phase are reset to zero. Secondly, the cluster representing the pile is not activated to avoid the extension of the soil material. Furthermore, the horizontal (Δu_x) and vertical (Δu_y) displacements are applied simultaneously at pile-soil boundary to simulate the installation effect of driven pile, if they are applied separately, leading to the inaccuracies of the numerical results. Finally, to avoid a big distortion of the mesh in one phase, the horizontal and vertical displacements are increased step by step and the check box “reset displacement to zero” is not activated in these phases. The magnitudes of the prescribed displacements are given in Tables 5.4 and Table 5.5 .

Table 5.4: Prescribed displacements applied in calculation phases

Case	Point 10 & 11		Point 12 & 5		Point 6	
	$\Delta x^1(\text{cm})$	$\Delta y^1(\text{cm})$	$\Delta x^2(\text{cm})$	$\Delta y^2(\text{cm})$	$\Delta x^3(\text{cm})$	$\Delta y^3(\text{cm})$
Case 1	0	1	2	4	0	50
Case 2	0	1	6	4	0	50
Case 3	0	1	2	6	0	50
Case 4*	0	2	18	8	0	74
Case 5	0	2	14	8	0	74
Case 6	0	2	16	8	0	74
Case 7	0	2	20	8	0	74
Case 8	0	2	22	8	0	74
Case 9	0	2	18	4	0	74
Case 10	0	2	18	6	0	74
Case 11	0	2	18	10	0	74
Case 12	0	2	18	12	0	74
Case 13	0	2	18	8	0	70
Case 14	0	2	18	8	0	72
Case 15	0	2	18	8	0	76
Case 16	0	2	18	8	0	78
Case 17	0	2	18	8	0	80
Dense**	0	2	18	8	0	74
Loose***	0	2	18	8	0	74

5.3.5 Numerical results

The first trial is made with a small magnitude of the prescribed displacements applied at the pile-soil boundary. Then these values will change based on its results in terms of the void ration distribution at the pile shaft and the average vertical stress at the pile tip. The measured results from Dijkstra J. et al. [10] are used to validate the numerical results. In the first analysis, the magnitudes of the horizontal (Δx^2) and vertical (Δy^2) prescribed displacements applying at the part 2 of the model are 2.0 cm and 4.0 cm respectively. Furthermore, the vertical prescribed displacements at the part 1 (Δy^1) and part 3 (Δy^3) are correspondingly selected 1.0 cm and 50 cm. In the calculation phases, these displacements are increased step by step to avoid a big distortion of the mesh in one phase (the calculation phases include 20 steps).

Table 5.5: Prescribed displacements and numerical results

Case	Part 1	Part 2		Part 3	e (-)	σ'_{yy} (kPa)
	Δy^1 (cm)	Δx^2 (cm)	Δy^2 (cm)	Δy^3 (cm)		
Case 1	1	2	4	50	0.738	10,520
Case 2	1	6	4	50	0.761	8,290
Case 3	1	2	6	50	0.746	10,632
Case 4*	2	18	8	74	0.821	6,586
Case 5	2	14	8	74	0.807	7,863
Case 6	2	16	8	74	0.814	7,213
Case 7	2	20	8	74	0.826	5,990
Case 8	2	22	8	74	0.831	5,447
Case 9	2	18	4	74	0.816	6,328
Case 10	2	18	6	74	0.819	6,432
Case 11	2	18	10	74	0.823	6,719
Case 12	2	18	12	74	0.825	6,818
Case 13	2	18	8	70	0.821	6,210
Case 14	2	18	8	72	0.821	6,447
Case 15	2	18	8	76	0.821	6,795
Case 16	2	18	8	78	0.821	6,955
Case 17	2	18	8	80	0.821	7,202
Dense**	2	18	8	74	0.798	9,015
Loose***	2	18	8	74	0.845	5,263

* The case gives expected result for medium dense sand

** and *** are cases for dense and loose sand respectively, remaining case for medium dense sand.

The results from the first analysis shows that there is an increase of the void ratio along the pile shaft (part 2) leading to a shear band as mentioned by many authors [8, 18, 32]. Especially, a compacted zone appears at a distance from the pile shaft which is also found from the simulation of Henke & Grabe [18]. The zone directly below the pile tip is also loosened similar to the zone near the pile shaft and this phenomenon can be considered similar to Chong's findings [8]. So far, the results are quite promising even the fact that the void ratio at the pile shaft is far small than the measured one and the average vertical stress at the pile tip is much bigger than the measured one (see Table 5.5 for more detail).

In the next steps, only the horizontal or vertical prescribed displacements at the pile shaft (part 2) are changed while keeping those at other parts in order to see how the change of the soil behaviour in terms of stresses and void ratio respect to displacement changes. In general, when the horizontal displacement at the pile shaft (Δx^2) is increased leading to a raise of the void ratio at the pile shaft and a large reduction of the vertical stress at the pile tip. The width of the shear band also increases. On the other hand, when the vertical displacement at the pile shaft (Δy^2) is increased, results in a small growth of the void ratio at the pile shaft and the vertical stress at the pile tip. But the width of the shear band decreases.

For the medium dense case, after varying the magnitudes of the prescribed displacements, the numerical results fit very well with the centrifuge test results when the magnitudes of the horizontal (Δx^2) and vertical (Δy^2) displacements applying at the pile shaft are 18 cm (72% radius of the pile) and 8 cm (32% radius of the pile) respectively while the vertical displacements (Δy^3) applying at the pile tip to be 74 cm (10.6% the length of the jacked pile). Then, the results from this case will be analyzed in the following sections.

5.3.5.1 Change of void ratio

Fig. 5.8 shows the void ratio around the jacked pile after 7 m of penetration in initially medium dense Baskarp sand. As can be seen, the void ratio increases along the pile shaft until the distance of approximately 1.0 to 1.5 times the diameter of the pile, making a shear band as mentioned by Chong [8] or Henke & Grabe [18]. The width of the shear band is larger than the previous authors' finding, the reason could be due to the properties of Baskarp sand itself with strongly dilatant behaviour. At a distance from the pile shaft, the soil body is compacted leading to a decrease of the void ratio. The highest degree of compaction is located near the pile tip. This compaction could be explained by the increase of the volumetric strain at a zone close to the pile tip resulting in the decrease of the volumetric strain in the compacted zone.

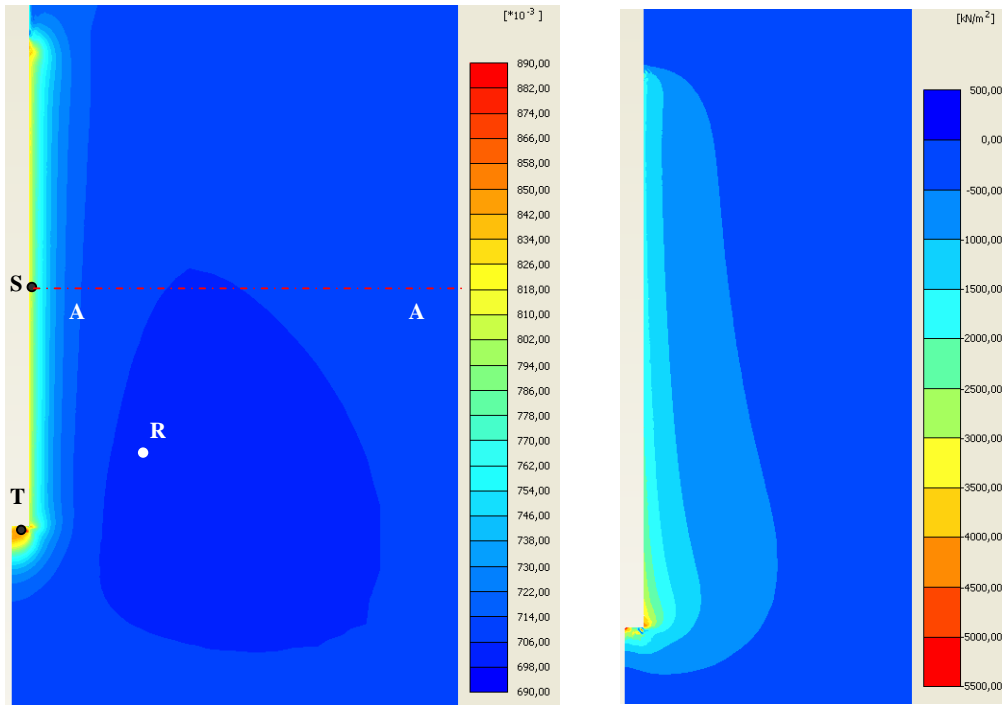


Fig. 5.8: Void ratio (left) and horizontal stress distribution (right) after 7 m of pile jacking

The effect of pile jacking at cross section A-A can be seen in Fig. 5.9. Until the distance of 1D, the void ratio rises notably (5 to 15%) while between 2D and 10D the soil is compacted. Additionally, below the pile tip the soil body is loosened up to a distance of 3D. This loosening is shown much more than in the pile shaft, mostly by the bigger prescribed displacements. This phenomenon is in good accordance with the finding by Chong [8] for initially dense sand. This effect will be checked again for initially loose sand, come later on.

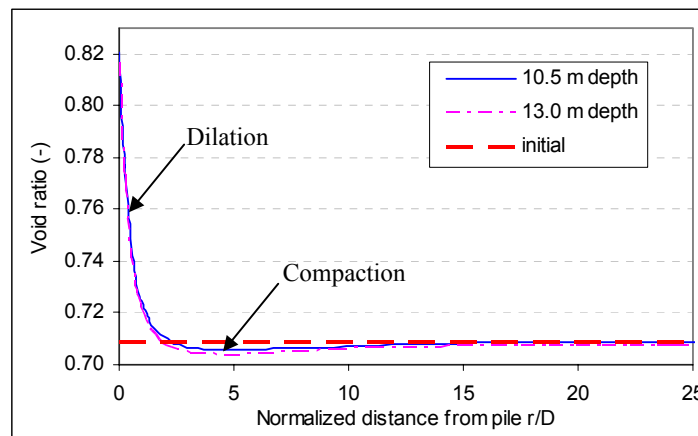


Fig. 5.9: Void ratio distribution at cross-section AA after 7 m of pile jacking

5.3.5.2 Stress distributions

It can be seen from Fig. 5.8 and Fig. 5.10 that the horizontal stress decreases by moving away from the pile. The significant increase of horizontal stress can be found until the distance of more than 5D. Moreover, there is also an increase of the horizontal stress leading to an increase of the shear stress along the pile shaft (Fig. 5.11). These stress distribution is similar to the measurements by White & Lehane [37]. But it differs from the measured results by Klotz & Coop [20] as well as the numerical results by Broere & Van Tol [6], in which the horizontal stress shows a decrease towards the pile tip. Obviously, the ratio between the shear stress and the horizontal stress after installation is smaller than in findings from Broere & Van Tol [6], could be due to smaller the mobilized friction angle found in this analysis.

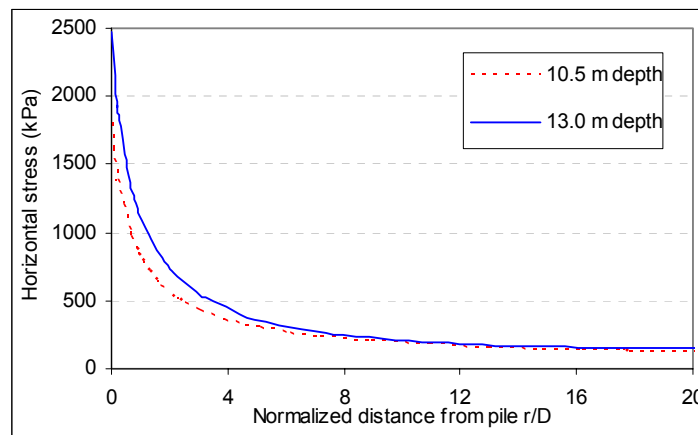


Fig. 5.10: Horizontal stress distribution at cross-section AA after 7 m of pile jacking

The vertical stress distribution can be seen in the Fig. 5.12, which reaches a maximum value at the bottom of the pile. This maximum stress and a strong shear force near the pile tip (Fig. 5.12) can lead to a stronger compaction of the soil around the pile tip as mentioned before. This phenomenon fit quite well with finding by Henke & Grabe [18]. However, a strange zone appears at the corner of the pile which is similar to the horizontal and shear stresses. This drawback could be due to the numerical scheme with large displacement below the pile tip.

The total displacement of the soil body can be seen in Fig. 5.13. Here, the irregular movements of the soil particles close to the pile tip results in an appearance of the strange zone as mentioned before. Furthermore, the rotation of the principal stress direction near pile corner can be observed.

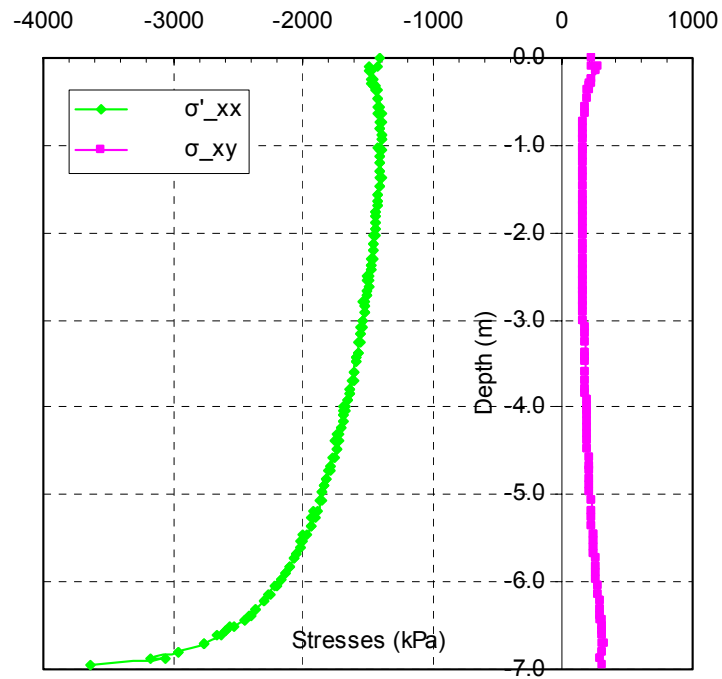


Fig. 5.11: Horizontal and shear stresses distribution along the pile shaft after 7 m of pile jacking

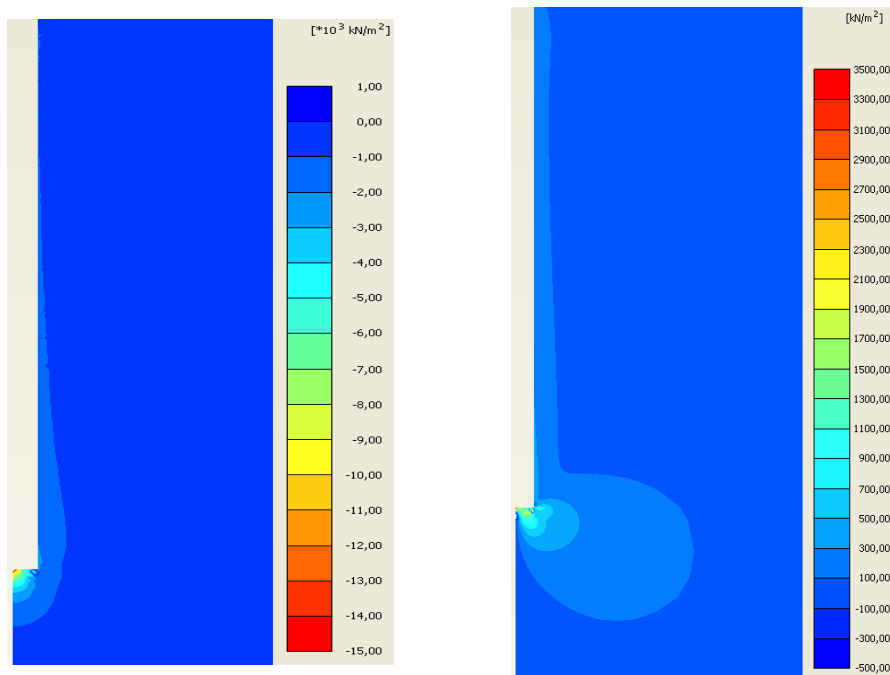


Fig. 5.12: Vertical stress (left) and shear stress distribution (right) after 7 m of pile jacking

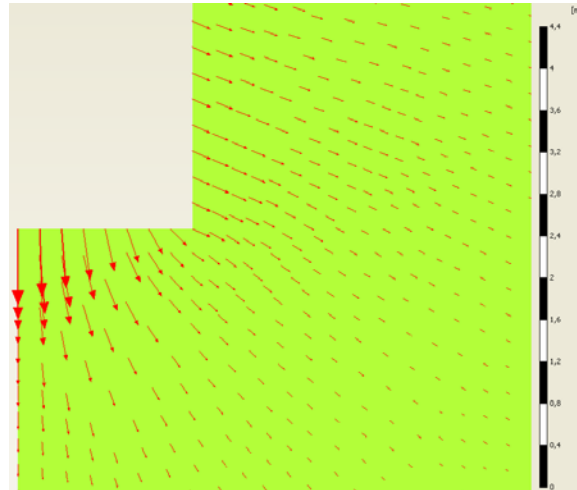


Fig. 5.13: Total displacement field after 7 m of pile jacking

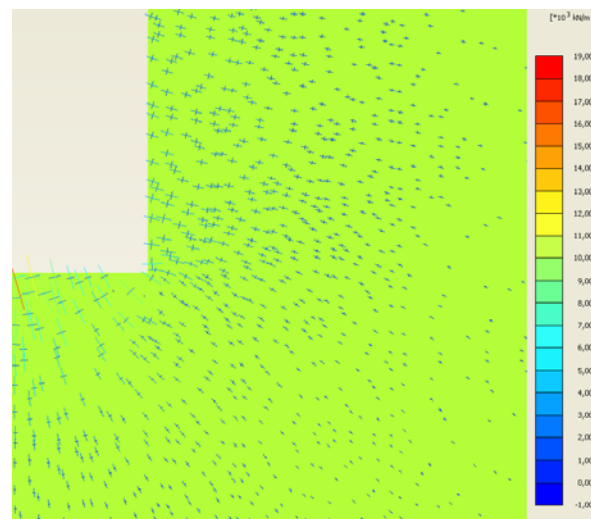


Fig. 5.14: Principal stresses direction after 7 m of pile jacking

5.3.5.3 Void ratio evolution

In Fig. 5.15, the evolution of the void ratio during the simulation of the installation effect of several points is plotted (see point locations in Fig. 5.8). Both point S (near the pile shaft) and point T (below the pile tip) display a dilatant behaviour. This can be explained by an increase of the volumetric strain accompanied by an increase of the prescribed displacements at the pile-soil boundary. However, point T shows higher the void ratio and the mean stress at every calculation phases due to higher values of prescribed displacements of point T. On the other hand, at point R (a distance of $2D$ from the pile), there is a compaction. This occurs as an decrease of the volumetric strain at this point that explained before. So far, this procedure gives promising result in terms of the void ratio evolution. By increasing displacements at the pile-soil boundary step

by step, the soil behaviour around a driven pile is more or less similar to the reality.

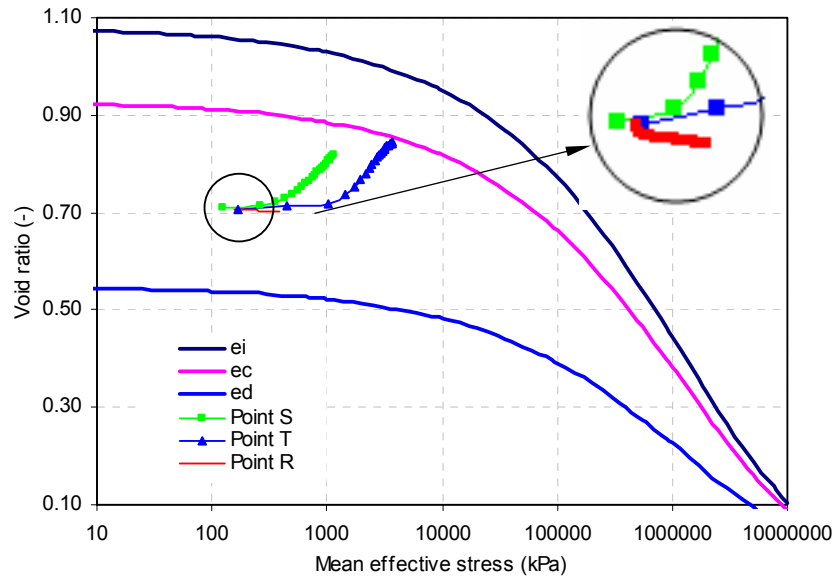


Fig. 5.15: Void ratio evolution during the jacking phases, the point locations according to Fig. 5.8

5.3.6 Influence of prescribed displacements

In this section, the influences of the prescribed displacements on the soil behaviour in terms of stresses and void ratio are investigated. The case 4 (Table 5.5) is chosen as the reference case. First, only the horizontal displacement at the pile shaft (part 2) is varied while keeping the others constant. Similarly, the sensitivity of the soil behaviour around the pile to the variation of the vertical displacement at the pile shaft (part 2) and at the pile tip is also investigated.

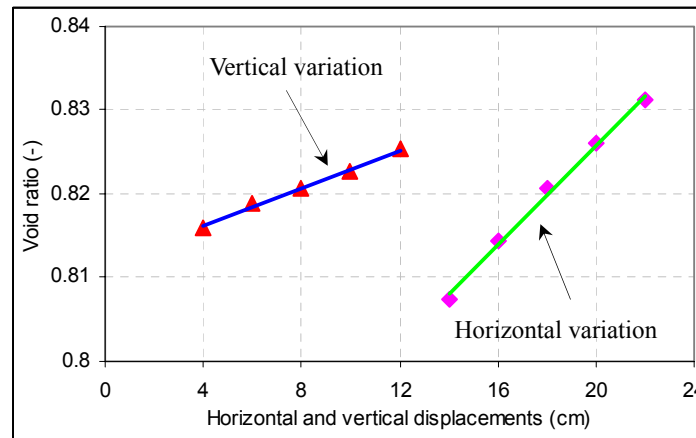


Fig. 5.16: Influence of prescribed displacements at the pile shaft on void ratio

As can be seen, the void ratio at the pile shaft linearly increase accompanied by the rise of either the horizontal or vertical displacements at the pile shaft. But, the horizontal component shows a higher influence than the vertical one on the soil behaviour in terms of the bandwidth and the void ratio (see Fig. 5.16).

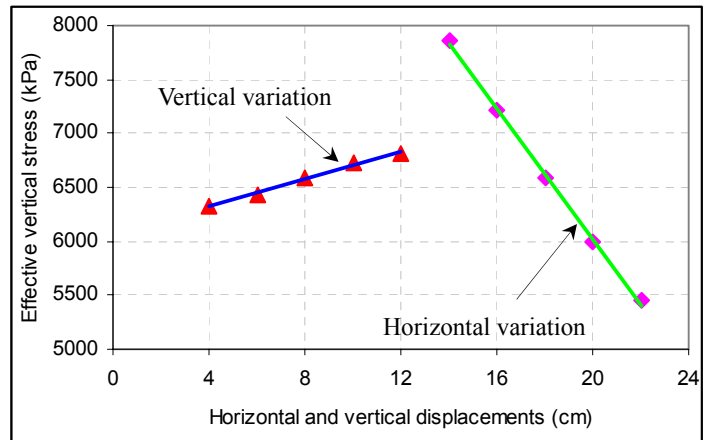


Fig. 5.17: Influence of prescribed displacements at the pile shaft on effective vertical stress

On the other hand, the effective vertical stress at the pile tip increases when rising the vertical component but decreases when increasing the horizontal component (Fig. 5.17). Once again, the horizontal displacement shows a stronger influence than vertical displacement. This finding is also confirmed by Broere & Van Tol [6]. Moreover, the vertical stress at the pile tip also linearly increase accompanied by the rise of the vertical displacements at the pile tip (Fig. 5.18).

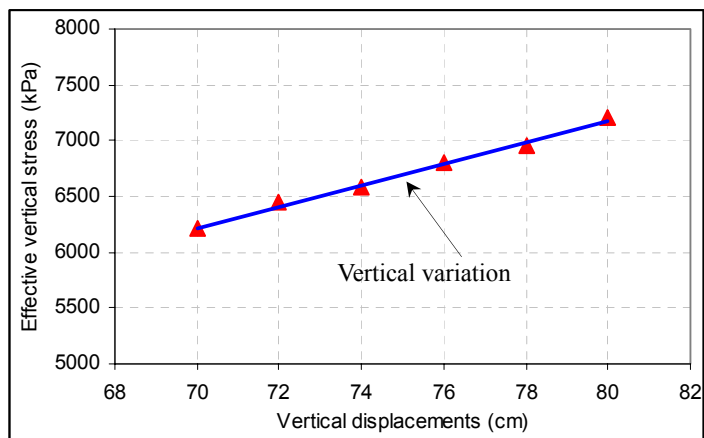


Fig. 5.18: Influence of prescribed displacements at the pile tip on effective vertical stress

Finally, the dense sample ($e_o = 0.637$) and loose sample ($e_o = 0.783$) are investigated by applying the same amounts of the prescribed displacements at the

pile-soil boundary as for medium dense sample. For the dense case, the results demonstrate a higher void ratio than the measured one at the pile shaft but much lower the vertical stress as expected at the pile tip. These discrepancies can be solved by reducing the amount of the horizontal displacement at the pile shaft and increase the amount of the vertical displacement at the pile tip. For the loose sample, the differences are also found but reversely to the dense case. Moreover, no compaction zone can be found below the pile tip for the loose case as mentioned by Chong [8]. From this point, it could be concluded that there may be a relation between the amount of the prescribed displacements applied at the pile-soil boundary and the relative density or density index. The higher relative density leads to the higher prescribed displacements applied at the pile tip but the smaller prescribed displacements at the pile shaft.

5.3.7 Modelling of shearing effect

This section investigates the bearing capacity of the model pile in terms the evaluation of the shaft friction. After applying the horizontal and vertical prescribed displacements at the pile-soil boundary in order to simulate the installation effects, the pile is allowed to shear by increasing the vertical component at the pile shaft while keeping the horizontal component, subsequently the soil close to the pile shaft come to the critical state (failure). At this state, the shear strength of the soil is equal to the shear stress.

As can be seen in Fig. 5.19, the horizontal stress at a reference point (point S as shown in Fig. 5.8) increases gradually during the jacking phases. However, it decreases rapidly due to the shearing process, subsequently becomes plateau at failure. The horizontal stress at failure is much smaller than after jacking phases, reduced by 80%. On the other hand, the shear stress at failure is only smaller of 9% than that after jacking phases. During the shearing phases, the shear stress increases enormously at the beginning then decreases steadily until the failure (Fig. 5.20).

Taking the ratio between the shear stress and the horizontal stress, the mobilised friction angle can be calculated ($\tan\delta = \sigma_{xy}/\sigma_{xx}$) in Fig. 5.21. The results show that these values are small and mostly remain constant during the jacking phases. This phenomenon is also found by Klotz & Coop [20]. However, during the shearing phases, the mobilised friction angle is in the range of 30° and 28° . It mean that only the friction reduction factor $R = 0.87$ and 0.82 could be found at peak state and at failure respectively (the internal friction angle of medium sand is $\phi = 34.5^\circ$, see appendix B for more detail)

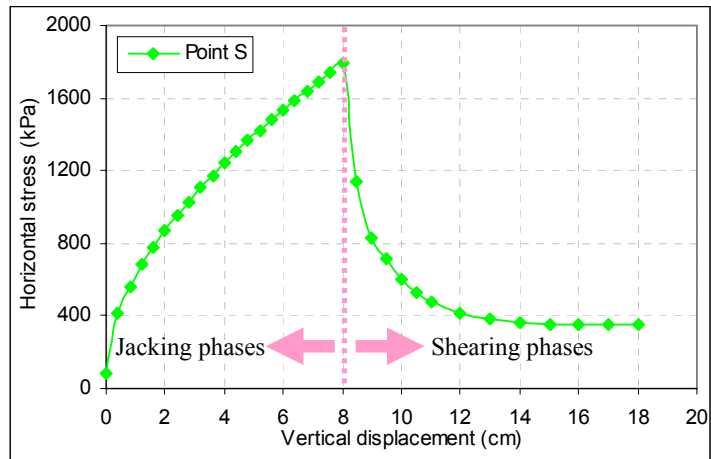


Fig. 5.19: Horizontal stress development during shearing process

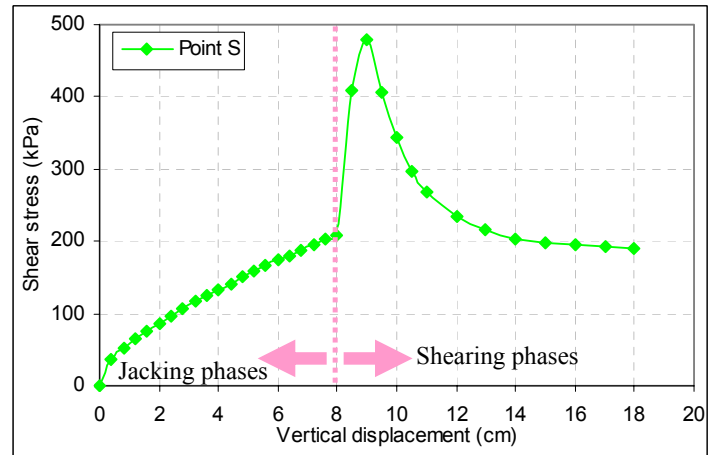


Fig. 5.20: Shear stress development during shearing process

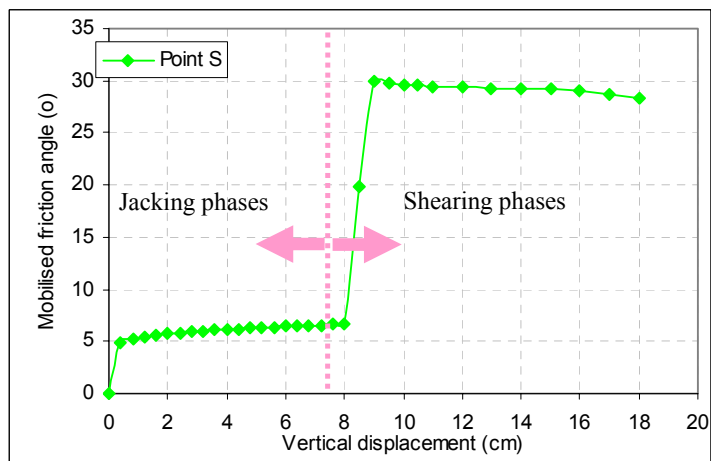


Fig. 5.21: Mobilised friction angle development during shearing process

Fig. 5.22 shows the stress path p - q at point S. During the jacking phases, there is a linear increase of the effective mean stress p' with the deviatoric stress q . However, it decreases in the shearing phases accompanied by a reduction of the deviatoric stress q . Moreover, it can be seen in Fig. 5.23 that the volumetric strain at point S increases in both the jacking phases and shearing phases due to an increment of the prescribed displacements applied at the pile-soil boundary. This phenomenon leads to an increase of the void ratio as seen in Fig. 5.24. Lastly, the void ratio evolution at point S is plotted in Fig. 5.25. Clearly, the dilatant behaviour occurs in both the jacking phases and shearing phases and this void ratio reaches the critical line at the end of the shearing phases (at failure).

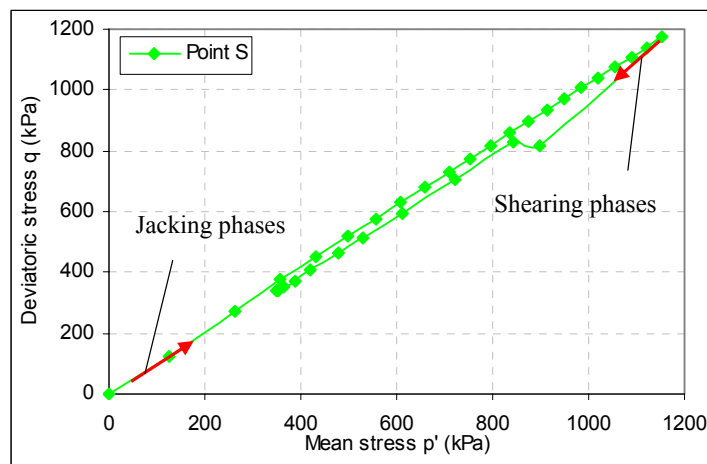


Fig. 5.22: Stress path in p - q plane during shearing process

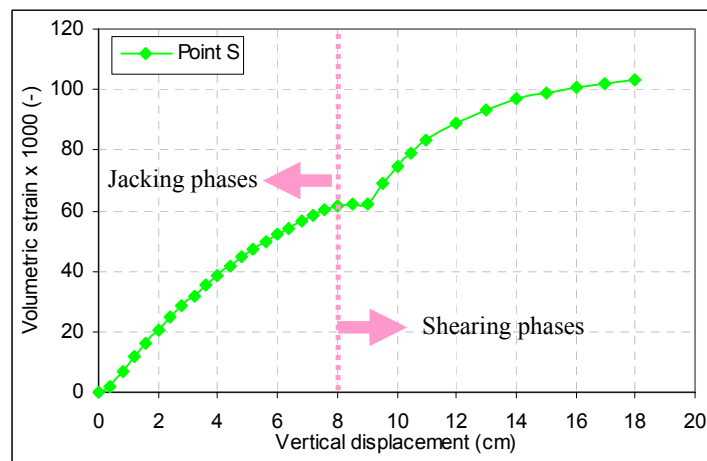


Fig. 5.23: Volumetric strain development during shearing process

Jacking phases: Increasing both the horizontal and vertical displacements simultaneously.

Shearing phases: Increasing the vertical displacements while keeping the horizontal displacement

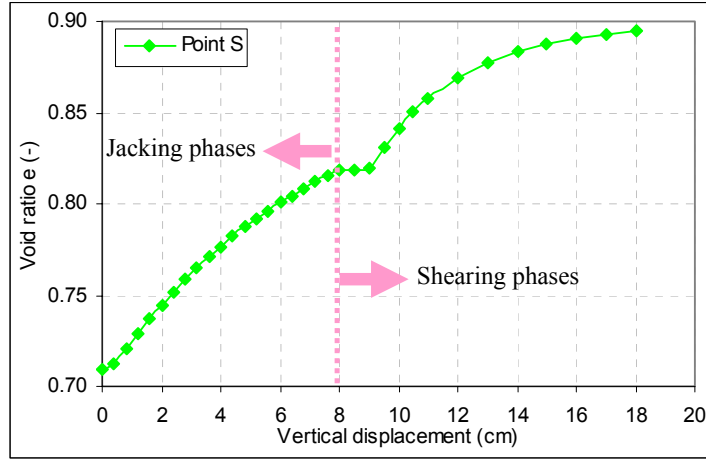


Fig. 5.24: Void ratio development during shearing process

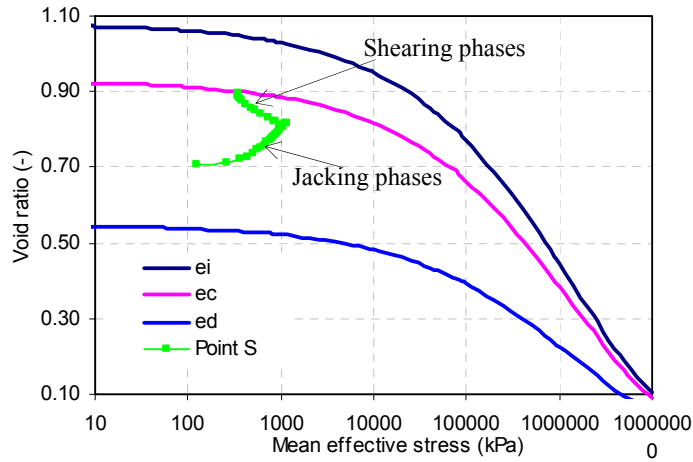


Fig. 5.25: Void ratio evolution in e - p' plot during shearing process

5.4 Conclusion

This chapter proposes a procedure to simulate the pile installation process in Plaxis 2D, based on the suggestions as showed by Broere & Van Tol [6] and Said et al. [33], where the installation effect is taken into account by applying the prescribed displacements at the pile-soil boundary. The centrifuge pile test performed by Dijkstra et al. [10] is chosen in order to validate the numerical simulation. The hypoplastic model formulated by Von Wolfferdorff [36] with the intergranular strain is used for the soil material. The hypoplastic parameters are derived from laboratory tests by Elmi Anaraki [13], while the intergranular strain parameters are estimated in such a way that the soil responses from the HP model without intergranular strain are similar to those obtained from the HP model with intergranular strain.

In the numerical framework, the calculations phases are applied directly after the initial phase. Moreover, the horizontal and vertical displacements are increased step by step to avoid a big distortion of the mesh in one phase. In this way, the installation effects of driven piles are modelled. For the case of a pile with 0.5 m diameter and 14 m length, jacking into medium dense Baskarp sand to the depth of 7 m, the numerical results fit very well with the centrifuge test results when the magnitudes of the horizontal and vertical displacements applying at the pile shaft are 18 cm (72% radius of the pile) and 8 cm (32% radius of the pile) respectively while the vertical displacements applying at the pile tip to be 74 cm (10.6% the length of the jacked pile).

The numerical results show that the void ratio increases along the pile shaft until a distance of approximately 1.0 to 1.5 times the diameter of the pile, leading to a shear band as mentioned by Chong [8] or Henke & Grabe [18]. At a distance from the pile shaft, the soil body is compacted leading to a decrease of the void ratio. The highest degree of compaction is located nearby the pile tip. This compaction could be explained by the increase of the volumetric strain at the zone close to the pile tip, resulting in an decrease of the volumetric strain in the compacted zone.

On the other hand, the horizontal stress decreases by moving far away from the pile. A significant increase of the horizontal stress can be found until a distance of more than 5D. Moreover, there is also an increase of the horizontal stress leading to an increase of the shear stress along the pile shaft. These stress distribution is similar to the measurements by White & Lehane [37]. But it differs from the measured results by Klotz & Coop [20] as well as the numerical results by Broere & Van Tol [6], in which the horizontal stress shows a decrease towards the pile tip.

Moreover, the influences of the prescribed displacements on the soil behaviour in terms of stresses and void ratio are investigated. From the results, it can be concluded that the void ratio at the pile shaft linearly increases accompanied by the rise of either the horizontal or vertical displacements at the pile shaft. But the effective vertical stress at the pile tip increases when rising the vertical component, and decreases when increasing the horizontal component. Furthermore, the horizontal displacement shows a stronger influence than the vertical displacement. This finding was also discovered by Broere & Van Tol [6].

The same amount of the prescribed displacements as for medium dense sample are also applied for dense and loose samples. For the dense case, the results demonstrate a higher void ratio as measured at the pile shaft but much a lower vertical stress as expected at the pile tip. For the loose sample, the differences are also found but reversely to the dense case. Moreover, no compaction zone can be found below the pile tip for the loose case as mentioned by Chong [8]. From this point, it is concluded that there could be a relation between the amount of prescribed displacements applied at the pile-soil boundary and the relative density or density index. A higher relative density

leads to a higher prescribed displacement applied at the pile tip but a smaller prescribed displacement at the pile shaft.

Finally, the model pile is sheared by increasing the vertical component at the pile shaft while keeping the horizontal component from jacking phases, subsequently the soil close to the pile shaft come to failure. The results show that both the horizontal and shear stress decrease during the shearing phases, but the magnitude of the horizontal stress reduces by 80% while only 9% can be found for the shear stress. Especially, only the friction reduction factor $R = 0.87$ and 0.82 could be found at peak state and at failure respectively. This finding could be investigated further in order to apply in the calculation of the bearing capacity of driven piles.

Chapter 6

Numerical Modelling of Cyclic Loading on Pile Shaft

6.1 Introduction

The previous chapters already discussed the hypoplastic model and its capacities to simulate the soil behaviour for the pile jacking method by using the FEM (Plaxis 2D finite element code). Herein, a procedure is introduced to simulate the pile installation process based on the proposals as showed in [6, 33], where the installation effect is taken into account by applying the prescribed displacements at the pile-soil boundary. The results show good agreements with experimental and other numerical results from previous authors [8, 18, 37]. However, the development of stresses and void ratio with respect to cyclic loading is more complicated. This process leads to a loosening of the soil body, causing a reduction of the void ratio and shear resistance in the surrounding zone [17, 18, 29]. In this chapter, the soil behaviour around a driven pile with respect to the vibrating method will be investigated by using Plaxis 2D. For simplification, only the cyclic effects in the vicinity of the pile shaft are considered. In these analyses, two soil models are used: the hardening soil and the hypoplastic model without intergranular strain, afterwards the results are compared in order to evaluate its capacities in modelling of cyclic loading effect.

6.2 Mesh and boundary conditions

Similar to Chapter 5, the numerical simulations are also performed using Plaxis 2D finite element code [5] in which the geometry is defined in an axisymmetric mesh. Due to a difficulty in modelling of a full pile, the main aim of this chapter is to examine the soil behaviour around only a part of the pile under cyclic loading. In the analysis, the pile dimensions are 7 m length and 0.4 m diameter. Subsequently, the length of the mesh is chosen to be equal to the pile length while the width of the mesh is 15 m (more than two times the pile length). The soil cluster is modelled by 15-noded triangular elements. In the model, the left side of the geometry is fixed at a distance of 0.2 m from the axial line, representing the pile-soil boundary. For boundary conditions, the left and the right sides of the geometry are applied horizontal fixity whereas the bottom is fixed both horizontally and vertically. A distributed load of 100 kPa is applied on the top of the boundary to create high stresses in order to simulate a real situation of the pile installation at certain depth of penetration (See Fig. 6.1 for more detail).

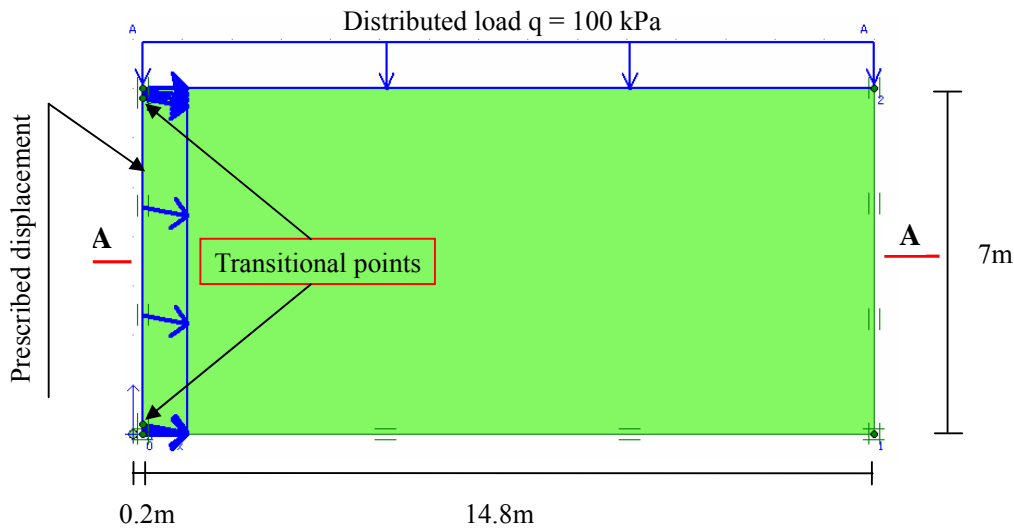


Fig. 6.1: Geometry of the model

In order to have a better prediction of the soil behaviour around the pile where the big displacements take place, the zones near the pile are made finer than other parts of the mesh (Fig. 6.3). This requirement is realized by choosing a different *Local element size factor* in Plaxis 2D. Two points situated at the right side of the geometry are set to 1.0 while other points located at the left side are set to 0.05. Otherwise, this requirement could be completed by choosing the *Refine cluster* option for the zones close to the pile. Furthermore, two transitional points (point 4 and 5) are also added at the pile-soil boundary to avoid a big distortion of the mesh when applying prescribed displacements, this necessity will be explained later on (Fig. 6.2).

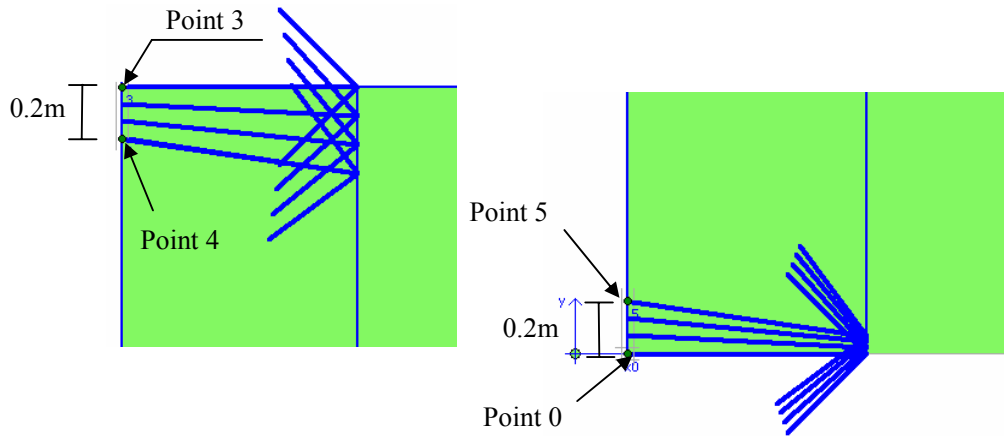


Fig. 6.2: Detail of top-left corner and bottom-left corner of the geometry

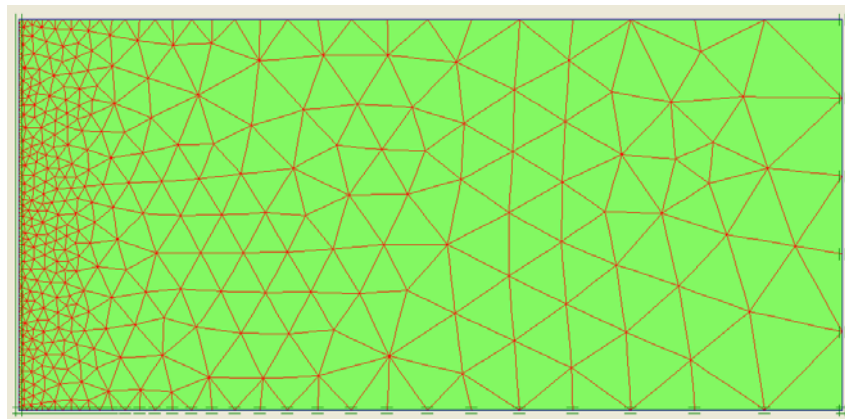


Fig. 6.3: Finite element mesh of the model geometry

6.3 Simulation of installation effect

As mentioned in Chapter 5, the installation effect of the pile jacking can be simulated by applying the prescribed displacements, both horizontally and vertically, at the pile-soil boundary. Based on this principle, the simulation of the cyclic loading is also developed. It means that, after applying the horizontal and vertical prescribed displacements at the pile-soil boundary, in order to simulate the pile jacking process, and then the vertical component is cycled while keeping the horizontal component to be constant, to model the cyclic loading process.

On the other hand, the magnitude of the horizontal and vertical components of the prescribed displacements as well as the amount of the cyclic vertical part depend on various factors, such as the pile diameter, the penetration depth of the pile, soil

properties, vibrating frequency, etc. Nevertheless, the main aim of the investigation is to see how the soil behaves under the cyclic loading which results from the vibrating process at certain depth of the pile penetration. Therefore, it is recommended to apply the total amount horizontal and vertical components equal to $0.25D$ (10 cm) and $0.125D$ (5 cm) respectively in order to simulate the pile jacking process at a certain penetration depth, while the amplitude of the oscillation of the vertical part equivalent to $0.05D$ (2 cm) with respect to the simulation of the vibrating process.

6.4 Constitutive model and parameters

Once again, Baskarp sand is chosen as material set. Baskarp sand is an uniform sand, the grains are classified as angular to sub-angular with D_{50} of approximately $140\mu\text{m}$ [13]. This sand has a total unit weight of 20 kN/m^3 , and shows a strongly dilatant behaviour when prepared in a dense state [10]. The initial soil state is varied between loose and dense condition, in order to see the density dependency of the soil behaviour under cyclic loading. Consequently, the initial void ratio is selected 0.83 ($D_r = 0.26$) and 0.65 ($D_r = 0.73$) respectively.

For the hypoplastic model, all parameters are shown in Table 6.1. They were derived from laboratory tests by Elmi Anaraki [13]. Unfortunately, the intergranular strain is not included, because of numerical problems in calculation phases.

Table 6.1: Hypoplastic parameters for Baskarp sand [13]

Parameters	φ_c (o)	h_s (MPa)	n	e_{d0}	e_{c0}	e_{i0}	α	β
Values	30	4000	0.42	0.548	0.929	1.08	0.12	0.96

Furthermore, the hardening soil model is also used in the numerical simulation for a consistency check and comparison with the hypoplastic model. The material set of the hardening soil model is derived from definitions by Brinkgreve & Broere [5] using the *Soil tests* facility in Plaxis 2D, in such a way that the soil responses from the hardening soil model are similar to those obtained from the hypoplastic model (see appendix B for more detail). The parameters of the hardening soil model for Baskarp sand are suggested in Table 6.2.

Table 6.2: Estimation of hardening soil parameters for Baskarp sand

Parameters	E_{50}^{ref}	$E_{\text{eod}}^{\text{ref}}$	$E_{\text{ur}}^{\text{ref}}$	φ	ψ	m	v_{ur}	P^{ref}
Unit	(kPa)	(kPa)	(kPa)	(o)	(o)	-	-	(kPa)
Dense	40,500	50,000	121,500	37	9	0.5	0.2	100
Loose	31,000	33,000	93,000	31.3	2	0.5	0.2	100

6.5 Calculation procedures

6.5.1 Initial stresses

In Plaxis 2D, the initial stresses in the soil body are influenced by the weight of the material [5]. The initial horizontal stress is calculated from the initial vertical stress by using K_0 procedure ($K_0 = 1 - \sin\phi$). Furthermore, the water level is also selected at the ground surface level to make fully saturated soil mass.

Once again, for the hypoplastic model the void ratio is a state variable which is dependent on the pressure level. Therefore, after the initial stresses are generated, the void ratio in the soil body varies according to Bauer's formula referred in Chapter 3. In the analysis, the stress level at middle cross-section (A-A) of the geometry is chosen to define the initial void ratio. As a result, the initial void ratios at zero pressure using in Plaxis 2D are 0.838 and 0.657 in order to get the loose and dense states after generating the initial stresses.

6.5.2 Calculation phases

This phase is applied directly after the initial phase. All calculation phases are carried out under drained analysis. Firstly, the distributed load at the top is activated while all displacements from the initial phase are reset to zero. Then the horizontal (Δu_x) and vertical (Δu_y) prescribed displacements are applied simultaneously at pile-soil boundary to simulate the installation effect of the pile jacking process as discussed in the Chapter 5. In these phases, the check box "*reset displacement to zero*" is not activated. To avoid a big distortion of the mesh in a phase, the horizontal and vertical prescribed displacements are increased step by step, and they reach the magnitude of 0.25D (10 cm) and 0.125D (5 cm) respectively after 5 phases. Next, the effect of cyclic loading is simulated by cycling the vertical component whilst keeping the horizontal component from previous phases. As chosen, the amplitude of the oscillation of the vertical part equivalent to 0.05D (2 cm). Two transitional points (point 4 and 5) are also added at the pile-soil boundary in order to avoid a big distortion of the mesh at the corners when applying the vertical prescribed displacements. Therefore, the horizontal and vertical components are applied at two transitional points (point 4 and point 5), while two remaining points (point 0 and 3) are only applied horizontal component (Fig. 6.2). The magnitudes of the prescribed displacements are given in Table 6.3.

Table 6.3: Calculation phases in numerical simulation

Phase order	Point 4 & 5		Point 0 & 3		Note
	Δu_x (cm)	Δu_y (cm)	Δu_x (cm)	Δu_y (cm)	
1	0	0	0	0	Distributed load
2	2	1	2	0	Jacking phase
3	4	2	4	0	Jacking phase
4	6	3	6	0	Jacking phase
5	8	4	8	0	Jacking phase
6	10	5	10	0	Jacking phase
7	10	3	10	0	1st unloading
8	10	5	10	0	1st reloading
9	10	3	10	0	2nd unloading
10	10	5	10	0	2nd reloading
11	10	3	10	0	3rd unloading
12	10	5	10	0	3rd reloading
13	10	3	10	0	4th unloading
14	10	5	10	0	4th reloading

6.6 Result and discussions

Herein, the results of the loose and dense cases for the hypoplastic and hardening soil models will be analyzed and compared, then validated with the findings from previous studies [18, 37]. To quantify the installation effect around the pile, stresses and void ratio distribution at the middle cross-section of the geometry (cross section A-A, see Fig. 6.1) will be chosen.

6.6.1 Dense case

6.6.1.1 After jacking process

Fig. 6.5 plots the void ratio distribution at cross-section A-A after jacking phases (phase 6 in Table 6.3). In the hypoplastic model, the void ratio is taken directly from the output while in the hardening soil model the void ratio is calculated from the volumetric strain. As can be seen, the void ratio distributions are almost the same for the hardening soil and hypoplastic models after jacking phases. They also demonstrate a decrease of the void ratio when going far away from the pile shaft and create a shear zone close to the pile shaft until a distance of $2D$. On the one hand, both models also show a compaction zone between the distance of $4D$ and $8D$ but the degree of the compaction is very small

because the soil mass is in an initially dense state. On the other hand, the void ratio in the hardening soil model is little higher than those in the hypoplastic model after jacking phases, this can be explained by not completed compatibility of model parameters.



Fig. 6.4: Visualisation of void ratio distribution after jacking phases (phase 6) for HP

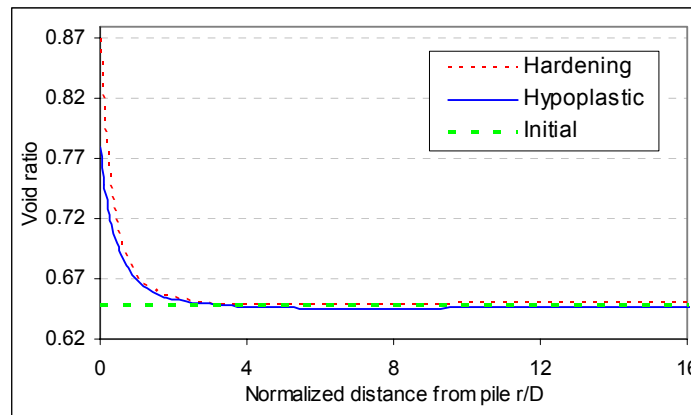


Fig. 6.5: Void ratio distribution after jacking phases (phase 6) at cross AA

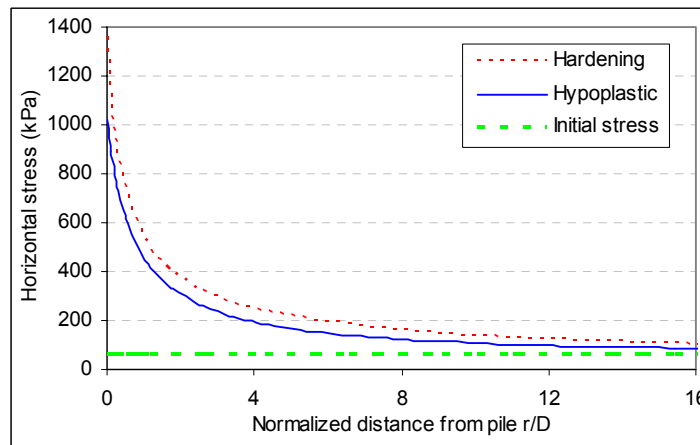


Fig. 6.6: Horizontal stress distribution after jacking phases (phase 6) at cross AA

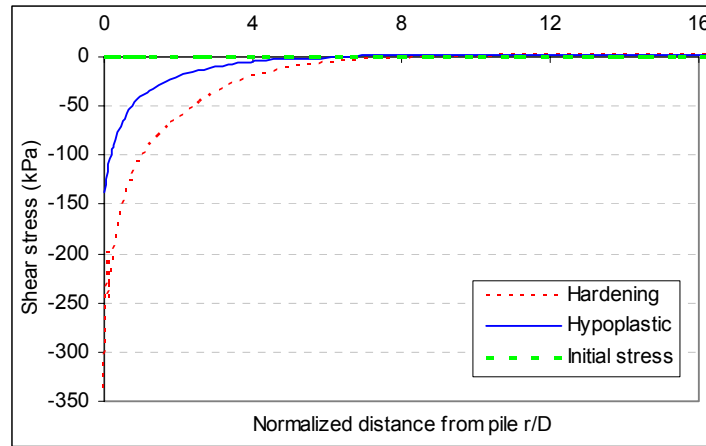


Fig. 6.7: Shear stress distribution after jacking phases (phase 6) at cross AA

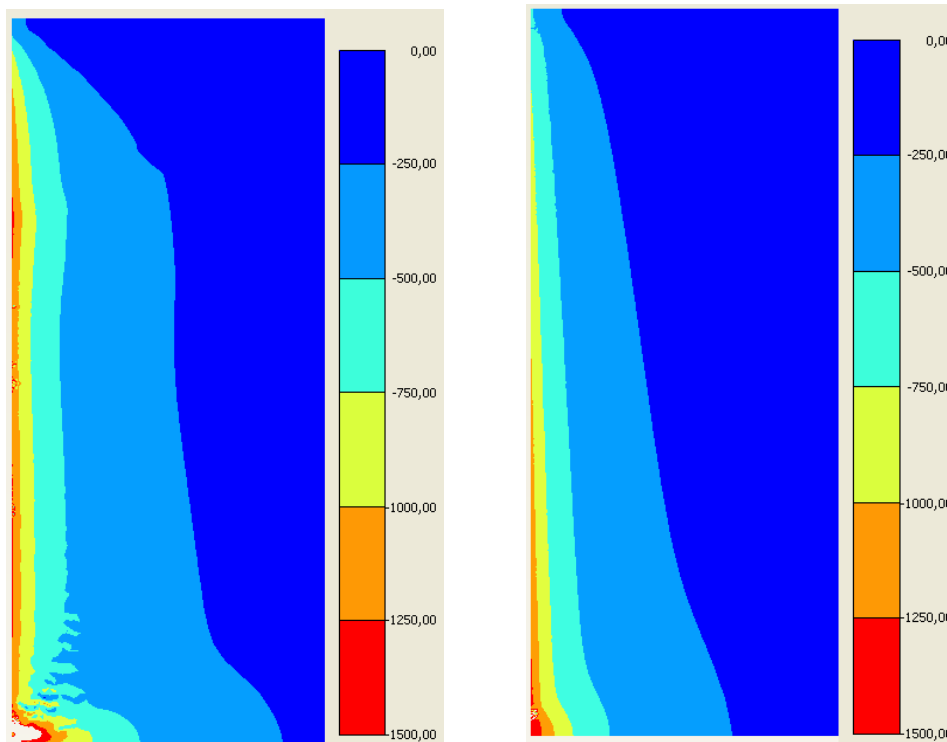


Fig. 6.8: Visualisation of horizontal stresses distribution after jacking phases (phase 6) for HS (left) and HP (right)

In terms of the horizontal stress distribution, the numerical results from the hardening soil and hypoplastic models can be similar. They display an increase along the depth and a decrease far way from the pile. But numerical problems appear at the pile corner with the high concentration of tresses. This could be due to a large displacement and big distortion at the pile corner that does not totally incorporate the numerical scheme in Plaxis 2D. For both models, the influenced zone in which the

horizontal stress increases considerably is until 4 times the diameter of the pile (Fig. 6.6). At a further distance, the horizontal stress is close to the initial one. However, the hardening soil model gives a higher values of σ_{xx} than those from the hypoplastic model, approximately 40÷50 kPa in average, as the hardening soil model has a higher void ratio as explained before. This discrepancy leads to an increment of the shear stress for HS model in comparison with HP model (Fig. 6.7)

6.6.1.2 After cyclic loading process

For the hypoplastic model, after the cyclic loading it can be seen that the void ratio increases close the pile-soil boundary ($r < 0.2D$) due to an increase of the volumetric strain caused by increasing of the prescribed displacements at the pile-soil boundary whilst further away until a distance of 3 times the diameter of the pile the soil is compacted. This compaction appears in both the reloading and unloading phases. Because of this compaction resulting from the continuous cyclic shearing, the horizontal stress substantially reduces in the compaction zone, from the maximum value of 1000 kPa after jacking phases to 80 kPa after 3 cycles. Furthermore, the vertical stress also declines quickly, much more below the initial stress line, which is accompanied by a reduction in the void ratio. Also, the shear stress degrades rapidly because of the reduction of the void ratio due to cyclic loading. It can be seen that more cycles of cyclic loading leads to a higher reduction of stresses and void ratio. Promisingly, this phenomenon fits quite well with the soil response in reality caused by cyclic shearing (see Fig. 6.9 to Fig. 6.12 in more detail).

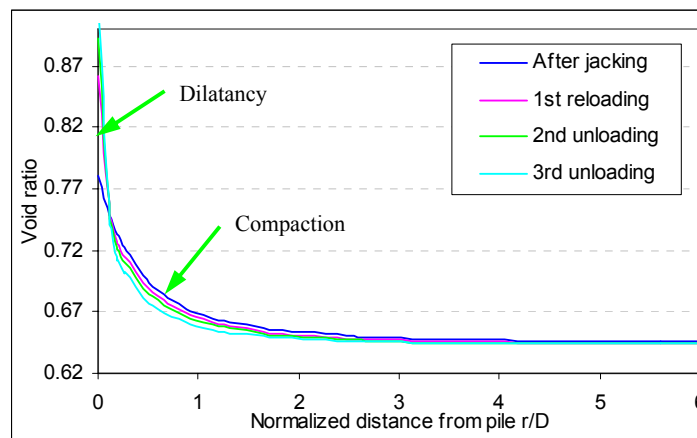


Fig. 6.9: Void ratio distribution at cross AA after cyclic loading for HP

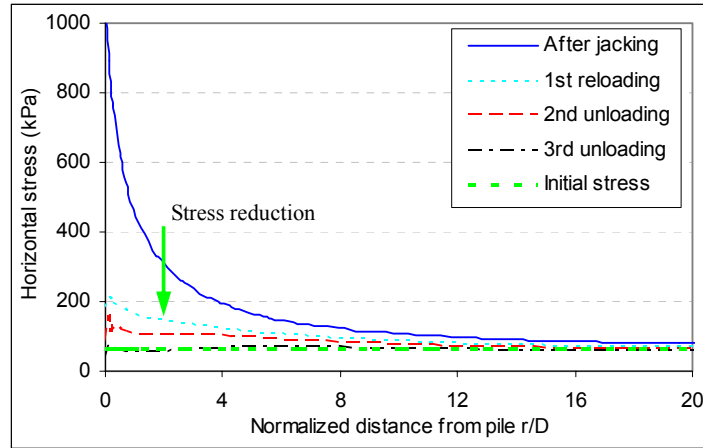


Fig. 6.10: Horizontal stress reduction at cross AA after cyclic loading for HP

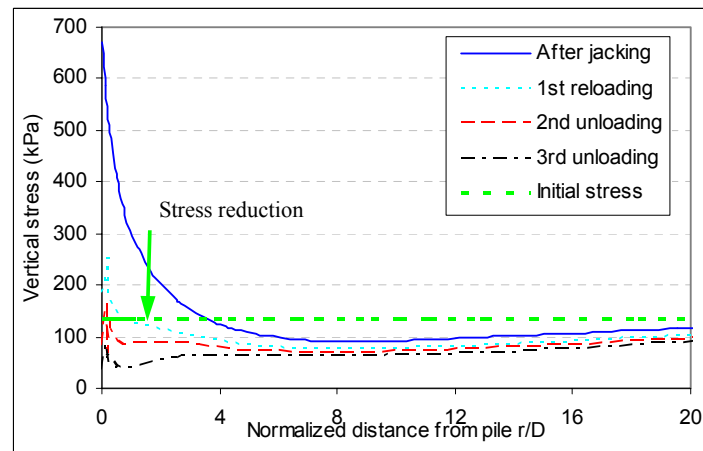


Fig. 6.11: Vertical stress reduction at cross AA after cyclic loading for HP

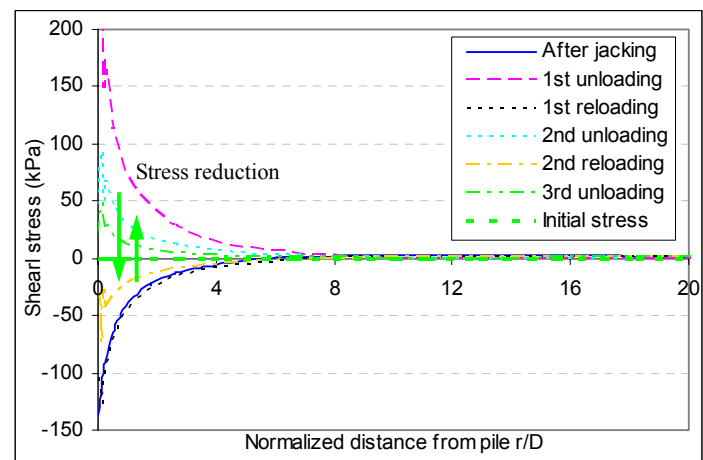


Fig. 6.12: Shear stress reduction at cross AA after cyclic loading for HP

On the other hand, the hardening soil model shows a different behaviour after cyclic loading phases. Evidently, the void ratio distribution does not change after cyclic loading except these points extremely close to the pile-soil boundary ($r < 0.2D$). Therefore, a compaction due to the cyclic loading does not incorporate in the hardening soil model. As a result, there is no reduction of the horizontal stress can be found in this model. Surprisingly, the vertical stress displays an increase and keeps this high stress after cyclic loading, this phenomenon happens reversely in comparison with the hypoplastic model. The shear stress also keeps a high stress level in cyclic loading. This could be explained by the limitations of the model itself, the HS model is an isotropic hardening model so it dilates continuously and does not incorporate the softening behaviour due to dilatancy and cyclic loading, (see Fig. 6.13 to Fig. 6.16).

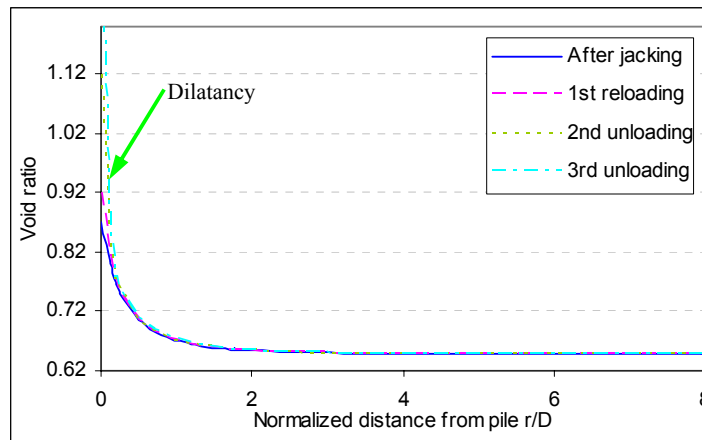


Fig. 6.13: Void ratio distribution at cross AA after cyclic loading for HS

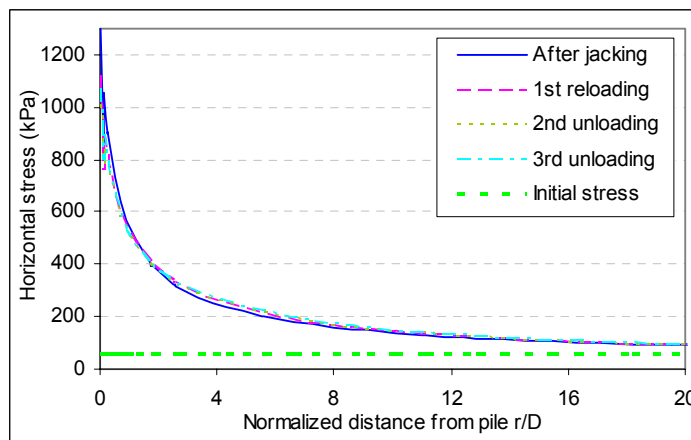


Fig. 6.14: Horizontal stress distribution at cross AA after cyclic loading for HS

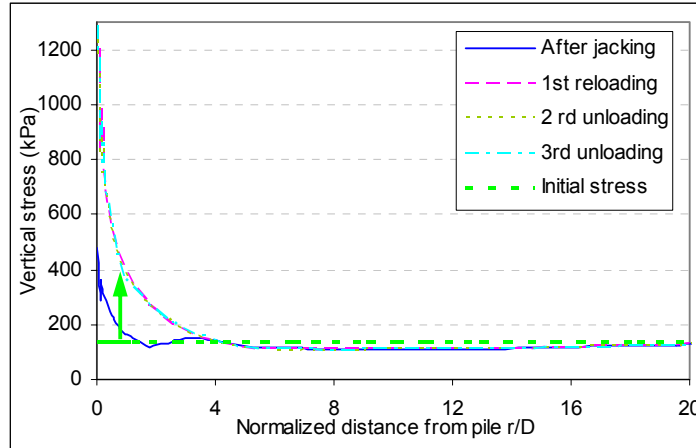


Fig. 6.15: Vertical stress distribution at cross AA after cyclic loading for HS

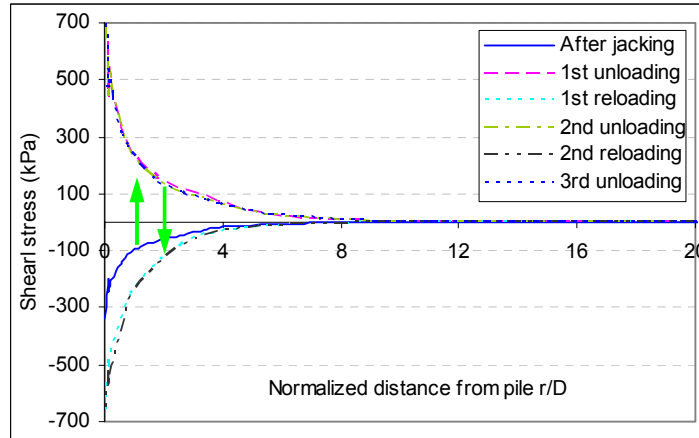


Fig. 6.16: Shear stress distribution at cross AA after cyclic loading for HS

For more evidently, several points at the cross section A-A (see Fig. 6.4 for more detail) are chosen to see the change of stresses and void ratio due to the cyclic loading process. The first point is located at pile-soil boundary (Point A, $r_A = 0$), the second and the third points are further away from the pile shaft, (Point B, $r_B = 0.2D$ and Point C, $r_C = 0.5D$). Fig. 6.17 displays how the soil behaves around the pile due to the installation effects including the jacking and cyclic loading phases for the HP model. Clearly, for initially dense sand the zone which is close to the pile shaft ($r < 2.0D$) dilates during the jacking phases which is accompanied by an increase of mean stress and void ratio. Subsequently, the void ratio evolution of three points (A, B and C) is mostly similar in the jacking phases. However, the soil behaves differently in cyclic loading whereas the void ratio at point C decreases as the illustration of the compaction due to cyclic loading. No compaction can be found at point A and B, the void ratio at point B mostly doesn't change while the void ratio at point A continues to rise and

reaches the critical state after some cycles. This fact is caused by an increase of the volumetric strain due to applying the prescribed displacement at pile-soil boundary.

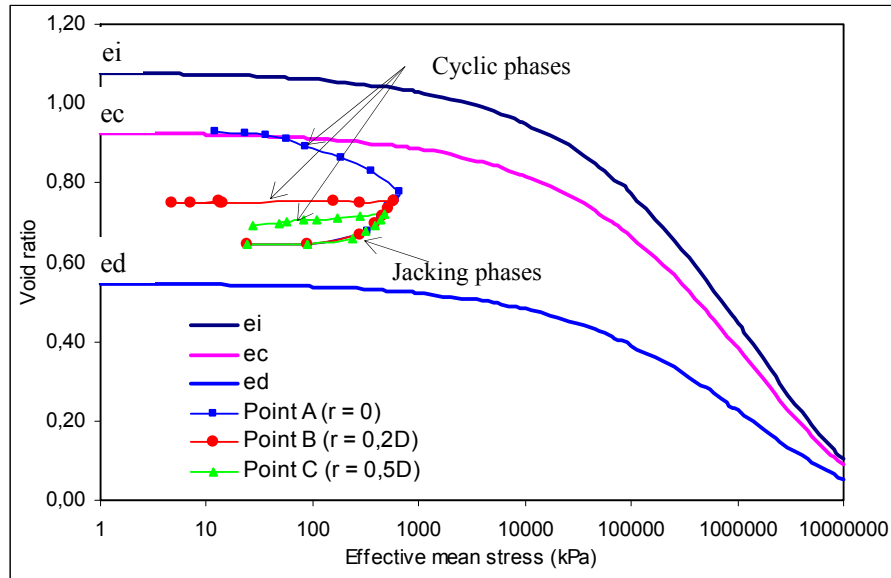


Fig. 6.17: Void ratio evolution at several points at cross AA for HP, point locations given in Fig. 6.4

For the HP model, the stress reduction due to the cyclic loading is illustrated in Fig. 6.18 and Fig. 6.19 where the point C is chosen. During the jacking phases, the soil dilates causing an increase of the soil volume, consequently the stresses rise significantly. Nevertheless, all stresses degrade quickly in the cyclic phases because the soil is compacted. After some cycles the stresses reduce to nearly zero, the soil reaches an isotropic state, and then the calculation phase will finish since several points in the soil mass reach critical state.

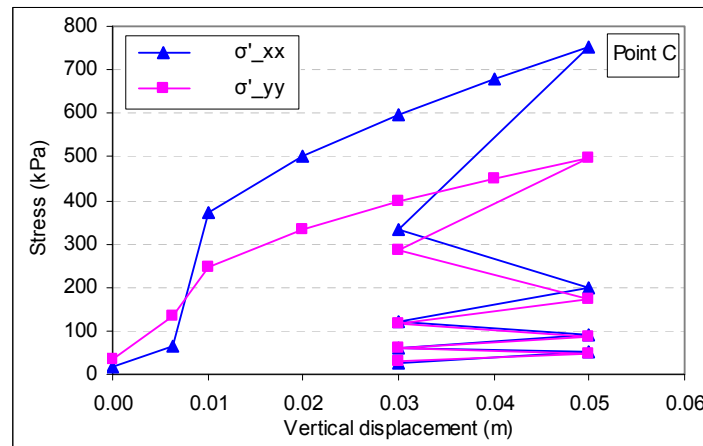


Fig. 6.18: Horizontal and vertical stresses reduction at point C for HP

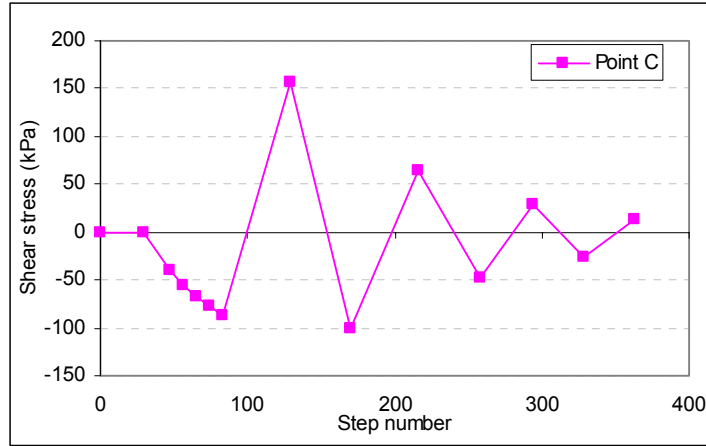


Fig. 6.19: Shear stress reduction at point C for HP

On the other hand, for the HS model the void ratio evolution at point B and C exhibit differently in comparison with the HP model. They always dilate in both jacking and cyclic phases. In the cyclic phase, the dilatancy is much larger with the points close to the pile-soil boundary. This fact can be explained by the capacity of HS model itself which is mentioned before. As a result, no reduction of stresses at point C appears whereas the vertical, horizontal and shear stresses always stay at high level (see Fig. 6.20 to Fig. 6.22 in more detail).

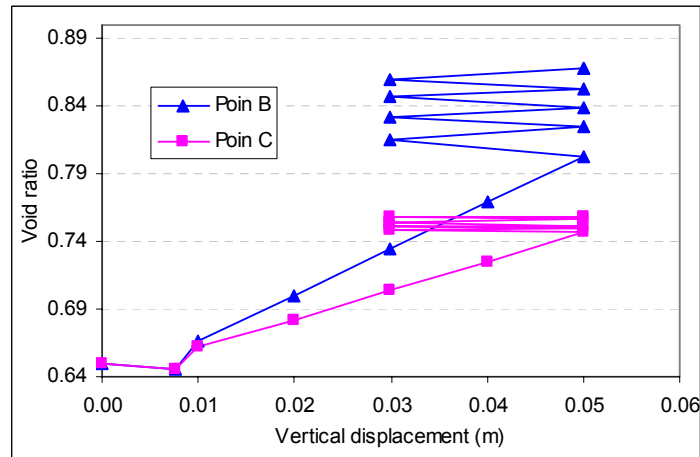


Fig. 6.20: Void ratio evolution at several points for HS, point locations given in Fig. 6.4

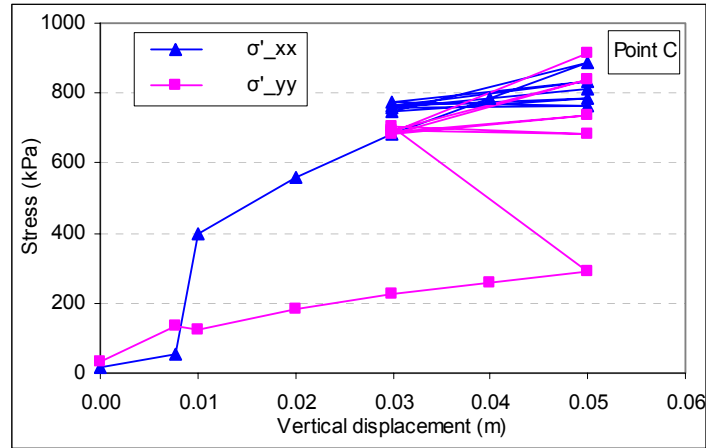


Fig. 6.21: Horizontal and vertical stresses developments at point C for HS

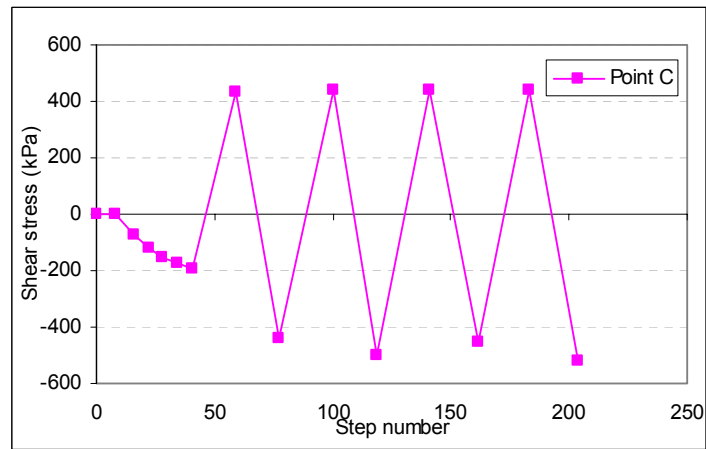


Fig. 6.22: Shear stress development at point C for HS

6.6.2 Loose case

6.6.2.1 After jacking process

When the same amounts of prescribed displacements are applied at the pile-soil boundary as the dense case, similar results can be found. The tendency of the void ratio and stresses are mostly the same as mentioned in the dense case for both the hypoplastic and hardening soil models. One exception is a wider compacted zone after the jacking phase between the distance of 1D and 10D, this can be explained by an initially loose state of the soil so that the soil body has more the pore volume than the dense case. The degree of this compaction is also much higher than the dense case (Fig. 6.24). Furthermore, the magnitude of stresses after the jacking phase is also smaller compared to the dense case.

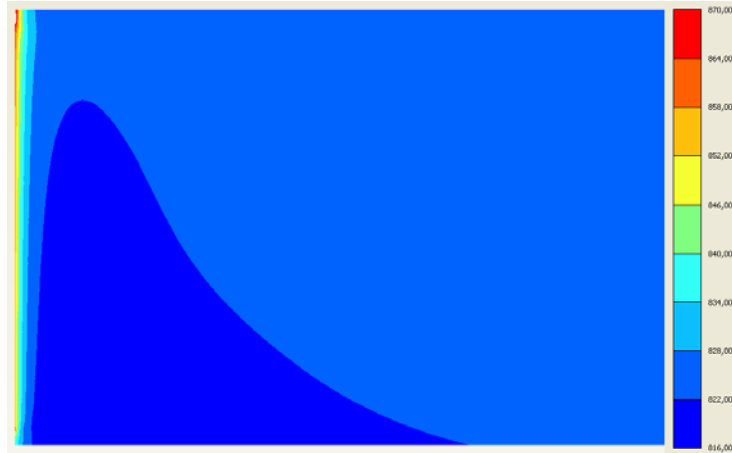


Fig. 6.23: Visualisation of void ratio distribution after jacking phase (phase 6) for HP

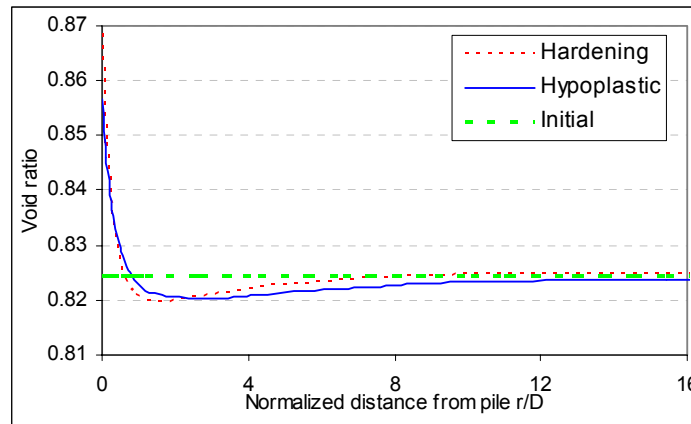


Fig. 6.24: Void ratio distribution after jacking phase (phase 6) at cross AA

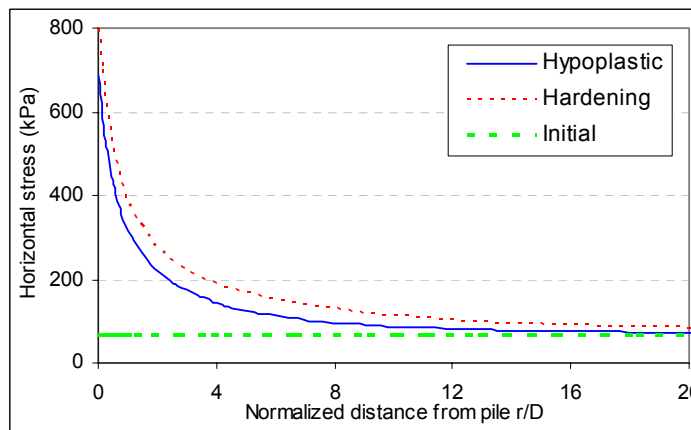


Fig. 6.25: Horizontal stress distribution after jacking phase (phase 6) at cross AA

6.6.2.2 After cyclic loading process

It can be seen that the mechanism of the soil around the pile after the cyclic loading for the loose sand exhibit similarly to those for the dense sand for both the HP and HS model. For the hypoplastic model, the void ratio increases close the pile-soil boundary ($r < 0.2D$) due to dilatancy as explained before while further away until the distance of 5 times the diameter of the pile the soil is compacted. This compaction is much more evident than in the dense case, in particular up to the distance of $2D$. The more cycles leads to the movement of compaction zone to the pile. Because of this compaction resulting from the continuous cyclic shearing, the stresses around the pile also decrease as for the dense case (see Fig. 6.26 to Fig. 6.29 for more detail)

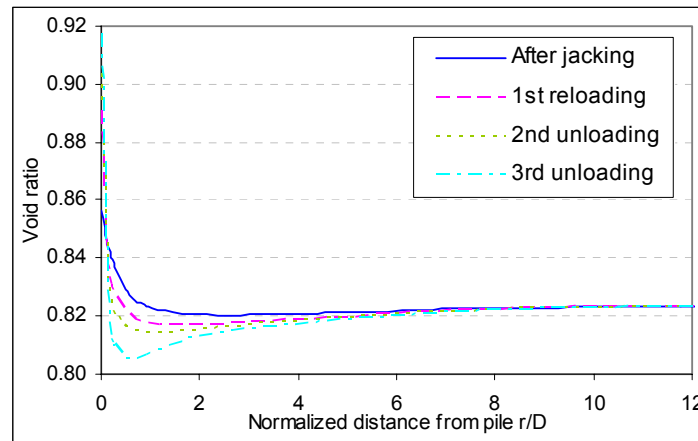


Fig. 6.26: Void ratio distribution at cross AA after cyclic loading for HP

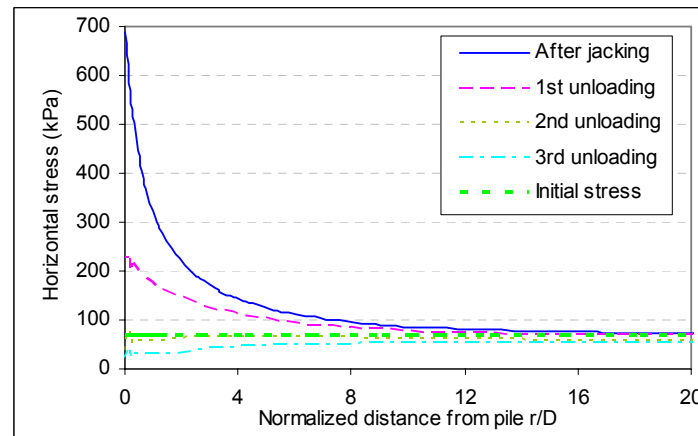


Fig. 6.27: Horizontal stress reduction at cross AA after cyclic loading for HP

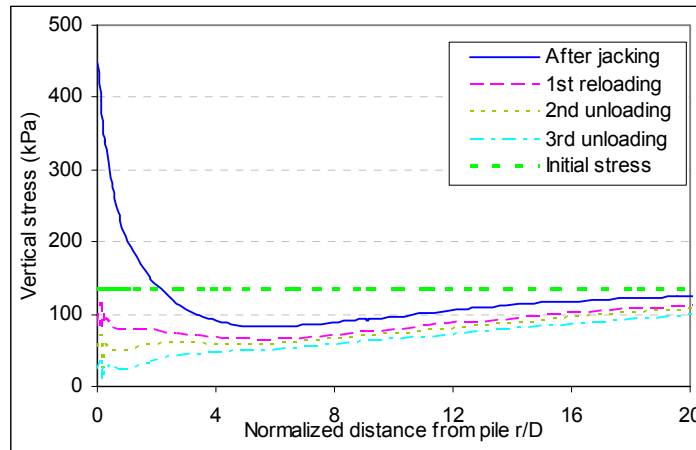


Fig. 6.28: Vertical stress reduction at cross AA after cyclic loading for HP

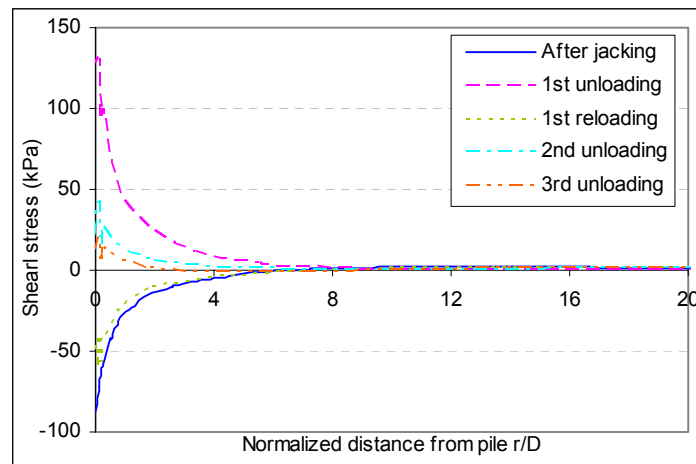


Fig. 6.29: Shear stress reduction at cross AA after cyclic loading for HP

Conversely, for the HS model the void ratio distribution does change after the cyclic loading except these points extremely close to the pile-soil boundary ($r < 0.2D$). It means that a compaction due to the cyclic loading does not appear in the hardening soil model. Consequently, no reduction of the horizontal stress can be found as in the hypoplastic model. This can be explained by the limitation of the model itself as mentioned before.

The effects of cyclic loading can be seen clearly in the Fig. 6.34, whereas the evolution of point A ($r_A = 0$) and point C ($r_C = 0.5D$) are plotted. Once again, the dilatancy occurs at the zone close to the pile shaft in both jacking phases and cyclic phases. This is confirmed by an increase of the void ratio at the point A in the whole processes. However, at a distance from the pile shaft the compaction appears leading to a decrease of the void ratio at point C during cyclic loading phases.

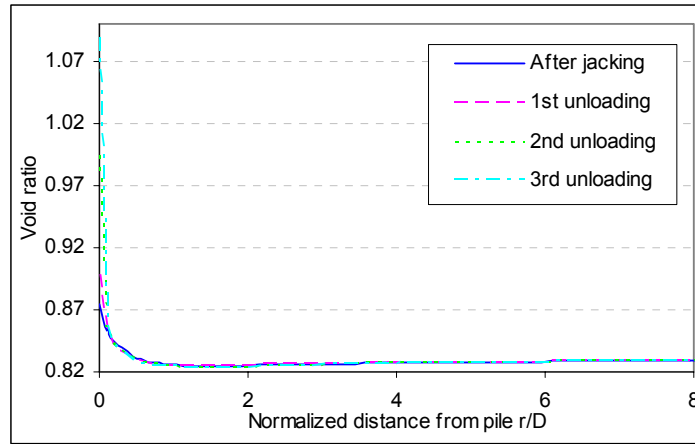


Fig. 6.30: Void ratio distribution at cross AA after cyclic loading for HS

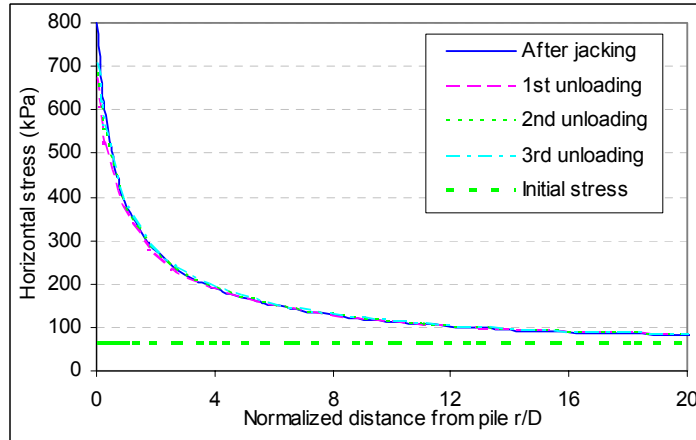


Fig. 6.31: Horizontal stress distribution at cross AA after cyclic loading for HS

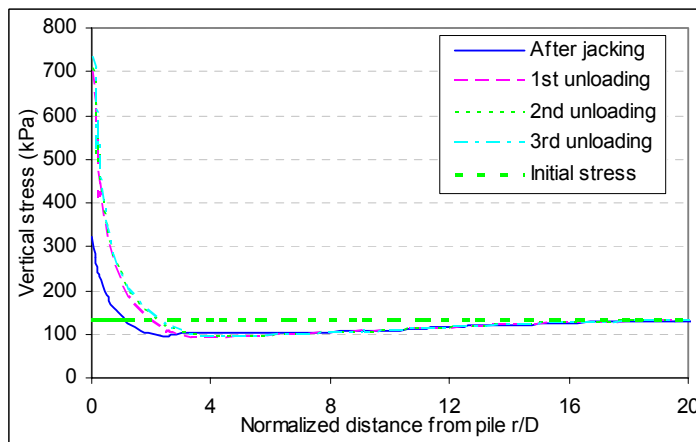


Fig. 6.32: Vertical stress distribution at cross AA after cyclic loading for HS

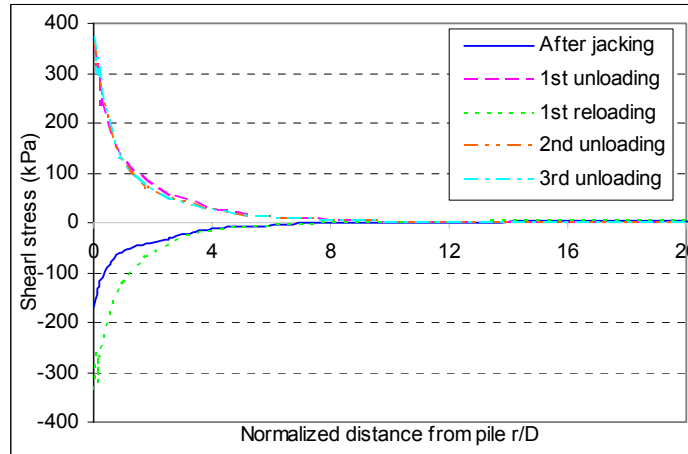


Fig. 6.33: Shear stress distribution at cross AA after cyclic loading for HS

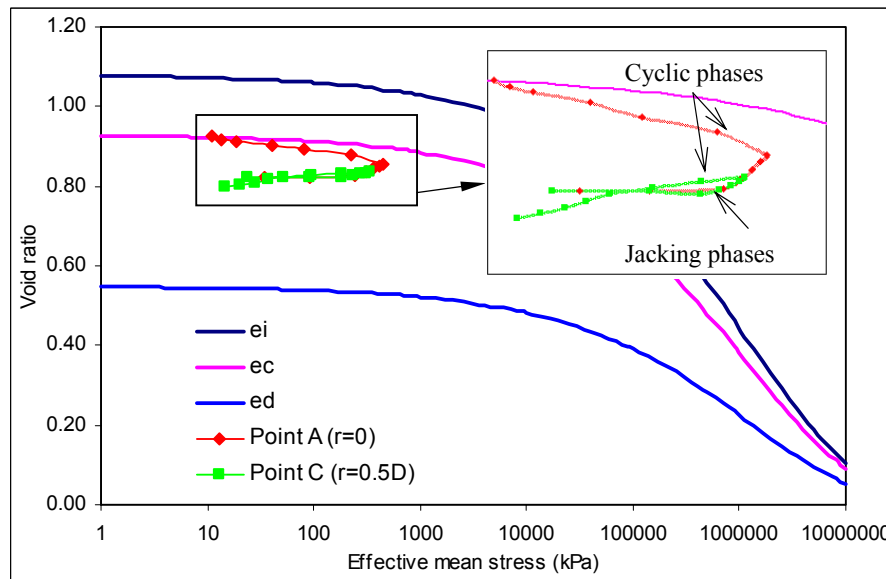


Fig. 6.34: Void ratio evolution at several points at cross AA for HP, point locations given in Fig. 6.4

6.6.3 Modelling of shearing effect

Herein, the development of the shear stress is investigated. The effect of cyclic loading is also considered. Similar to the previous chapter, the shearing process is simulated by increasing the vertical prescribed displacement at the pile shaft while keeping the horizontal component from previous phases. This process is applied after jacking phase and after few cycles of cyclic loading. At the end of this process, the shear strength of the soil is equal to the shear stress.

The developments of the shear stress at a point close to the pile shaft (point A) are plotted in Fig. 6.35. As can be seen, when the shearing processes are applied directly after jacking phases, the similar results are found compared with Chapter 5. During the shearing phases, the shear stress increases enormously at the beginning then decreases steadily until failure.

However, when the cyclic loadings are included, no increase of the shear stress during the shearing phases could be found. It always decreases until failure. Importantly, the soil strength at failure is also decreased due to the effect of cyclic loadings, more cycles of cyclic loading leads to a larger decrease of the soil strength. By the simplified simulation, the peak strength decreases by 38% and 60% whilst the residual strength decreases by 26% and 48% after 1 and 2 cycles respectively.

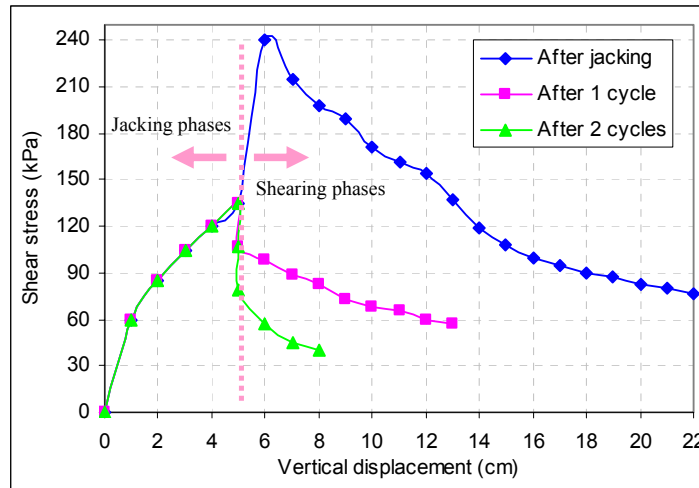


Fig. 6.35: Shear stress development during shearing process

6.7 Conclusion

This chapter investigates the soil behaviour of Baskarp sand under cyclic loading using the FEM with Plaxis 2D whereas the hardening soil and hypoplastic model without the intergranular strain are used. The installation effect of the cyclic loading in the vicinity of the pile shaft is simply modelled. First, the horizontal and vertical prescribed displacements are applied at the pile shaft in order to simulate the pile jacking process, subsequently the vertical component is cycled while keeping the horizontal component. The development of stresses and void ratio around the pile are utilized to evaluate the capacities of both soil models.

Generally, both models show a similar soil behaviour after the jacking process. It means that they both demonstrate a decrease of the void ratio when going far away

from the pile shaft and create a shear zone close to the pile shaft until a distance of $2D$. Moreover, both models also show a compaction zone between the distance of $4D$ and $8D$ but the degree of compaction is higher when the soil mass is in an initially loose state. Subsequently, the stress distribution of both models display an increase over the depth and a decrease far way from the pile shaft. Of course, the dense state has higher stresses than the loose state.

However, after the cyclic loading phases the results are completely different. For the HS model, the void ratio distribution does not change after cyclic loading except these points extremely close to the pile-soil boundary ($r < 0.2D$). It means that a compaction due to cyclic loading does not appear which leads to the no reduction of stresses. The reasons could be related to model itself since the HS model is an isotropic hardening model so it dilates continuously and does not incorporate the softening behaviour due to dilatancy and cyclic loading.

Promisingly, after the cyclic loading the HP model without the intergranular strain shows that the void ratio increases close to the pile-soil boundary ($r < 0.2D$) caused by an increase of the volumetric strain due to applying the prescribed displacements, while further away until a distance of 5 times the diameter of the pile the soil is compacted. The amount of this compaction depends on the initial state where the loose state displays the higher compaction. Because of this compaction resulting from the continuous cyclic shearing, the stresses degrade quickly. This phenomenon fits quite well with the soil response in reality [26] caused by cyclic shearing and the findings from prior studies [18, 37].

Lastly, the effect of cyclic loading and shearing process on the soil behaviour is also investigated. The results show that the soil strength at failure decreases due to the effect of cyclic loading, more cycles of cyclic loading leads to a bigger decrease of the soil strength. The reductions of 38% & 60% for the peak strength and 26% & 48% for the residual strength could be found after 1 and 2 cycles respectively.

Chapter 7

Conclusions and Recommendations

7.1 General

The installation effect of driven piles in sand, with respect to different installation methods is investigated by using the finite element method in Plaxis 2D. The soil is modelled with the hypoplastic model with and without the intergranular strain formulation.

7.2 Conclusions

7.2.1 Hypoplasticity

In this study, the hypoplastic model formulated by Von Wolffersdorff is chosen to model the soil. The constitutive law is given in the rate form, the stress rate is a function of the stress tensor, the current void ratio and the strain rate as $\dot{\mathbf{T}} = \mathbf{F}(\mathbf{T}, e, \mathbf{D})$. This property makes the hypoplastic model quite suitable for modelling the installation effect of driven piles, whilst the continuously changing of soil density is taken into account by the state variable-the void ratio. The model also accounts for stress-dependency and

density-dependency of stiffness and strength. The softening behaviour is included in this model to overcome the limitation of the hardening soil model (Chapter 4). In particular, the excessive accumulation of deformations in the region of small stress cycles of the hypoplastic model by Von Wolffersdorff is overcome by the introduction of intergranular strain. When the intergranular strain is included, the current stiffness is controlled by the direction of strain rates and the recent history of deformation.

From the simulation it can be concluded that, the initial void ratio (e_0) controls the soil behaviour as it is a state variable in the hypoplastic model. A reduction of the void ratio leads to a significant increase of stiffness and strength. A stronger dilatancy also occurs with a reduction of the initial void ratio.

Among other hypoplastic parameters, φ_c , e_{c0} , and e_{d0} have a significant influence on the soil response in triaxial tests. The parameters e_{i0} and β include only very small effects in terms of the initial stiffness. On the other hand, the exponent n has a huge influence on oedometer tests, followed by e_{d0} , e_{i0} , h_s and β , while the exponent α and e_{c0} have only slight effects on the stiffness at high stress level.

Finally, the influence of intergranular strain parameters is only found at very small strain and high pressure. An increase of β_r leads to a decrease of the initial stiffness and delays the occurrence of the dilatancy behaviour but does not have an influence on the magnitude of the dilatancy angle. In the oedometer test, an increase of β_r also results in a decrease of the modulus at high stress level. On the other hand, the influences of the parameter χ on the soil response are reversed in comparison with the parameter β_r .

7.2.2 Modelling of pile jacking

In this part, a procedure is proposed to simulate the pile installation process in Plaxis 2D, which based on the suggestions as showed by previous authors [6], where the installation effect is taken into account by applying the prescribed displacements at the pile-soil boundary. A centrifuge pile test [10] is chosen in order to validate the numerical simulation. In the centrifuge test, the pile has an initial embedment length of 205 mm into the sand, subsequently it is hydraulically jacked a further 200 mm into the soil body. As a result, different prescribed displacements are applied at the pile-soil boundary as mentioned in Section 5.3.2. The hypoplastic model formulated by Von Wolffersdorff with the intergranular strain is used in all analyses. The hypoplastic parameters are derived from laboratory tests [13], while the intergranular strain parameters are estimated as shown in Section 5.3.3.

The numerical simulation is performed in an axisymmetric mesh. The representative pile diameter and length are 0.5 m and 14 m, respectively. As it is confirmed that impossible to model completely the pile installation process, in which the

pile is jacked continuously from the surface to its final installation depth in Plaxis software [6]. Hence, the installation effect is model after the pile is jacked until the final depth of the penetration.

For initially medium dense Baskarp sand ($e_o = 0.709$), the numerical results fit very well with the centrifuge test results when the magnitudes of the horizontal and vertical displacements applied at the pile shaft are 18 cm (72% radius of the pile) and 8 cm (32% radius of the pile) respectively while the vertical displacement applied at the pile tip to be 74 cm (10.6% the length of the jacked pile).

The numerical results show that the void ratio increases along the pile shaft until the distance of approximately 1.0 to 1.5 times the diameter of the pile, making a shear band as similarly mentioned by previous authors [8],[18]. At a distance from the pile shaft, the soil body is compacted leading to a decrease of the void ratio. The highest degree of compaction is located near the pile tip.

On the other hand, the horizontal stress decreases by moving far away from the pile. A significant increase of the horizontal stress can be found until a distance of more than 5D. Besides, there is also an increase of the horizontal stress leading to an increase of the shear stress along the pile shaft. These stress distributions are similar to the measurements as shown in [37].

From the sensitivity analyses, it can be concluded that the void ratio at the pile shaft linearly increases accompanied by a rise of either the horizontal or vertical displacements at the pile shaft. Also the effective vertical stress at the pile tip increases when rising this vertical component, and decreases when increasing this horizontal component. However, the horizontal displacement applied at the pile shaft shows a stronger influence than the vertical displacement. This finding is also similarly mentioned in [6].

The same amount of the prescribed displacements as for medium dense sample are also applied for dense and loose samples. It is possible to conclude that there could be a relation between the amount of the prescribed displacements applied at the pile-soil boundary and the initial soil condition (e.g. the relative density). The higher relative density leads to a higher prescribed displacement applied at the pile tip but smaller prescribed displacement at the pile shaft.

Finally, the effect of the shearing process adjacent to the pile shaft is investigated by increasing the vertical component at the pile shaft while keeping the horizontal component from jacking phases. The results show that both the horizontal and shear stress decrease during the shearing phases, but the magnitude of the horizontal stress reduces by 80% while only 9% can be found for the shear stress. Especially, only the friction reduction factor $R = 0.87$ and 0.82 could be found at peak state and at failure respectively. This finding could be investigated further in order to apply in the calculation of the bearing capacity of driven piles.

7.2.3 Modelling of cyclic loading

Based on the previous procedure for modelling the installation effect of driven piles, a simplified procedure is used in order to investigate the cyclic loading effect near the pile shaft. Only a part of a pile is considered due to the difficulty in the modelling of the full pile. First, the horizontal and vertical prescribed displacements are applied at the pile-soil boundary to simulate the pile jacking process, subsequently the vertical component is cycled whilst keeping the horizontal component. The hypoplastic model formulated by Von Wolfferdorff without the intergranular strain is used, since the limitation of the existing numerical scheme for the use of the intergranular strain. The hardening soil model, where the parameters are derived from the hypoplastic model, has also been used for evaluating the capacities of both soil models.

Generally, both models show similar results after the jacking process. An increase of the void ratio resulting in a shear zone close to the pile shaft and a compaction at a distance from the pile is observed. Moreover, the horizontal stress distribution of both models display an increase over the depth and a decrease far way from the pile shaft.

However, the soil behaves differently during cyclic loading. For the hardening soil model, the void ratio distribution does not change after cyclic loading except for the points extremely close to the pile-soil boundary ($r < 0.2D$). No compaction is found from cyclic loading. As a result, no reductions of stresses are found either.

On the other hand, for the hypoplastic model a compaction occurs at a distance from the pile shaft. More loading cycles lead to more compaction of the soil. The initially loose state displays the highest compaction. This compaction results from continuous cyclic shearing, therefore the stresses degrade quickly. This phenomenon fits quite well with the soil response found in reality [26] caused by cyclic shearing and the findings from prior studies [18, 37].

Finally, the effect of cyclic loading on the soil strength is also investigated. The results show that the soil strength at failure is also decreasing due to cyclic loading, more loading cycles leads to a larger reduction of soil strength at failure. The reductions of 38% & 60% for the peak strength and 26% & 48% for the residual strength could be found after 1 and 2 cycles respectively.

7.3 Recommendations

The hypoplastic model with intergranular strain is suitable for the modelling of driven piles. The current simulations performed without the intergranular strain formulation shows the reasonable results for the cyclic loading. However, future studies should incorporate the intergranular strain. Furthermore, the influence of the number of cycles and the amplitude of the oscillation on the stress reduction and soil compaction could be also considered.

In these analyses, a zone near the pile is refined by reducing the *Local element size factor* in Plaxis 2D. Further studies could consider the influence of the finite element meshes (i.e. fine mesh or coarse mesh) on the numerical results.

Additional numerical simulations should incorporate the experimental results, to investigate a possible relation between the amount of the prescribed displacements applied at the pile-soil boundary and the penetration depth, the pile diameter and (or) the initial soil conditions (i.e. the relative density).

The current numerical simulation could be continued to evaluate the bearing capacity of driven piles in terms of the base resistance and the shaft friction. As shown in [6], after the pile installation process is modelled the pile cluster is activated then the distributed load applied at the pile head is increased until failure, in order to evaluate the bearing capacity.

Finally, another procedure could be tried in Palxis 2D to simulate the installation effect of driven piles by using the *Updated mesh* analysis. This method allows the continuous changing of the finite element mesh. In this procedure, the pile cluster is linearly increased step by step from a rectangular element, by applying the prescribed displacements around this element.

Appendix A

Estimation of intergranular strain parameters for Baskarp sand

In this part, the intergranular strain parameters for Baskarp sand are estimated. In fact, these parameters are derived by laboratory tests as given in Table 3.2. Here, the parameters for intergranular strain are simplified estimation by using the *Soil tests* facility in Plaxis 2D, in such a way that the soil responses from the hypoplastic model without intergranular strain are similar to those obtained from the hypoplastic model with intergranular strain.

As mentioned in Section 3.4, the intergranular strain includes 5 parameters. However, the increase of granular stiffness for 90° and 180° change of strain path direction by the factor m_T and m_R are usually taken the value of 2.0 and 5.0 respectively, as the “rule of thumb”. The radius of elastic range R varies between 10^{-7} and 10^{-3} , but normally is taken 10^{-4} . As a result, this section only considers the determination of parameters β_r and χ .

First, these parameters (β_r and χ) are assumed to be equal to those as for Karlsruhe sand. It means that β_r and χ have the values of 0.5 and 0.6 respectively. Then, they are corrected, based on their sensitivity to the soil response.

As can be seen in Fig. A.1, if the intergranular strain is included the initial stiffness is much higher than without the intergranular strain, and the dilatancy also occurs earlier. Moreover, the modulus is also much higher in oedometer test if the intergranular strain is included (Fig. A.2).

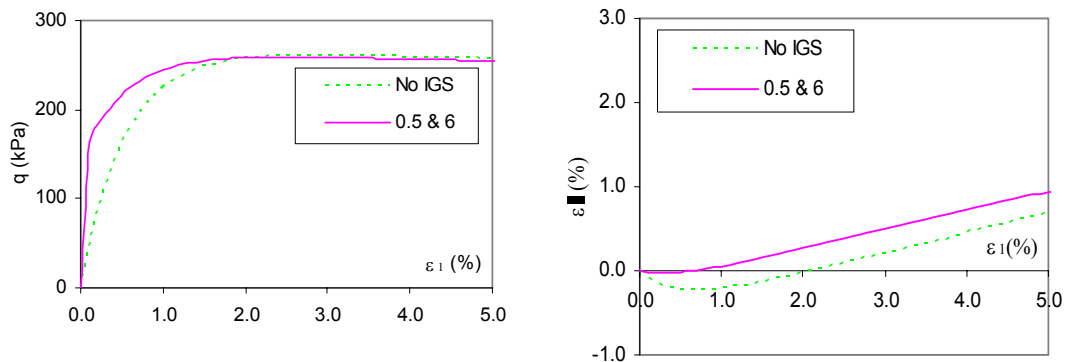


Fig. A.1: Drained triaxial tests for Baskarp sand without IGS and with IGS ($\beta_r = 0.5$ and $\chi = 6$)

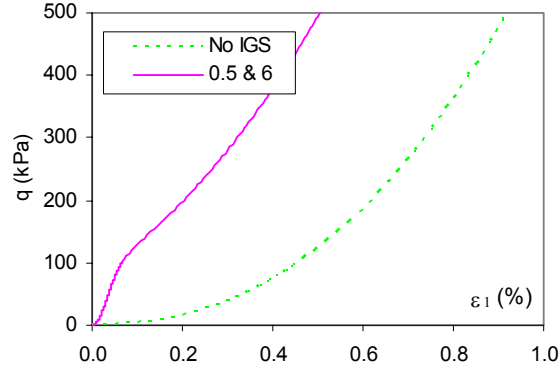


Fig. A.2: Oedometer tests for Baskarp sand without IGS and with IGS ($\beta_r = 0.5$ and $\chi = 6$)

As discussed in Section 4.4.4, an increase of β_r leads to a decrease of the initial stiffness and delays the occurrence of the dilatancy behaviour. In the oedometer test, an increase of β_r also results in a decrease of the modulus at high stress level. Therefore, the magnitude of β_r needs to be increased in order to make comparable results with the case of without the intergranular strain.

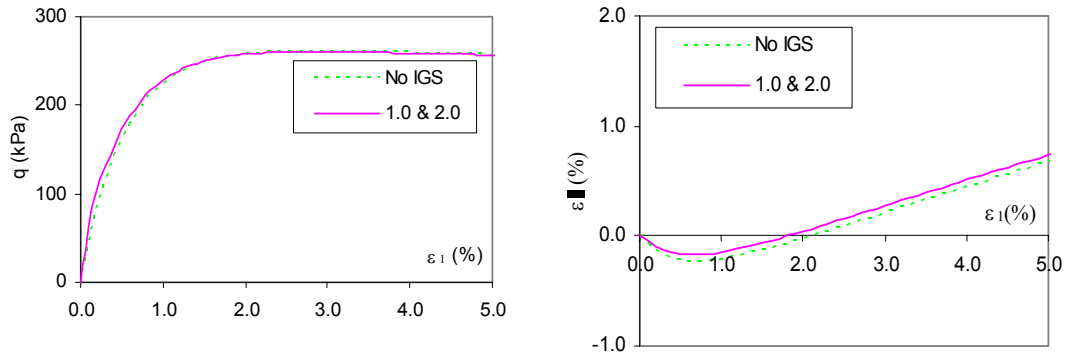


Fig. A.3: Drained triaxial tests for Baskarp sand without IGS and with IGS ($\beta_r = 1$ and $\chi = 2$)

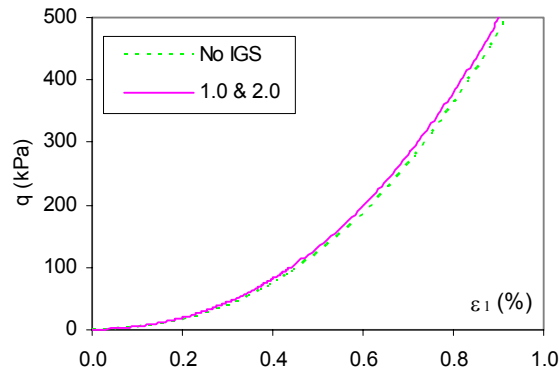


Fig. A.4: Oedometer tests for Baskarp sand without IGS and with IGS ($\beta_r = 1$ and $\chi = 2$)

On the other hand, the influences of the parameter χ on soil response are reversed in comparison with the parameter β_r . From these points, it is concluded that there should be the combination of increasing β_r and decreasing χ . After several trials, if β_r and χ have the values of 1.0 and 2.0 respectively, the soil responses from the hypoplastic model without intergranular strain fit very well with those obtained from the hypoplastic model with intergranular strain (Fig. A.3 and Fig. A.4). Finally, the intergranular strain parameters for Baskarp sand are suggested in Table A.1.

Table A.1: Estimated parameters of the intergranular strain for Baskarp sand

Parameters	m_T	m_R	R_{max}	β_r	χ
Values	2	5	0.0001	1.0	2.0

Appendix B

Estimation of Hardening soil parameters for Baskarp sand

As mentioned in Chapter 6, the hardening soil model is also used in the numerical simulation for a consistency check and comparison with the hypoplastic model. Here, the hardening soil parameter is derived from definitions by Brinkgreve & Broere [5], using the *Soil tests* facility in Plaxis 2D in such a way that the soil responses from the hardening soil model are similar to those obtained from the hypoplastic model.

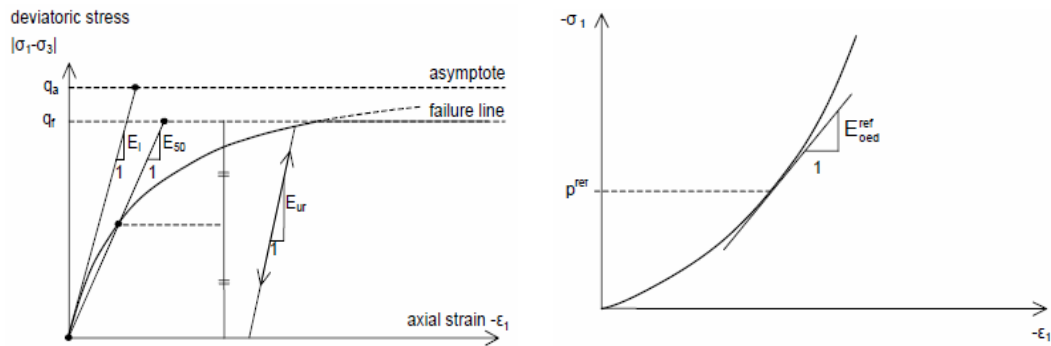


Fig. B.1: Determinations of E_{50}^{ref} , E_{ur}^{ref} , E_{cod}^{ref} , from drained triaxial and oedometer tests

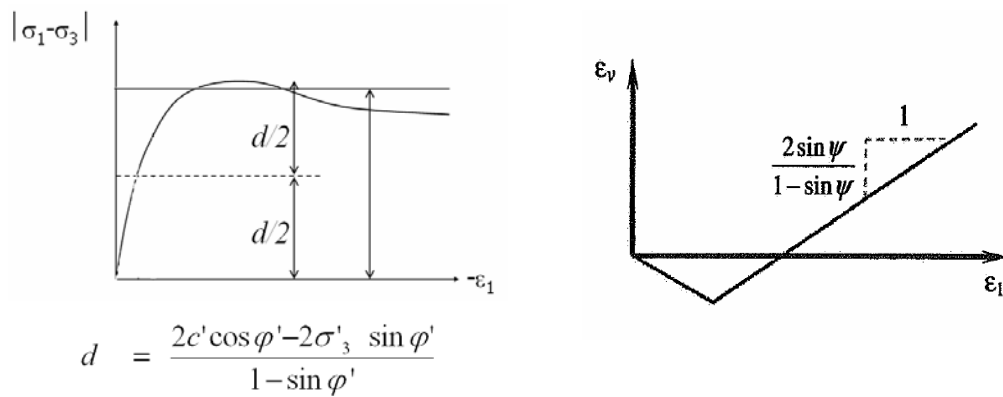


Fig. B.2: Determinations of φ and ψ from drained triaxial test

In Fig. B.1, the definition of stiffness parameters is visualised. E_{50}^{ref} and E_{ur}^{ref} are determined from a drained triaxial test while E_{cod}^{ref} is determined from an oedometer test. Moreover, the friction angle (ϕ) and the dilatant angle (ψ) are also determined from a drained triaxial test (Fig. B.2).

First, a drained triaxial test and an oedometer test are simulated by using the *Soil tests* facility in Plaxis 2D, in which the hypoplastic model are used as the input parameters. Based on its results, some parameters of the hardening soil model are defined as shown in Fig. B.1 and Fig. B.2. Remaining parameters (m , v_{ur} , P^{ref}) are taken as suggested by Brinkgreve & Broere [5]. Subsequently, they are improved so that the results of drained triaxial and oedometers tests from the hypoplastic and the hardening soil models are qualitatively similar (see Fig. B.3 to Fig. B.5 for more detail)

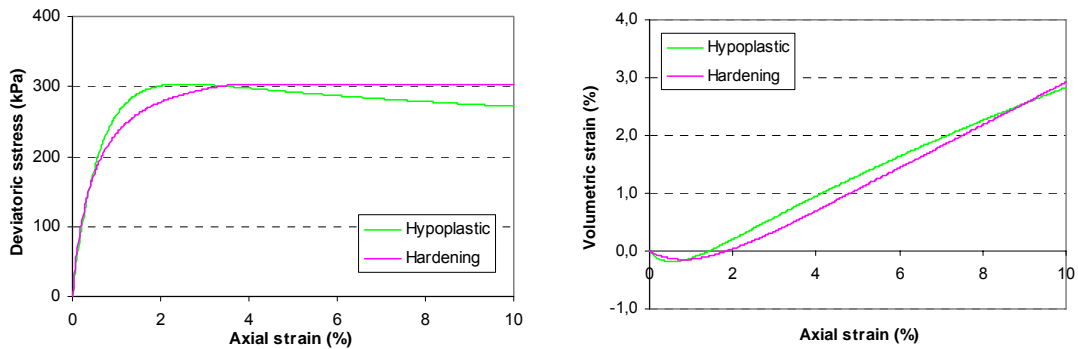


Fig. B.3: Result of drained triaxial tests at reference pressure (dense sample)

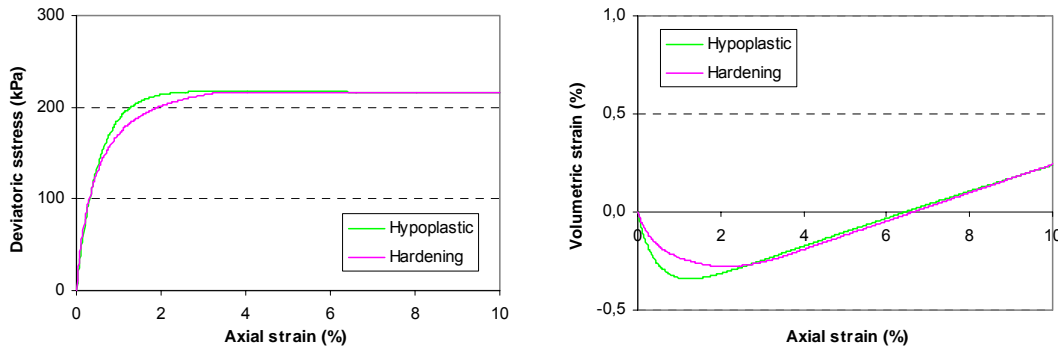


Fig. B.4: Result of drained triaxial tests at reference pressure (loose sample)

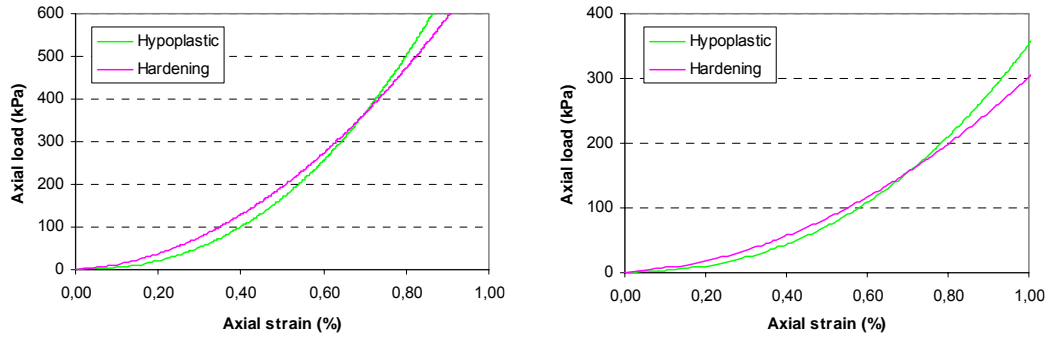


Fig. B.5: Result of oedometer tests on dense (left) and loose (right) samples

Finally, the parameters of the hardening soil model for Baskarp sand are suggested in Table B.1. In this analysis, the power for stress-level dependency of stiffness (m) of the hardening soil model is set to default value (0.5). However, it could be increased slightly to get more precise results in comparison with the hypoplastic model (Fig. B.5).

Table B.1: Estimated parameters of hardening soil model for Baskarp sand

Parameters	E_{50}^{ref}	$E_{\text{eod}}^{\text{ref}}$	$E_{\text{ur}}^{\text{ref}}$	φ	ψ	m	ν_{ur}	p^{ref}
Unit	(kPa)	(kPa)	(kPa)	(o)	(o)	-	-	(kPa)
Dense	40,500	50,000	121,500	37	9	0.5	0.2	100
Loose	31,000	33,000	93,000	31.3	2	0.5	0.2	100
Medium	36,000	38,000	108,000	34.5	2	0.5	0.2	100

References

1. Aronov, A.M. and Gudakov, Y.S., Evaluating the bearing capacity of driven piles in sandy soils. *Soil Mechanics and Foundation Engineering*, 1977. 14(1): p. 28-30.
2. Atkinson, J., Richardson, D., and Stallebrass, S., Effect of recent stress history on the stiffness of overconsolidated soil. *Geotechnique*, 1990. 40: p. 531-540.
3. Bauer, E., Calibration of a comprehensive hypoplastic model for granular materials. *Soils and Foundations*, 1996. 36(1): p. 13-26.
4. Bement, R.A.P. and Selby, A.R., Compaction of granular soils by uniform vibration equivalent to vibrodriving of piles. *Geotechnical and Geological Engineering*, 1997. 15(2): p. 121-143.
5. Brinkgreve, R.B.J. and Broere, W., Plaxis 2D. 2008. Version 9.
6. Broere, W. and Van Tol, A.F., Modelling the bearing capacity of displacement pile in sand. *Proceeding of the Institution of Civil Engineer, Geotechnical Engineering* 2006. 159(3): p. 195-206.
7. Chi, N.T., Investigation into soil displacement near a jacked-in pile in sand. 2008. MSc Thesis.
8. Chong, M., Density change of sand on cone penetration resistance. *Proceeding of first international symposium on penetration testing* 1988: p. 707-714.
9. Dijkstra, J., et al., Numerical simulation of pile installation in sand. *International Center of Computational Engineering*, 2008.
10. Dijkstra, J., et al., Density changes near advancing displacement pile in sand. *Proceeding of International Conference on Foundation*, 2008.
11. Dijkstra, J., Broere, W., and Van Tol, A.F., Experimental investigation into the stress and strain development around displacement pile. *In Proceeding of the Tenth International Conference on Piling and Deep Foundations*, 2006: p. 252-259.
12. Dijkstra, J., Broere, W., and Van Tol, A.F., Numerical investigation into stress and strain development a round a displacement pile in sand. *Sixth European Conference on Numerical Methods in Geotechnical Engineering*, 2006.
13. Elmi Anaraki, K., Hypoplasticity insvestigated. *Technical report, Delft University of Technology*, 2008.
14. Engin, H.K., Progress PhD report. 2009.
15. Gorbunov, M. and Posadov, Displacement and compaction of soil by

driven pile. *Soil Mechanics and Foundation Engineering*, 1968. 5(5): p. 313-318.

16. Gudehus, G., A comprehensive constitutive equation for granular materials. *Soils and Foundations*, 1996. 36(1): p. 1-12.

17. Henke, S. and Grabe, J., Numerical investigation of soil plugging inside open-ended piles with respect to the installation method. *Acta Geotechnica*, 2008. 3(3): p. 215-223.

18. Henke, S. and Grabe, J., Simulation of pile driving by 3-dimensional finite element analysis. In *Proceeding of 17th European Young Geotechnical Engineer*, 2006. Croatian Geotechnical Society: p. 215-233.

19. Herle, I. and Gudehus, G., Determination of parameter of a hypoplastic constitutive model from properties of grain assemble. *Mechanics of Cohesive-Frictional Material*, 2000. 4(5): p. 461-486.

20. Klotz, E.U. and Coop, M.R., An investigation of the effect of soil state on the capacity of driven piles in sands. *Geotechnique*, 2001. 51(9): p. 733-751.

21. Kolymbas, D., Introduction to hypaplasticity. *Advances in Geotechnical Engineering and Tunnelling*, 1999.

22. Kolymbas, D., A generalized hypoelastic constitutive law. *Proceeding of International Conference on Soil Mechanics and Foundation Engineering*, 1985.

23. Kolymbas, D. and Wu, W., Recent results of triaxial tests with granular material. *Powder Technology*, 1990. 60(99-119).

24. Kudella, P. and Reul, O., Hypoplastic analyses of piled refts. *Numerical Mehtods in Geotechnical Engineering*, 2002: p. 389-395.

25. Lehane, B.M., et al., Mechanisms of shear friction in sand from instrumented pile tests. *ASCE Journal of Geotechnical Engineering*, 1993. 119(1): p. 19-35.

26. Masoumi, H.R. and Degrande, G., Numerical modeling of free field vibration due to pile driving using a dynamic soil-structure interaction formulation. *Journal of Computational and applied mathematics*, 2008. 215(2): p. 503-511.

27. Niemunis, A., Extended hypoplastic models for soil. 2003. ISSN 1439-9342.

28. Niemunis, A. and Herle, I., Hypoplastic model for cohesionless soils with elastic strain range. *Mechanics of Cohesive-Frictional Material* 1997. 2: p. 279-299.

29. Pecker, A., Soil behaviour under cyclic loading. *Advanced Earthquake Engineering Analysis*, 2007: p. 1-13.

30. Puzrin, M. and Burland, J., Non-linear model of small strain behavior

of soils. *Geotechnique*, 1998. 48: p. 217-233.

31. Reyes, D.K., Rodriguez-Marek, A., and Lizcano, A., A hypoplastic model for site response analysis. *Soil Dynamic and Earthquake Engineering*, 2009. 29(1): p. 173-184.

32. Robinsky, E.I. and Morrison, C.F., Sand displacement and compaction around model friction piles. *Canadian Geotechnical Journal*, 1964. 1(2): p. 88-96.

33. Said, I., Gennaro, D.V., and Frank, R., Axisymmetric finite element analysis of pile loading tests. *Computers and Geotechnics*, 2009. 36(1-2): p. 6-19.

34. Schanz, T., Vermeer, P.A., and Bonnier, P.G., The hardening soil model: Formulation and verification. *Beyond 2000 in Computational Geotechnics*, 1999. Balkema, Rotterdam, ISBN 90 5809 040 X.

35. Schofield, A. and Wroth, C., Critical state soil mechanics. *McGraw-Hill, London*, 1968.

36. Von Wolffersdorff, P.A., A hypoplastic relation for granular materials with a predefined limit state surface. *Mechanics of Cohesive-Frictional Material*, 1996. 1: p. 251-271.

37. White, D.J. and Lehane, B.M., Friction fatigue on displacement piles in sand. *Geotechnique*, 2004. 54(10): p. 645-658.